ForskEL X-WiWa

Deliverable 1.3

MIKE 3 Coupling Added Value

Energinet.dk

Report

September 2016

This report has been prepared under the DHI Business Management System certified by Bureau Veritas to comply with ISO 9001 (Quality Management)

ForskEL X-WiWa

Deliverable 1.3

MIKE 3 Coupling Added Value

Prepared for	Energinet.dk
Represented by	Ms Aja Brodal

Offshore wind farm

Author	Rodolfo Bolaños Sanchez
Quality supervisor	Jacob Tornfeldt Sørensen

Project number	11812962
Approval date	9 September 2016
Revision	Final
Classification	Restricted

DHI • Agern Allé 5 • DK-2970 Hørsholm • Denmark
Telephone: +45 4516 9200 • Telefax: +45 4516 9292 • dhi@dhigroup.com • www.dhigroup.com

This page is intentionally left blank

CONTENTS

FIGURES

TABLES

1 Introduction

X-WiWa aims at improving the forecast of wind and waves during storm conditions and provide design parameters through better estimation of the extreme wind and waves (e.g. the 50-year return period). For this, coupling approaches are considered between atmospheric, wave and oceanic models.

One of the ocean-atmosphere interactions is via heat exchange where sea surface temperature (SST) plays a crucial role. The importance of the diurnal variability of sea surface temperature on air-sea interaction is being increasingly recognized. Kawai and Wada (2007) present a comprehensive review on the knowledge of the diurnal SST variation and its impact on the atmosphere and the ocean. They outline that a few numerical experiments have indicated that the diurnal SST variation can modify atmospheric properties over the Pacific warm pool or a coastal sea, but the processes underlying the modification have not yet been investigated in detail.

Other interactions occur between waves and current where ocean currents can produce modifications of the wave propagation, this is particularly important in areas with strong tidal currents (Benetazzo et al., 2013; Bolaños et al. 2014; Sørensen et al., 2006; Ardhuin et al., 2012). Currents modify wave properties by current refraction and the Doppler shift of wave frequency and, conversely, waves can generate currents through processes such as Stokes' drift and radiation stress. The velocity distribution in combined wave–current flows is important for the determination of sediment transport in coastal waters, wave height attenuation, and pollution dispersion.

For a fixed observer, the waves travel faster when they move in the same direction as the current (and vice versa). This is known as the 'Doppler effect', resulting in a change in the intrinsic wave frequency. The wave dispersion relation in a uniform current is modified such that waves of the same apparent (absolute) period will have a longer intrinsic (relative) period in a favourable (following) current and a shorter intrinsic period in an opposing current (Wolf and Prandle, 1999).

When talking about coupling between models it is common to refer to "offline" coupling or "online" coupling. Offline coupling meaning that exchange of information occurs in one direction, from one model to another one, while in an online coupling information exchange occurs in both directions during the simulation. Online coupling systems are more demanding from the computational point of view and it requires a system capable of performing the exchange of information between different models. Although large efforts have been done to develop these kind of systems (e.g. COAWST, Warner et al., 2010) there is not a clear evidence that an online system may bring significant benefits over an offline system. A situation where its benefit is evident is in a forecasting system for hurricanes (Zhu and Zhang, 2006), where sea-surface temperature variations are strongly coupled with the atmosphere and are critical to the correct hurricane simulation and thus an offline forecasting system would incorrectly estimate the hurricane intensity. However, for a hindcast system, typically used to derive extremes for design purposes, an online system with access to high quality forcing (e.g. satellite SST, reanalysis winds, etc.) would suffice. For this reason, this report focuses on the impact of the use of ocean variables in atmosphere and wave model in an offline coupling mode.

A three-dimensional (3D) ocean model can be used to estimate a high temporal and spatial resolution of SST and spatially varying currents. For this purpose, the model MIKE 3 has been implemented in the North Sea. This report describes the model set-up and discusses the model results and implications for atmospheric and wave modelling in the North Sea with special focus on the Danish waters. The report is structured as follows: Section 2 gives a brief description of the three-dimensional ocean model, MIKE 3. Section 3 describes the implementation of MIKE 3 for the North Sea. In Section 4 model validation is discussed while in Section 5 the impact of ocean variables on wind and wave modelling are discussed. Finally, Section 6 summarizes the conclusions of this report.

2 MIKE 3 Model Description

MIKE 3 is a component of the MIKE Powered by DHI software (MIKEpoweredbyDHI, 2016; Pietrzak et al., 2002). It is based on the solution of the three-dimensional incompressible Reynolds averaged Navier-Stokes equations, subject to the assumptions of Boussinesq and of hydrostatic pressure. The transports of temperature and salinity follow the general transport-diffusion equations (Pietrzak et al., 2002). The small-scale turbulence can be approximated using sub-grid scale models, several turbulence models can be applied: a constant viscosity, a vertically parabolic viscosity and a standard k-ε model (Rodi, 1984). The turbulence is described separately for the vertical and the horizontal transport. The free surface is taken into account using a σ-coordinate system but a combined σ and z-layer distribution is possible within the model. In the horizontal plane, an unstructured grid is used. The spatial discretization is performed using a cell-centred finite volume method. The heat in the water can interact with the atmosphere through heat exchange, which is calculated on the basis of the four physical processes: latent heat, sensible heat, short wave radiation and long wave radiation. The model is able to also take into account tidal potential (Pugh, 1987), evaporation/precipitation, wind stress, two-dimensional (2D) wave radiation stresses and the open boundaries can be forced by elevation, velocity, salinity and temperature. Wind stress is based on a drag formulation dependent on wind speed (Wu, 1984).

This page is intentionally left blank

3 MIKE 3 Implementation in the North Sea

This section provides a general description of MIKE 3 implementation in the North Sea regarding model domain and forcing. A more detailed description can be found in the X-WiWa deliverable D1.15.

3.1 Model Domain

The model domain covers the North Sea, Norwegian Sea and Barents Sea. The most northern latitude of the domain is at 81° N and the most southern lies at 47.9° N. The western limit is delimited by 4.5° W and the eastern one by 47.8° E as seen in Figure 3.1. The mesh resolution goes from 0.2 degrees in the most offshore part of the Norwegian Sea up to 0.05 degrees in the coastal part of the southeast North Sea. In the vertical the model uses combined sigma and z-levels, with 13 sigma levels in the top 61 m and 20 z-levels underneath with a variable vertical distribution. The model has been implemented for the years 2011 and 2013.

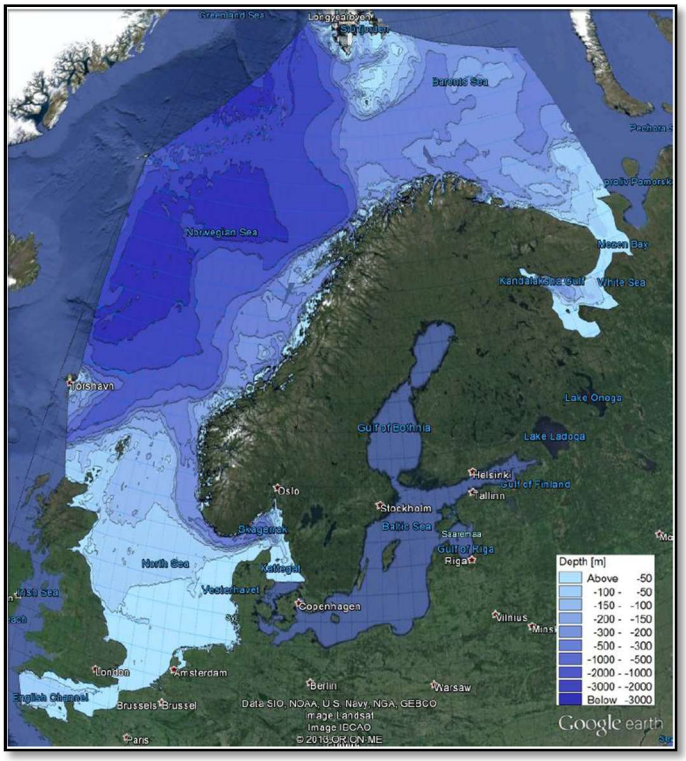

Figure 3.1 Model domain covering the North Sea

3.2 Open Boundary Forcing and Initial Conditions

A downscaling approach has to be used to model the 3D ocean dynamics of the North Sea with high spatial resolution. This requires the generation of open boundaries and initial conditions derived from global ocean models. My-Ocean data (now Copernicus) have been used to provide temperature, salinity and large-scale (not tidal) surface elevation and ocean currents to MIKE 3.

3.2.1 My-Ocean Data

Operational Oceanography has been acknowledged by the European Commission as one of the 3 key-domains covered by its GMES programme. As a consequence, the European Commission co-funded a 3-year period called My-Ocean in the 7th framework programme for European research and Development. That project was undertaken in April 2009 and came to an end in March 2012. It was dedicated to the preparation of GMES (Global Monitoring for Environmental and Security). It had a free access and provided available information on the global ocean based on the combination of space and in situ observations and their assimilation into 3D models. Some of the variables available are temperature, salinity, currents, sea ice, sea level, wind and biogeochemical parameters. These models rely on the aggregation of European modelling tools and the scientific methodology is a result of a strong collaboration between operational and research communities. The continuation of the efforts done by My-Ocean is being carried out by Copernicus (http://marine.copernicus.eu/). Global ocean data have been used for the MIKE 3 implementation in the North Sea using a similar approach as in Bolaños et al. (2014b).

3.3 Tidal Forcing

Tidal currents and tidal surface elevation variations are included in the downscaling methodology. A 2D tidal simulation is done by imposing a tidal surface elevation in the model boundaries. This 2D model run generates the tidal boundary currents that are used to force the 3D model in combination with the baroclinic current provided by My-Ocean data. The tidal surface elevation is produced by the DTU10 (altimetry based) global tidal model (Chen and Andersen, 2010), which is part of the MIKE Powered by DHI software tools.

3.4 Atmospheric Forcing

The atmospheric forcing employed was provided by CFSR (Climate Forecast System Re-analysis) and included hourly fields of clearness coefficient, air temperature, humidity, precipitation, atmospheric pressure and wind velocity components.

The CFSR data set was established by the National Centers for Environmental Prediction (NCEP). CFSR is a coupled meteorological and oceanographic model system that uses synoptic data for initialization. The data are available on an hourly basis from 1 January 1979 to present. The CFSR data cover the 31-year period from 1979 to 2010, and since then the operational data set (denoted CFSV2) is available. The underlying model in CFSV2 is the same as for CFSR. However, the spatial resolution of wind was increased from 0.3° to 0.2° while the resolution of atmospheric pressure is 0.5° for the entire period.

4 MIKE 3 Validation

The X-WiWa deliverable D1.15 presented the MIKE 3 implementation together with model validation using satellite SST (from the Advanced Very High Resolution Radiometer (AVHRR) and Advanced Microwave Scanning Radiometer (AMSR) on the NASA Earth Observing System satellite) and current data from ADCP (Acoustic Doppler Current Profiler) in the Norwegian area. Here we have extended the validation to use current data from the FINO 1 and FINO 3 platforms (Figure 4.1) which are closer to Danish areas. Validation of surface elevation has also been done with data from Thorsminde (Figure 4.2).

FINO 1 and FINO 3 are two platforms in the southern North Sea intended to improve knowledge of ocean and atmosphere processes. Atmospheric and oceanic variables are available from

different instrumentations in the platforms (http://www.fino-offshore.de). In this report, ADCP measurements have been used to validate MIKE 3.

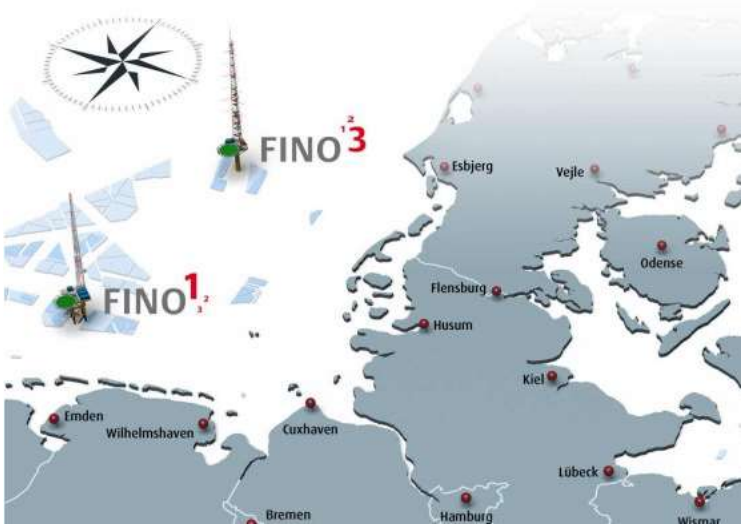

Figure 4.1 FINO platforms in the North Sea (http://www.fino-offshore.de).

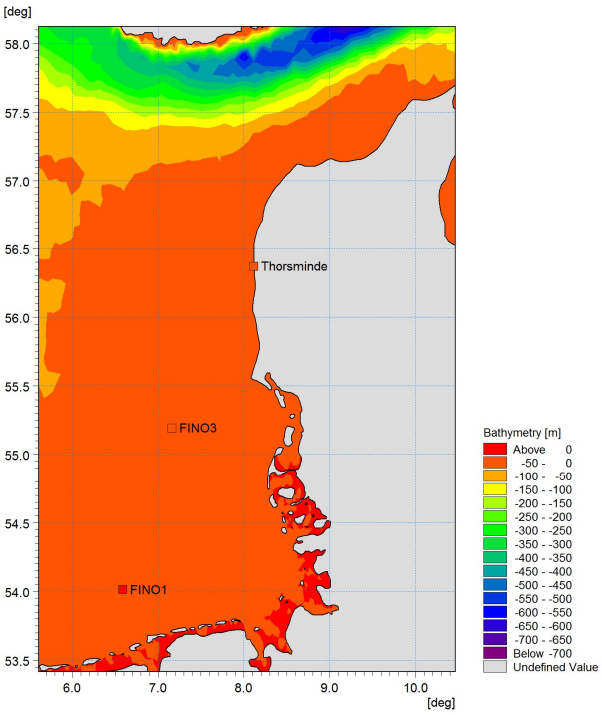

Figure 4.2 Location of Thorsminde SSH measurements

Output of the ocean model is 3D fields of salinity, temperature, and current components as well as 2D fields of depth-averaged current and surface elevation. Figure 4.3 shows an example of the distribution of surface currents on 21 November 2011. Large velocities can be seen in the English Channel mainly triggered by tides. Figure 4.4 shows the spatial distribution of salinity where the contribution of fresh water from the Baltic Sea is clearly shown. Figure 4.5 shows sea

surface temperature, where warmer water coming from the English Channel and colder from the Baltic Sea are appreciable.

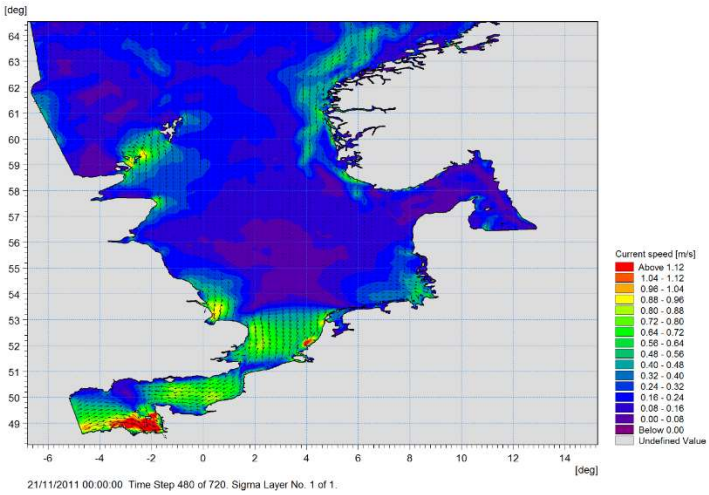

Figure 4.3 Spatial distribution of surface currents on 21 November 2011

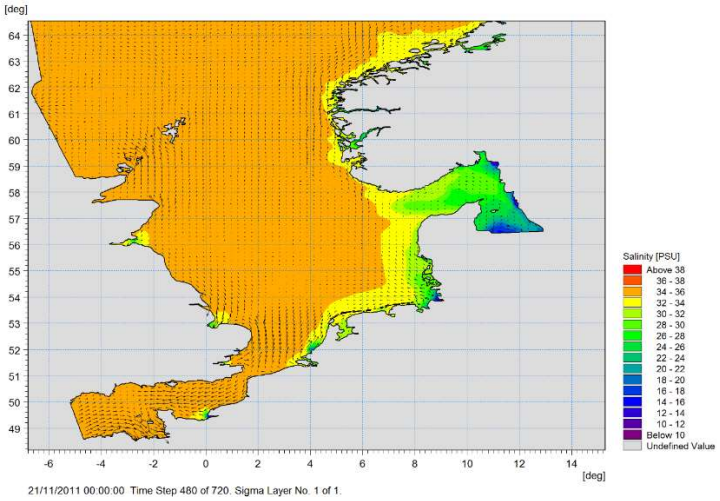

Figure 4.4 Spatial distribution of surface salinity on 21 November 2011

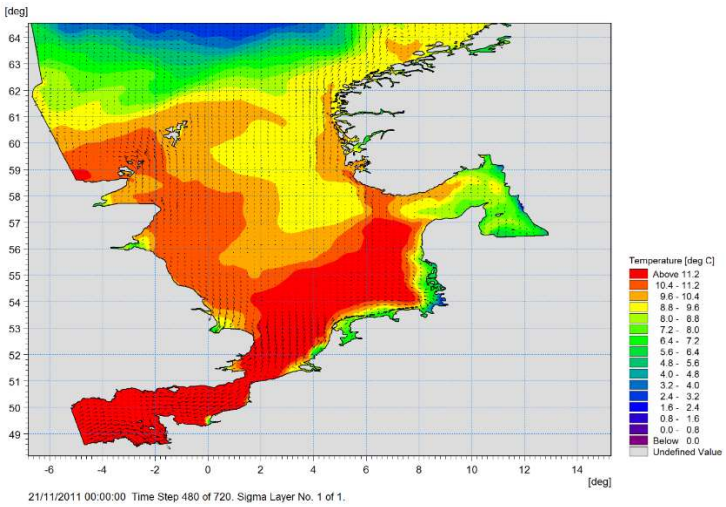

Figure 4.5 Spatial distribution of sea surface temperature (SST) on 21 November 2011.

Figure 4.6 to Figure 4.10 show scatter plots of current speed from model and measurements at FINO 1 at 28 m depth during 2012. Figure 4.6 shows the scatter plot showing a phase problem producing the circular pattern in the scatter plot. Figure 4.7 to Figure 4.10 show scatter plots with different time shifts of model data, showing that the less scatter is produced by 1 hour time shift (Figure 4.9). Similarly, Figure 4.11 to Figure 4.15 show comparisons at FINO 3 at 22 m depth for 2011. However, for FINO 3, slightly better results (less scatter) are obtained with a time shift of 90 min). Currents at both locations have a significant tidal component due to their location relative to the amphidromic point in the southern North Sea, and the phase error could indicate errors on tidal wave propagation along the domain.

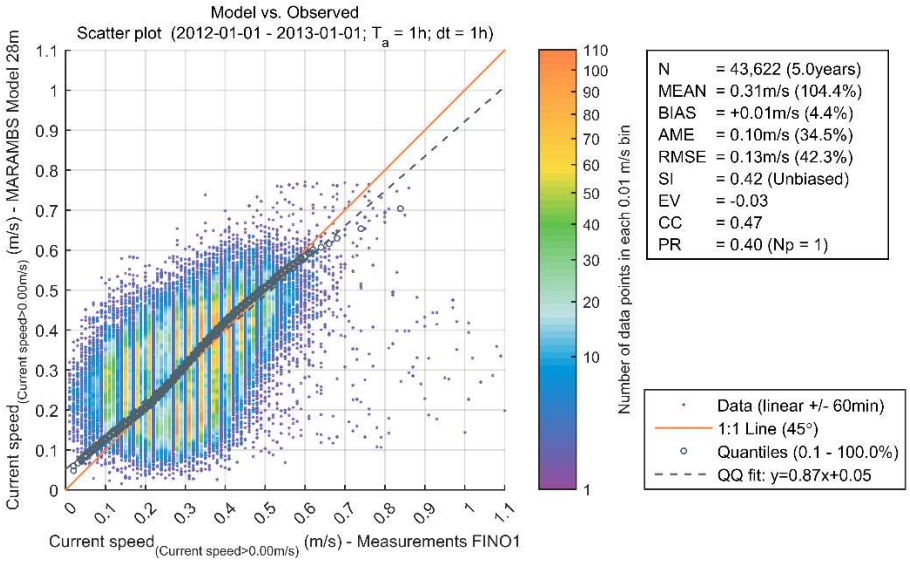

Figure 4.6 FINO 1 current speed scatter plot at 28 m depth with no time shift of time series.

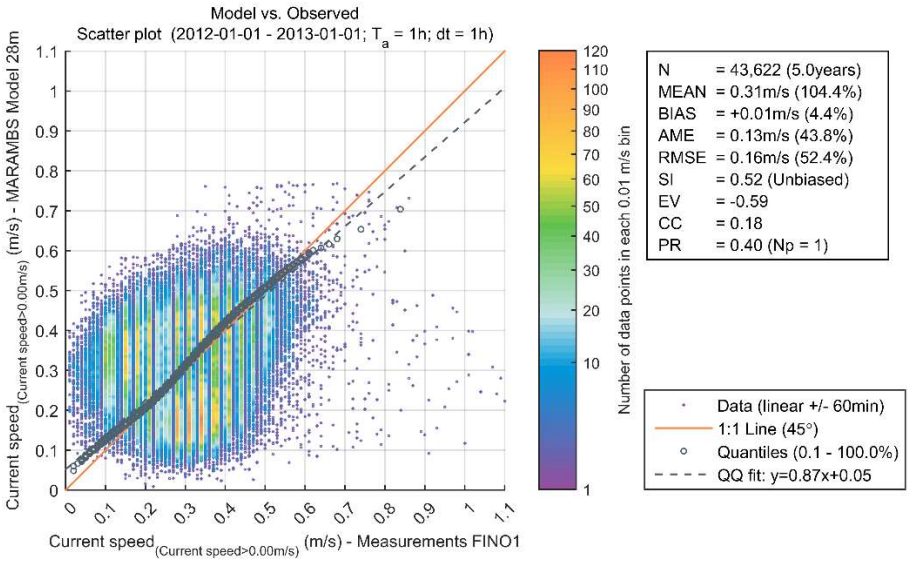

Figure 4.7 FINO 1 current speed scatter plot at 28 m depth with +30 time shift of model time series.

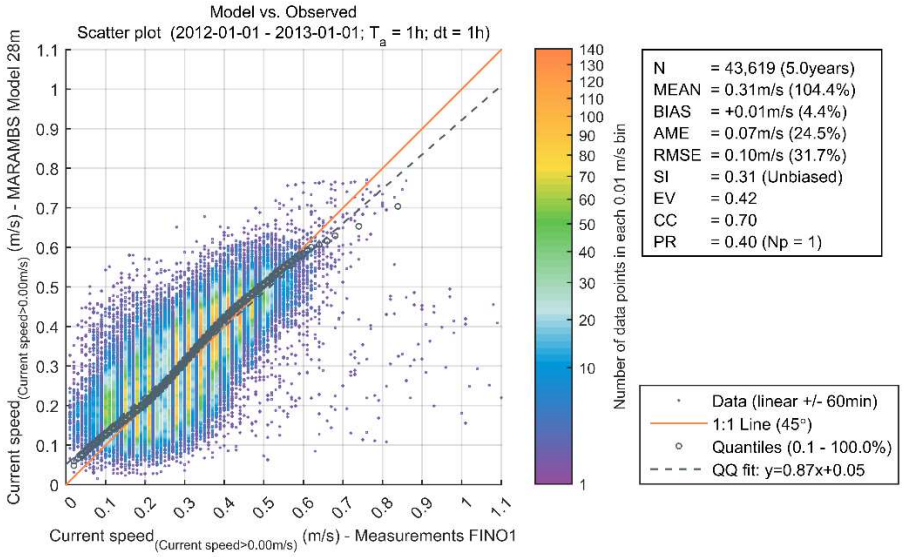

Figure 4.8 FINO 1 current speed scatter plot at 28 m depth with -30 time shift of model time series.

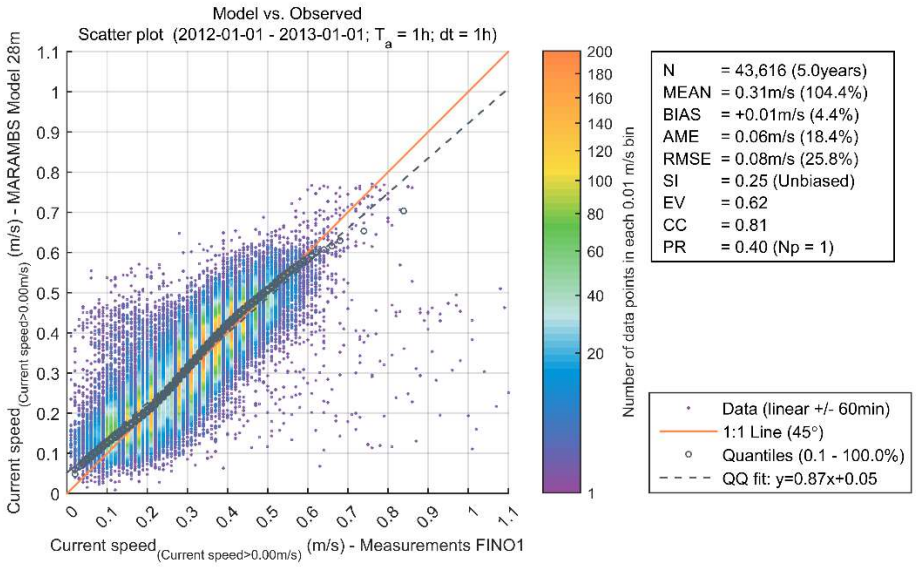

Figure 4.9 FINO 1 current speed scatter plot at 28 m depth with -60 time shift of model time series.

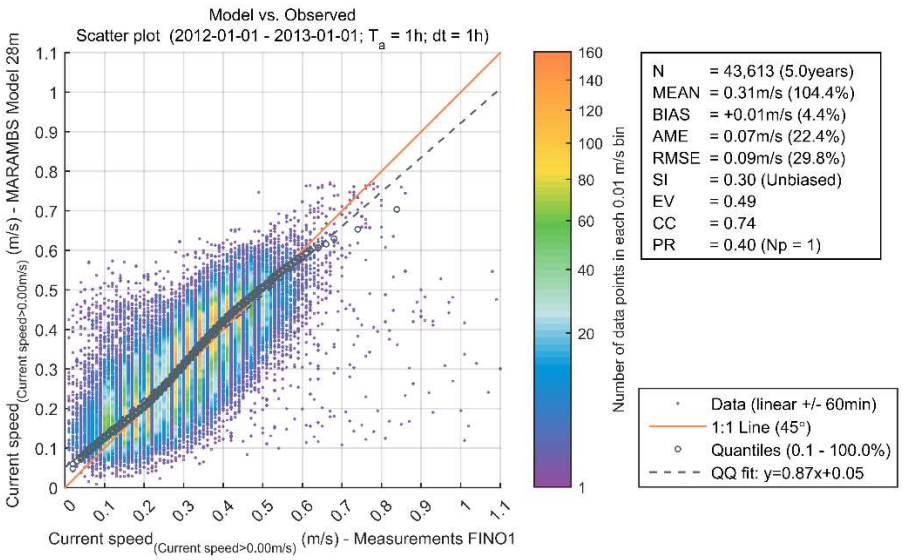

Figure 4.10 FINO 1 current speed scatter plot at 28 m depth with -90 time shift of model time series.

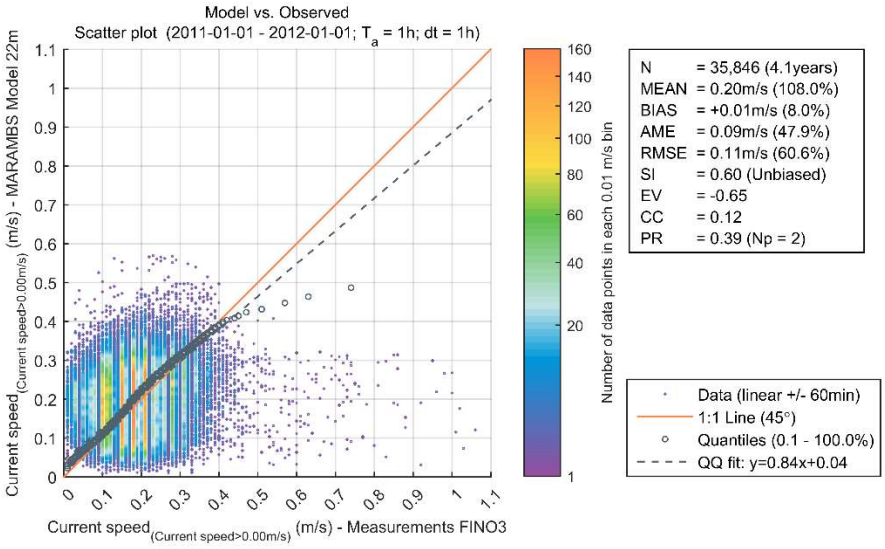

Figure 4.11 FINO 3 current speed scatter plot at 22 m depth with no time shift of model time series.

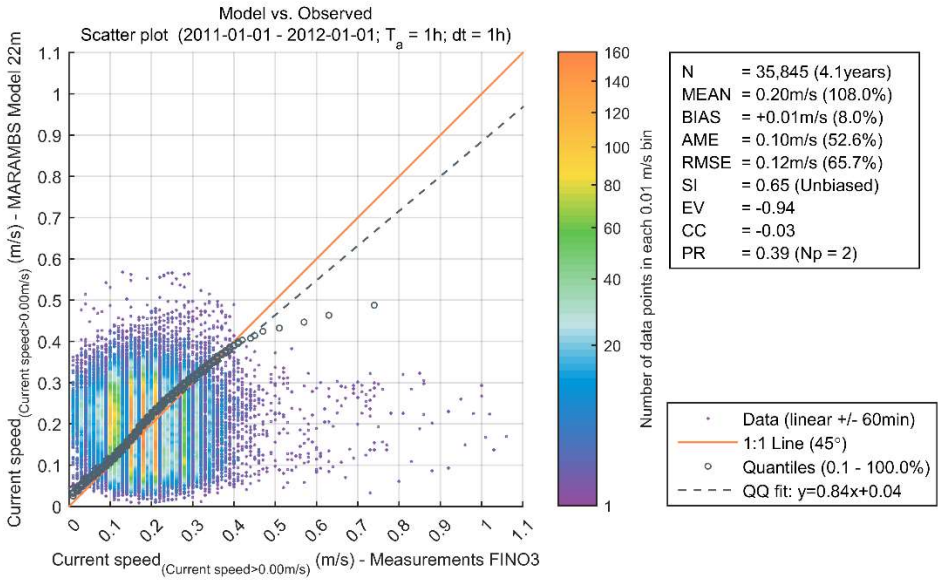

Figure 4.12 FINO 3 current speed scatter plot at 22 m depth with +30 time shift of model time series.

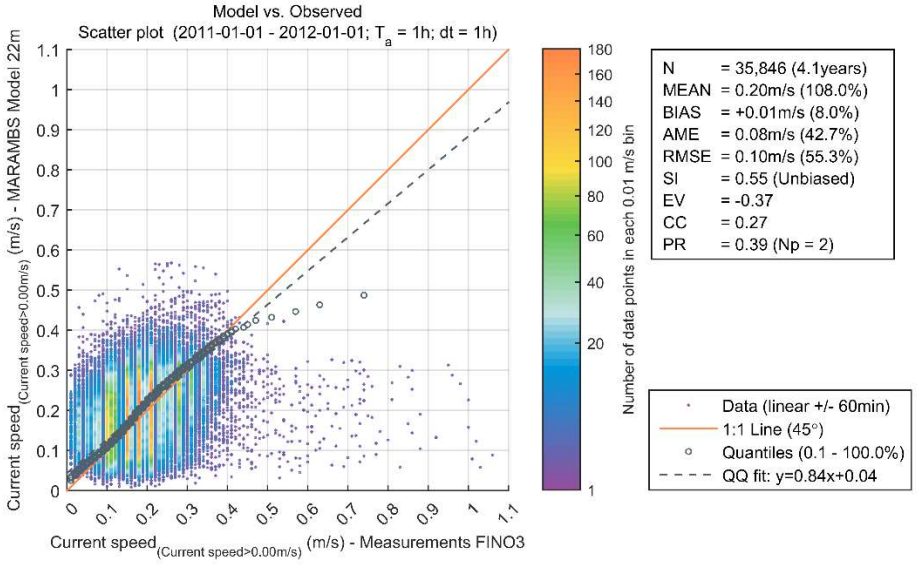

Figure 4.13 FINO 3 current speed scatter plot at 22 m depth with -30 time shift of model time series.

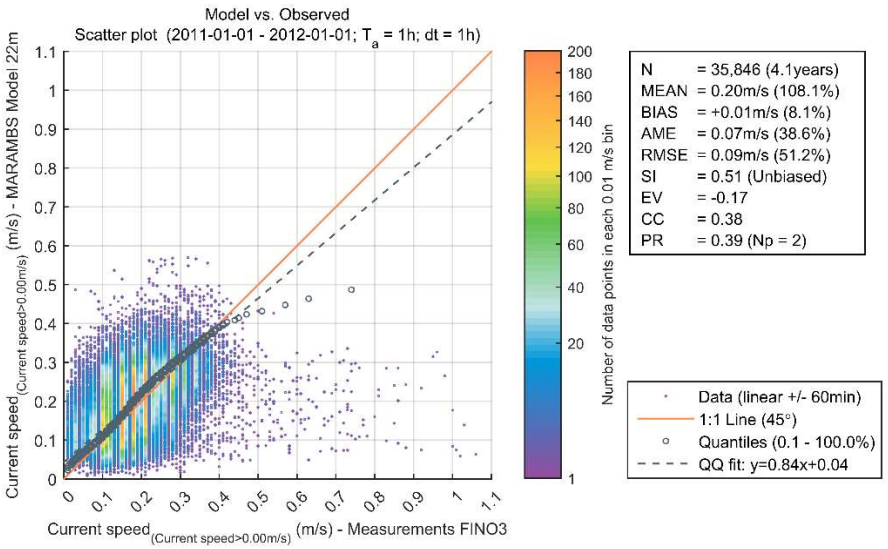

Figure 4.14 FINO 3 current speed scatter plot at 22 m depth with -60 time shift of model time series.

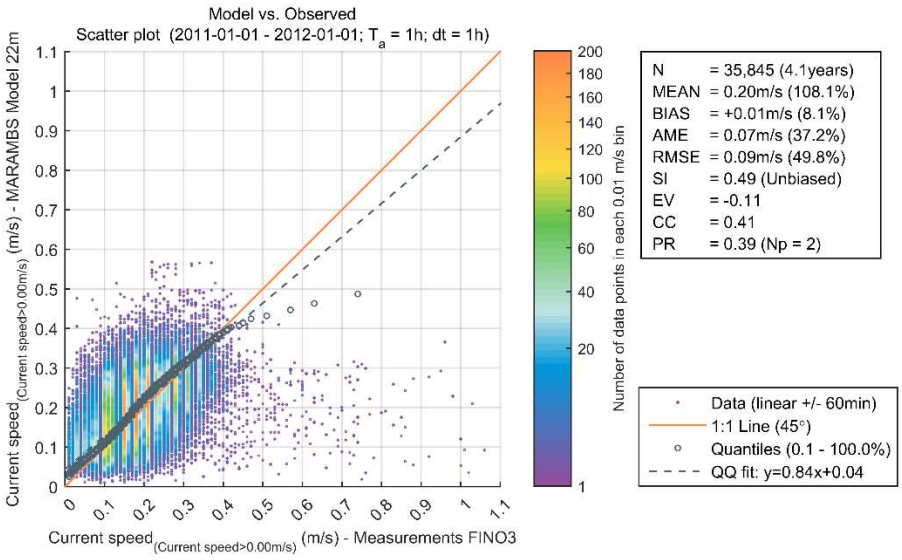

Figure 4.15 FINO 3 current speed scatter plot at 22 m depth with -90 time shift of model time series.

Figure 4.16 shows the Thornsminde time series of observed and modelled surface elevation for 2012 together with the scatter plot and some statistics. The model follows the general pattern of the observation showing a high correlation. However, it seems that it tends to predict lower high tide and higher low tides.

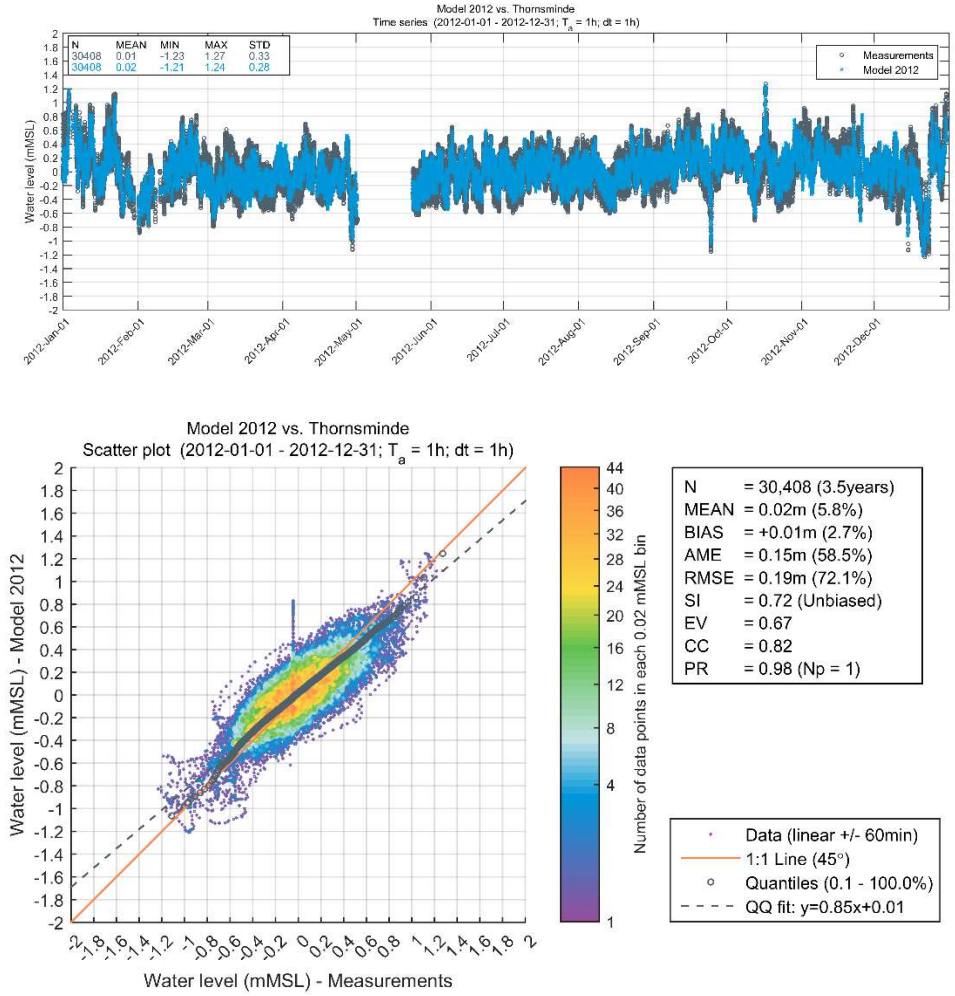

Figure 4.16 Surface elevation at Thornsminde. Top panel: time series of model and measurements. Bottom panel: scatter plot with some statistics indices.

5 Impact of Ocean Modelling on Atmospheric and Wave Modelling

5.1 Impact of Surface Elevation on Waves

Surface elevation (or sea surface height, SSH) can be important for waves in shallow areas, where surface elevation variations are significant in relation to water depth. This effect has been observed during storm conditions at Horns Rev where the inclusion of surface elevation significantly improved the wave modelling. An implementation of the wave model, MIKE 21 SW, was done for the North Sea with special focus on the Horns Rev area as seen in Figure 5.1. A spatial resolution of about 800 m was used for the Horns Rev area to simulate a storm (also used in Deliverable 3.1) that occurred during 19-22 March 2004. Measurements show significant wave height of up to 3.5 m at Horns Rev. The wave model was forced with CFSR winds, the spectral discretisation was done with 32 frequencies and 24 directions. The storm approached from west with CFSR winds reaching 23 m/s offshore Horns Rev.

Simulations with and without surface elevation were done to outline its importance. Surface elevation fields were obtained from DHI hindcast fields. During the 2004 storm, surface elevation reached more than 2 m, which is a significant change of water depth for the shallow sand banks in the Horns Rev area. Figure 5.2 shows the time series of measurements and model results. It shows that the consideration of surface elevation significantly improves model results by increasing wave height due to a reduced bottom induced dissipation. It has to be noted that modelling of surface elevation can be performed from both 2D and 3D models with equal accuracy, and thus the more expensive 3D is not justifiable for this purpose. It is also noted that a two way coupling is not necessary because in case of hindcast studies a calibrated database of surface elevation would suffice for the wave modelling purpose. For the case of online coupling, due to the relatively small influence of waves on surface elevation out of the surf zone this is not expected to have a significant impact compared to the case of offline coupling.

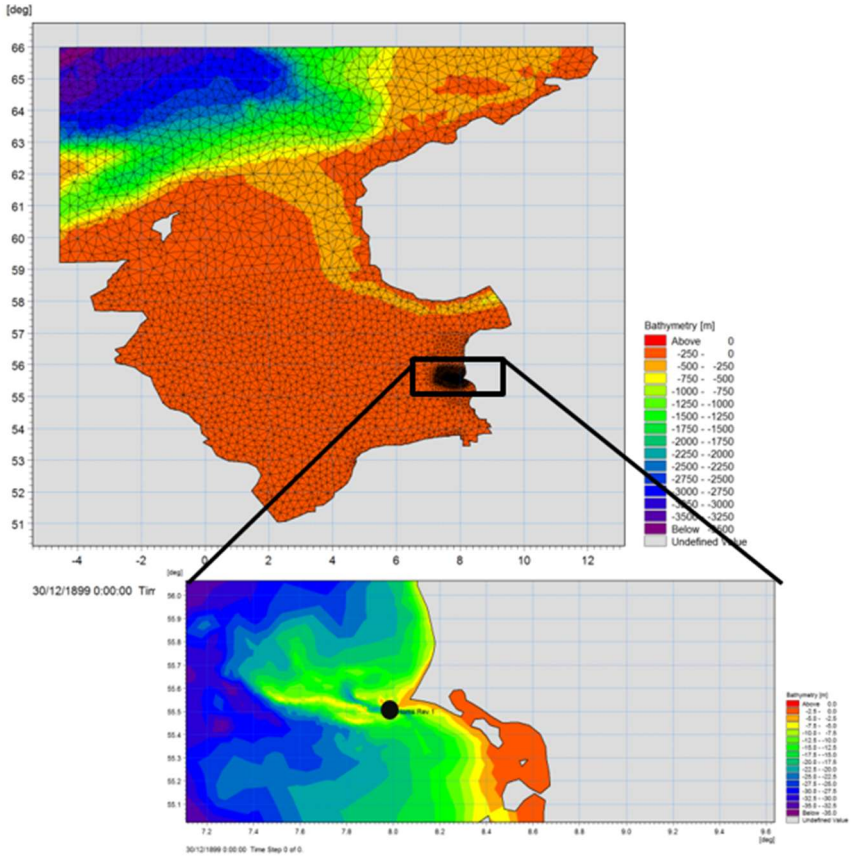

Figure 5.1 Model domain and location of buoy (black circle) measurements at Horns Rev for the storm which occurred in 2004.

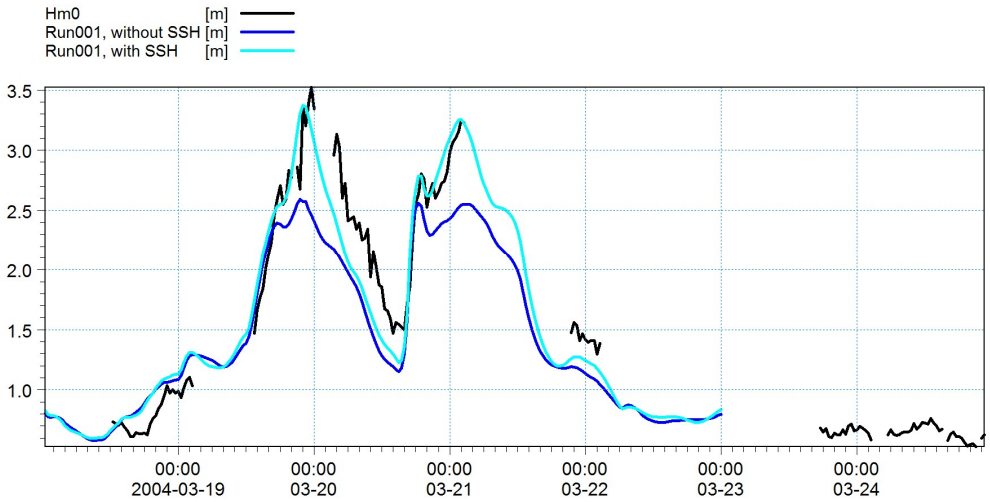

Figure 5.2 Observed and modelled significant wave height (H_{m0}) at Horns Rev.

5.2 Impact of SST on the Atmospheric Modelling

In X-WiWa Deliverable 1.16 some experiments regarding heat exchange were presented in order to investigate the impact of resolving the daily sea surface temperature (SST) cycle in an atmospheric model. The MIKE 3 implementation allows the generation of SST fields with high

spatial and temporal resolution. Modelled (hourly) SST has been used as an input to the atmospheric model WRF to be able to assess if there is any benefit from the high temporal resolution instead of the commonly used SST daily values. The studied period was November 2011, which presents a strong wind event reaching up to 20 m/s (u_{10}) within the North Sea, with waves with significant wave height (H_{m0}) of about 8 m at Sleipner and Ekofisk.

Results of WRF for the two model configurations were assessed at three locations; two of them are offshore locations (Ekofisk and FINO 3). The third location is a nearshore location at Horns Rev (Mast-8). The use of modelled high-resolution SST presented slight variations on the atmospheric model results. Wind speed variations were of the order of up to 2 m/s (~10 %) while air temperature variations of about 0.5 ^{o}C (~5 %). The largest differences in the results were found in the coastal location (Horns Rev).

The largest difference in wind speed is seen at Horns Rev, which is related to the large difference in SST. These SST differences at HR show high-frequency oscillations not observed in far-offshore locations. The response of WRF to the SST from MIKE 3 was mainly observed in the air temperature, and with some effect on wind speed at the coastal location. The difference was due to the different SST mean, and not due to the magnitude of temporal oscillations of the SST. The small daily variations in SST are not of significance for this storm case. The high-frequency differences at the coastal location seem to have a tidal origin, due to their semidiurnal frequency. The identification of six cases with large warming diurnal events has shown that they occurred during low wind conditions and, although significant impact of using a high-resolution SST could be expected, this will not have a direct impact in extreme wind conditions.

However, the results show that the mean of SST is an important parameter for storm intensity. This brings the question of the quality of SST used, while the default WRF SST data have a spatial resolution of 0.5 degree (about 50 km). Other higher resolution products (resolution of 5 – 3 km) could potentially outperform and provide a better SST forcing to the atmospheric modelling during storms. For hindcast of extreme events the use of such high-resolution products would be recommended and thus an online coupling would not give additional value. As discussed earlier, a different case is the forecasting of events (e.g. hurricanes) where the lack of SST products and the importance of SST variations for storm evolution requires an online coupled model.

It has to be noted that a coupling with a short coupling interval (1 - 3 h) between an atmospheric and ocean model can produce diurnal ocean variations (Danabasoglu et al., 2006). However, as pointed out by Kawai and Wada (2007), even if correct diurnal SST variations are supplied to an atmospheric model as a lower boundary condition, the model may not correctly respond to the diurnal variations of SST without appropriate heat flux parameterizations. These atmospheric parameterizations also need to be improved in order to study air-sea interaction on a diurnal time scale.

5.3 Impact of Currents on Waves

The spectral wave model, MIKE 21 SW, accounts for depth-averaged currents in the dispersion relation (MIKEpoweredbyDHI, 2016). The impact of currents on waves following this approach is noticeable in areas with significant currents, in many cases of tidal origin. The 2004 storm is used here to illustrate the impact of currents within the North Sea and in particular the west coast of Denmark. Figure 5.3 shows the mean difference in H_{m0} between the model without and with currents. Differences in H_{m0} are only of a few centimetres while for mean periods (Figure 5.4) they are of about 0.1 s. In areas of relatively low currents and during storms (wave celerity is larger) the impact of currents on waves is expected to be small due to the relatively larger wave celerity compared to the current speed, as shown here.

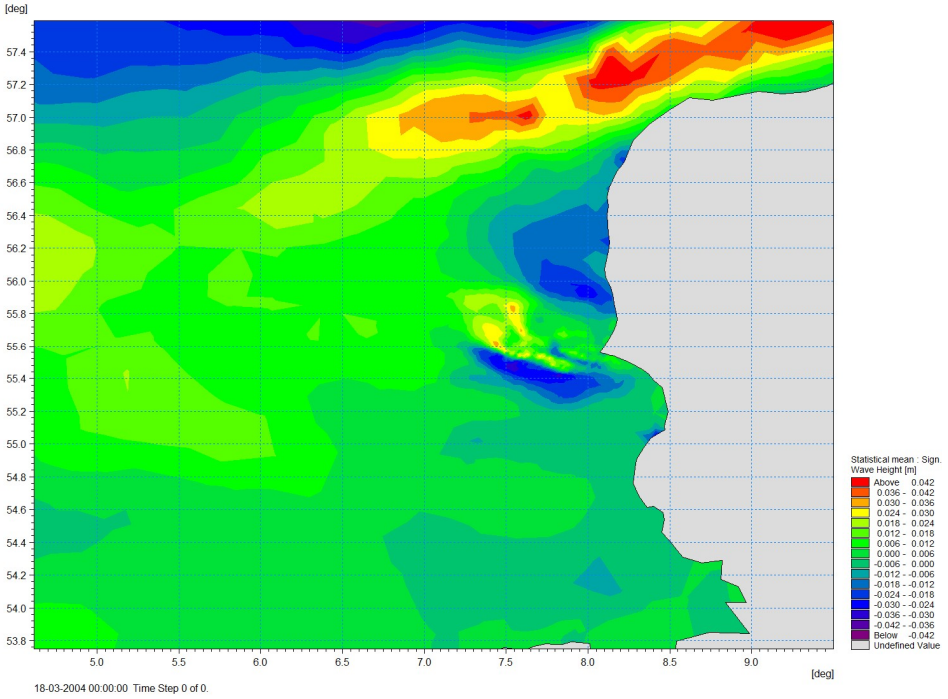

Figure 5.3 Mean of the difference in H_{m0} between the run without and with ocean currents.

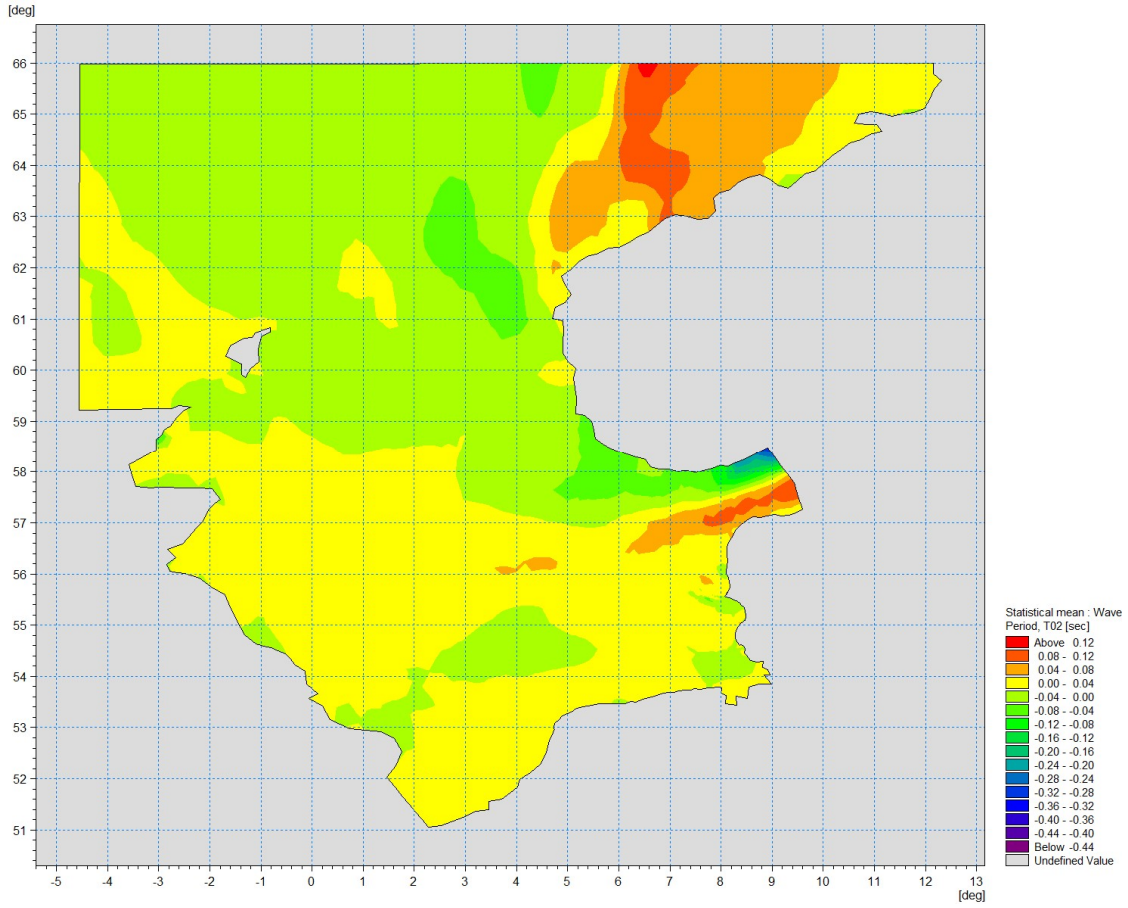

Figure 5.4 Mean of the difference in T_z between the run without and with ocean currents.

A different process that can modify the waves due to the current has been considered within the framework of X-WiWa. This consisted in modifying the wave celerity (c) in the wind input source function, where the wave growth rate (γ) reads as:

$$\gamma = \left(\frac{\rho_a}{\rho_w}\right)\left(\frac{1.2}{\kappa^2}\mu \ln^4 \mu\right)\sigma\left[\left(\frac{u_*}{c} + z_\alpha\right)\cos(\theta - \theta_w)\right]^2 \qquad \mu \le 1$$

$$\gamma = 0 \qquad \mu > 1$$

where:

ρ_a air density
ρ_w water density
κ von Karman constant
μ $k\, z_0 \exp(k/x)$
z_α constant = 0.11
k wave number
x $(u^*/c + z_\alpha)\cos(\theta - \theta_w)$
u^* wind friction velocity
c wave celerity
θ wave direction
θ_w wind direction

This correction is of particular importance for small waves (low celerity) within the wave spectrum, as wave growth can be significantly changed. For these small waves, the surface current is more representative than a depth-averaged current and thus two approaches have been tested, the first one where the surface current is approximated by a percent of the wind speed (2 %) and a second one where surface current is provided by MIKE 3.

During storms, a large wind-induced surface current is expected which could reduce the growth of waves. This is in line with the observed overestimation of waves under extreme wind conditions which has created the need of using a cap to the ratio of u^*/u_{10} (Jensen et al. 2006), with typical values between 0.05 and 0.06.

The test has been done for the storm that occurred in November 2011 and an entire year (2013). Two wave stations (Sleipner and Ekofisk, see Figure 5.5) are used for validation as they are located in the central part of the North Sea and record large waves during the November event. Figure 5.6 shows the time series of H_{m0} for observations and model results. It can be seen that using a percent of the wind has similar impact as the use of a cap to the fraction u^*/u_{10}. Figure 5.7 shows the maximum difference during the storm period for the entire North Sea. It is noticeable that the maximum difference follows the storm track, crossing the North Sea from west to east.

The use of a modelled surface current field is more physical than a parameterized one as it contains not only wind-induced current but also tidal induced, and thus can produce more spatial variations. For this reason the model domain was extended to simulate the entire 2013 and include areas with strong tidal currents. Figure 5.8 shows the mean H_{m0} difference indicating large differences in the southwestern North Sea. This was produced by small waves propagating against tidal currents which enhanced erroneous wave growth. To avoid this wave blocking when propagating against currents should be included in the implementation and it will be subject of future work.

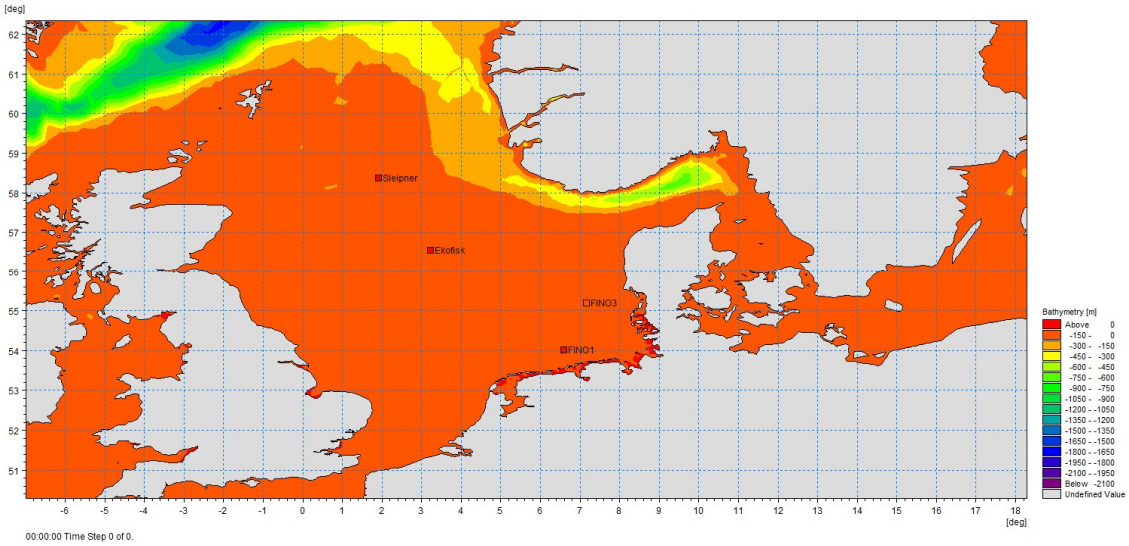

Figure 5.5 Location of Sleipner and Ekofisk wave measurements in the North Sea.

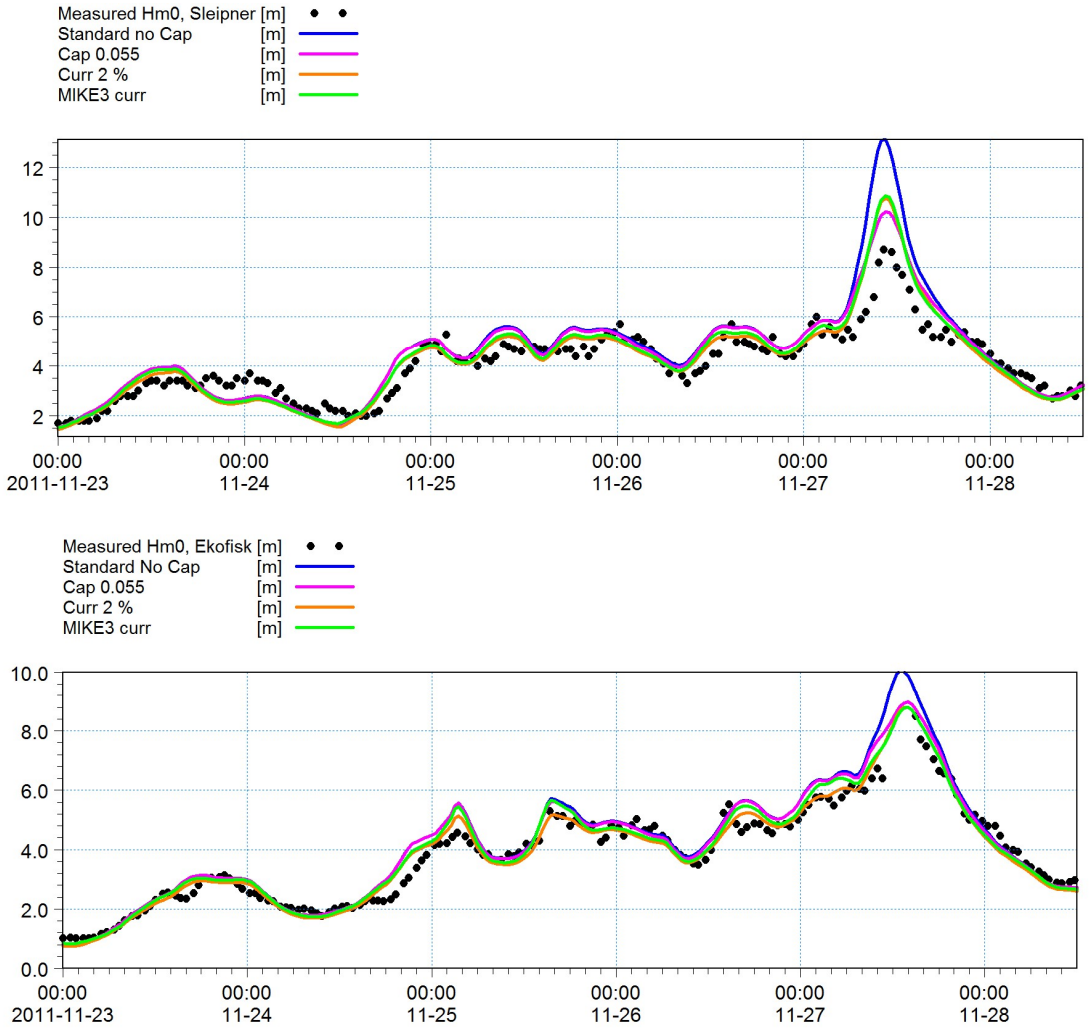

Figure 5.6 Time series of observed and modelled H_{m0} at Sleipner (top) and Ekofisk (bottom) during the November 2011 storm.

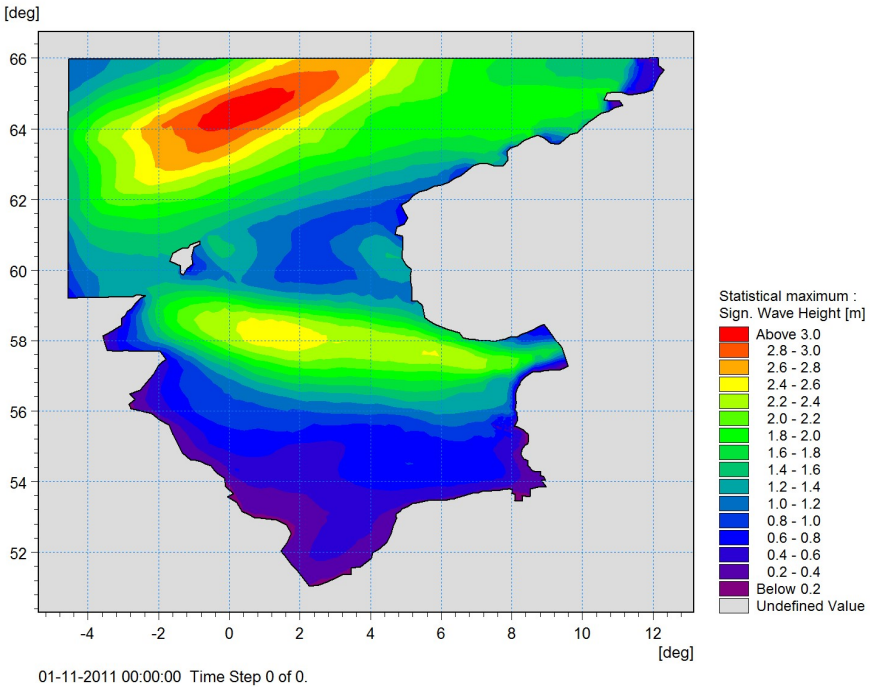

Figure 5.7 Maximum H_{m0} difference between not using and using MIKE 3 surface current to modify wave celerity in wave growth.

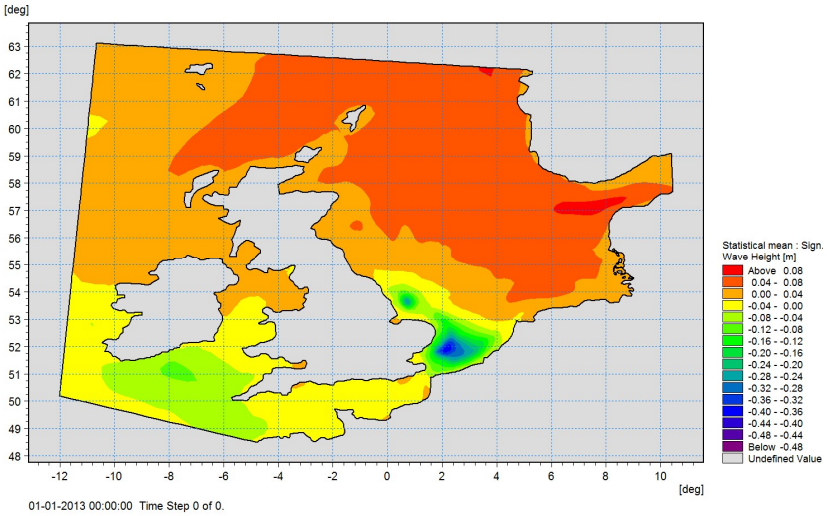

Figure 5.8 Mean of the difference in H_{m0} between the run without and with surface ocean currents from MIKE 3 to modify the input source term.

This page is intentionally left blank

6 Summary and Conclusions

The implementation of MIKE 3 for the North Sea provided good results in terms of the ocean currents. In terms of the sea surface temperature the model also presented good results, and although some bias with the satellite data was obtained the model allows us to assess the impact of high-resolution SST in the atmospheric model, WRF. In the present report we have extended the MIKE 3 validation to the FINO 1 and FINO 3 locations for current velocity and surface elevation at Thorsminde.

Three processes related to ocean coupling have been discussed: the impact of surface elevation on waves, the impact of SST on the atmosphere and the impact of ocean currents on waves. For these processes, a need of an online coupling has not been identified, especially when the interest is in hindcast modelling. Strong impact of SSH on waves was found, this is expected to be relevant in shallow areas when storm surge and tidal variations are significant. Surface elevation can be performed from both 2D and 3D models with equal accuracy, and thus the more expensive 3D is not justifiable for this purpose. The use of a high-resolution SST did not prove a significant benefit compared to standard SST fields in atmospheric modelling but outlines the importance of the use of an accurate SST field, for hindcast purposes there are available a series of reanalysis products. The impact of depth-averaged currents on waves was found not significant for Danish waters and storm conditions. However, a correction of wave growth with the surface current showed potential for improvement of wave modelling, although some other processes such as wave blocking should be considered in order to improve wave modelling under different scenarios.

Table 6.1 summarizes the processes discussed and the coupling needed in order to accurately do the modelling required within X-WiWa.

Table 6.1 Summary of processes and the type of coupling required

	Process	Offline coupling	Online coupling	Comments
Hindcast	Hurricane	✓		SST field available for hindcast
	SSH impact on waves	✓		SSH fields available for hindcast
	Currents impact on waves	✓		Current field available for hindcast
	SST impact on atmosphere	✓		SST field available for hindcast
Forecast	Hurricane		✓	Online coupling needed due to SST variation with the hurricane evolution
	SSH impact on waves	✓		Coupling could be done offline (serial sequence of model runs)
	Currents impact on waves	✓		Coupling could be done offline (serial sequence of model runs)
	SST impact on atmosphere	✓	✓	Depending on the impact of atmosphere on SST the coupling could be done offline or online.

7 Acknowledgments

Authors thank continuous interactions with other DHI colleagues (Morten Rugbjerg, Jacob Tornfeldt Sørensen, among others) during the development of this work. The BMWi (Bundesministerium fuer Wirtschaft und Energie, Federal Ministry for Economic Affairs and Energy) and the PTJ (Projekttraeger Juelich, project executing organization) are greatly acknowledged for providing FINO platform data. DONG Energy is also acknowledged for providing Horns Rev measurements data. Authors thank other X-WiWa members for support and contributions.

This page is intentionally left blank

8 References

Ardhuin, F., A. Roland, F. Dumas, A. C. Bennis, A. Sentchev, P. Forget, J. Wolf, F. Girard, P. Osuna and M. Benoit (2012). "Numerical wave modelling in conditions with strong currents: dissipation, refraction and relative wind." Journal of Physical Oceanography 42: 2101-2120.

Benetazzo, A., S. Carniel, M. Sclavo and A. Bergamasco 2013. "Wave-current interaction: effect on the wave field in a semi-enclosed basin." Ocean Modelling 70: 152-165.

Bleck, R., 2002. An oceanic general circulation model framed in hybrid isopycnic-Cartesian coordinates. Ocean Modelling 4, 55-88.

Bolaños, R., J. Brown and A. J. Souza 2014a. "Wave-current interactions in a tide dominated estuary." Continental Shelf Research 87: 109-123.

Bolaños, R., J. V. Tornfeld Sorensen, A. Benetazzo, S. Carniel and M. Sclavo 2014b. "Modelling ocean currents in the northern Adriatic Sea." Continental Shelf Research 87: 54-72.

Cheng, Y., Andersen, O.B., 2010. Improvement of Global Ocean Tide Models in Shallow Water Regions, Altimetry for Oceans and Hydrology OST-ST Meeting.

Danabasoglu, G., W. G. Large, J. J. Tribbia, P. R. Gent, B. P. Briegleb and J. C. McWilliams 2006. "Diurnal coupling in the tropical oceans of CCSM3." Journal of Climate: 2347-2365.

Halliwell, G.R., 1998. Simulation of North Atlantic decadal/multi-decadal winter SST anomalies driven by basin-scale atmospheric circulation anomalies. Journal of Physical Oceanography 28, 5-21.

Halliwell, G.R., R., B., Chassignet, E.P., Smith, L.T., 2000. Mixed layer model validation in Atlantic Ocean simulations using the Hybrid Coordinate Ocean Model EOS 80, OS304.

Jensen, R. E., V. J. Cardone and A. T. Cox 2006. Performance of third generation wave models in extreme hurricanes. 9th International Wind and Wave Workshop, Victoria, B.C.

MIKEpoweredbyDHI, 2016. MIKE 21 & MIKE 3 flow model FM. Hydrodynamic and Transport Module. Scientific Documentation. DHI, Hørsholm, Denmark, p. 50.

Pugh, D.T., 1987. Tides, surges and mean sea-level: a handbook for engineers and scientists. Wiley, Chichester.

Pietrzak, J., Jakobson, J.B., Burchard, H., Vested, H.J., Petersen, O.S., 2002. A three-dimensional hydrostatic model for coastal and ocean modelling using a generalised topography following co-ordinate system. Ocean Modelling 4, 173-205.

Reynolds, R.W., Smith, T.M., Liu, C., Chelton, D.B., Casey, K.S., Schlax, M.G., 2007. Daily high-resolution blended analyses for sea surface temperature. Journal of Climate 20, 5473-5496.

Rodi, W., 1984. Turbulence models and their application in hydraulics, in: IAHR (Ed.), Delft, p. 104.

Sørensen, O. R., H. Kofoed-Hansen and O. P. Jones 2006. Numerical modeling of wave-current interaction in tidal areas using an unstructured finite volume technique. International Conference on Coastal Engineering, World Scientific.

Warner, J. C., B. Armstrong, R. Y. He and J. B. Zambon 2010. "Development of a coupled ocean-athmosphere-wave-sediment transport (COAWST) modeling system." Ocean Modelling 35: 230-244.

Wolf, J., J. M. Brown, R. Bolaños and T. Hedges 2011. Waves in coastal and estuarine waters. Treatise on Estuarine and Coastal Science, Elsevier. 2: 171-212.

Wolf, J. and D. Prandle 1999. "Some observations of wave–current interaction." Coastal Eng. 37: 471-485.

Zhu, T. and D.-L. Zhang 2006. "The impact of the storm-induced SST cooling on Hurricane intensity." Advances in Atmospheric Science 23: 14-22.

Appendix C: D1.12

Report describing the tests performed and the model efficiency and sensitivities

Du J., Bolaños R., Larsén X. et al.

1. Overview of the existing coupling approaches in COAWST

This section gives an overview of the state-of-the-art of the existing wind-wave coupling approaches that are implemented in the COAWST coupling system. In COAWST, there are three roughness length (z_0) parameterization approaches: Taylor and Yelland (2001), Oost et al. (2002), and Drennan et al. (2005). In this project, we added one more approach, Fan et al. (2012), since it is used in MIKE 21 SW. In the four approaches, z_0 is parameterized as a function of the 10 m wind speed (u_{10}), the significant wave height (H_{m0}), the peak wave period (T_p) and peak wave length (L_p), see Imberger and Du (2016).

Coupling using these parameterization has been tested for two selected storms in the North Sea. One storm has the wind from the west covering the North Sea from 27th Jan 2002 to 29th Jan 2002. The other storm has the wind from the east covering the North Sea from 21st Nov 2002 to 23rd Nov 2002.

In addition to the above mentioned coupled experiments, a non-coupled experiment is also included, where z_0 is parameterized by the COARE3.0 scheme, in which z_0 is a function of wind speed only (Fairall, 2003).

The detailed model setups, the z_0 approach descriptions, and preliminary analysis of the results are described in Imberger and Du (2016). Here we focus on the analysis of the coupling impacts on the storm characteristics, in terms of the spatial distribution of the wind speed, significant wave height and friction velocity (Figure 1A, 1B, 1C, 1D and 1G), time series (Figure 1E) and the dependence of drag coefficient on the wind speed (Figure 1F).

Figure 1A shows a snapshot of the 10 m wind field at 12:00 28th Jan 2002 from the non-coupled simulation. The storm is centred at the west coast of Scotland with a maximum u_{10} of about 30 m/s. Wind direction in the North Sea is southwestly. Figure 1B, 1C and 1D shows the snapshots of u_{10}, H_{m0}, and u_*, respectively, for the same time as Figure 1A around the storm centre. Each subplot shows a different coupling approach. Significant differences can be seen in u_{10} and H_{m0} around the storm centre between these subplots. These differences are caused by the z_0 parameterization approaches.. For instance, the values of u_* calculated in Oost (2002) are much higher than those with other approaches around the storm centre. The high u_* gives higher z_0, which in turn reduces u_{10}. Accordingly, the simulated waves are significantly lower than those with the other approaches because they are forced by lower wind speed.

Time series of wind speed at 15 m (u_{15}), Wind direction at 28 m (WD_{28}), friction velocity (u_*), drag coefficient (C_d), H_{m0}, and T_p at Horns Rev 1, mast 2 (M2), during the storm are shown in Figure 1E. At M2, the turbulence is measured by sonic anemometer at 50 m, where u_* and C_d are calculated. Wave properties are measured by a buoy located in the south of Horns Rev 1 wind farm. Time series of u_{15} simulated by WRF generally follows the measurement data, except for an 1 to 2 hour delay of the storm peak. Using COARE3.0 (non-coupled), Taylor and Yelland (2001) and Fan et al. (2012) overestimates the maximum u_{15} for about 2 m/s; Using Drennan et al. (2005) gives the best prediction of maximum u_{15}; Using Oost et al. (2002) underestimates maximum u_{15} for about 3 m/s. The difference in H_{m0} from the use of different coupling approaches is not as significant as u_{15}, except for Oost et al. (2002), which corresponds to an underestimation of H_{m0} at the storm peak for about 0.5 m (Figure 1E). It should be noted that the underestimation of H_{m0} on the first day shown in Figure 1E is caused by the spinning up time of the modelling from the initial condition. One interesting phenomenon is that all the

simulations underestimate u_* before the storm peak and overestimate u_* after the storm peak. This phenomenon is also clearly seen in the time series of C_d.

Figure 1F shows C_d as a function of u_{10} at 12:00 28th Jan 2002 for all grid points over the whole simulation area. Black marks with error bars are from laboratory and field measurements from various places by different authors. Red and green curves are two C_d parameterization options in the SWAN model. Blue dots are calculated from different z_0 approaches from our experiments. In the non-coupled (COARE3.0) simulation, C_d is only a function of u_{10}, so the calculated C_d is distributed in a line with u_{10}. In the coupled simulation, C_d is not only a function of u_{10}, but also a function of H_{m0}, T_p, or L_p, so that the distribution of C_d with u_{10} is scattered. It should be noted that in the Taylor and Yelland (2001) approach, the calculated C_d can sometimes be too large, resulting in technical and numerical errors in the WRF simulation. Thus we need to set an upper and lower limit to according to Davis et al. (2008) to ensure numerical stationarity. It is shown that both the Taylor and Yelland (2001) and Oost (2002) approaches significantly overestimate C_d in comparison with measurements. Drennan et al. (2005)'s approach fits the measurements better but still tends to overestimate C_d. In Fan et al. (2012)'s approach, the wave dependence are so weak that the wind-wave coupling does not show any added values.

To summarize, these simple approaches for parameterizing z_0 with wind speed and a few wave parameters such as H_{m0}, T_p, and L_p, are not satisfactory. The approaches might be too simple to take into consideration some important elements such as the misalignment of wind and wave direction and the combination of wind wave and swells.

A dynamical coupling interface is therefore needed to take into account the complex sea state and account for the momentum conservation in the air-sea interface, which makes sure the momentum loss of the atmosphere equals to the momentum gained by the waves and currents.

Currently, one of the most widely used dynamical coupling approaches is from Janssen (1991, hereafter JANS). In JANS approach, z_0 (or wind stress) is calculated from the wind-input source function of SWAN, which makes sure that the momentum conserves at the air-sea interface. We applied JANS approach in the coupling system for storm simulations. Figure 1G shows the spatial distribution of u_{10}, H_{m0}, and u_* from the non-couple simulation and JANS coupled simulation during the storm 2004-09-20, at 01:00. JANS approach gives much larger u_* than COARE3.0, resulting in higher z_0, leading to that u_{10} is significantly reduced. There is also a significant phase shift of the wave field in the coupled result. Figure 1H shows C_d as a function of u_{10} from the non-coupled and JANS coupled simulation. It is clearly seen that JANS approach significantly overestimates C_d in comparison with measurements.

Through the overview of the currently existed wind-wave coupling approaches, we conclude that the adding value of roughness parameterization coupling approaches is very limited and may cause uncertainties to the whole system. Though the dynamical coupled approach of JANS, the surface stress estimation is so large that cannot be used in the coupling system without limiters. Thus it is necessary to develop our own coupling approach to fill the gaps. In the following section we explain the use of a wave boundary layer model in SWAN and how it improves the coupling system.

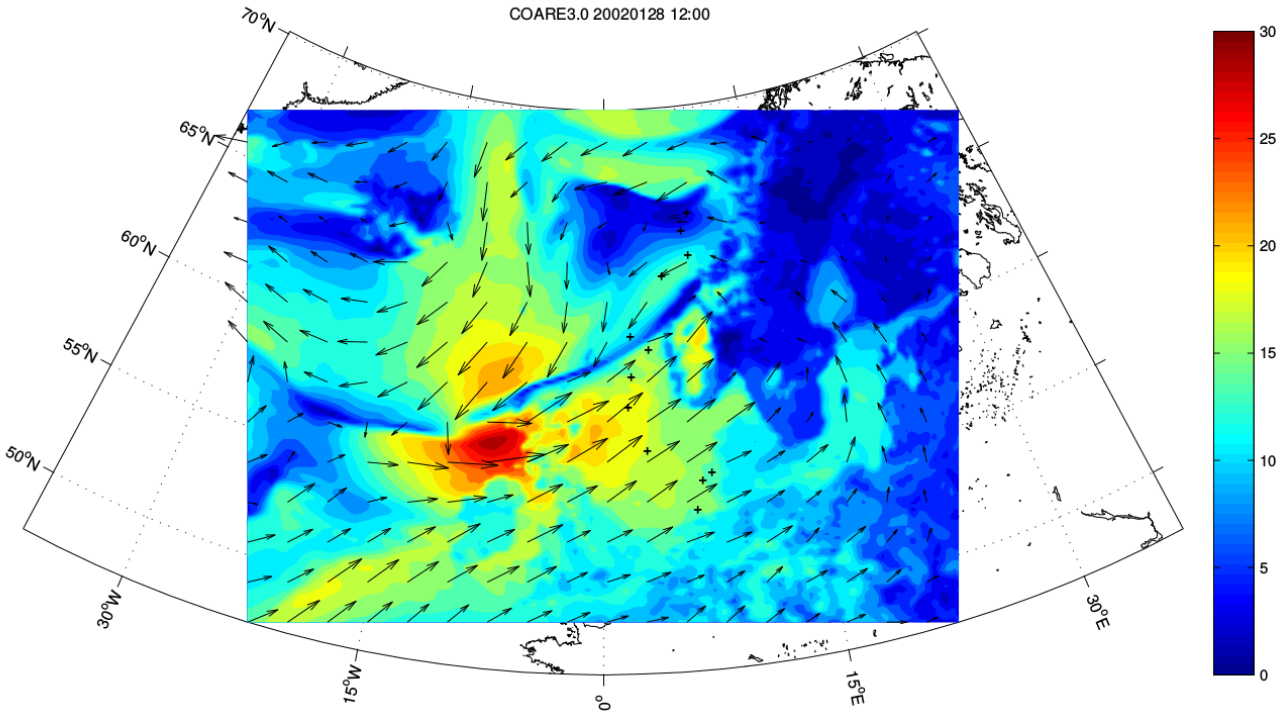

Figure 1A. Snapshot of u_{10} at 12:00 28th Jan 2002 from the non-coupled WRF simulation.

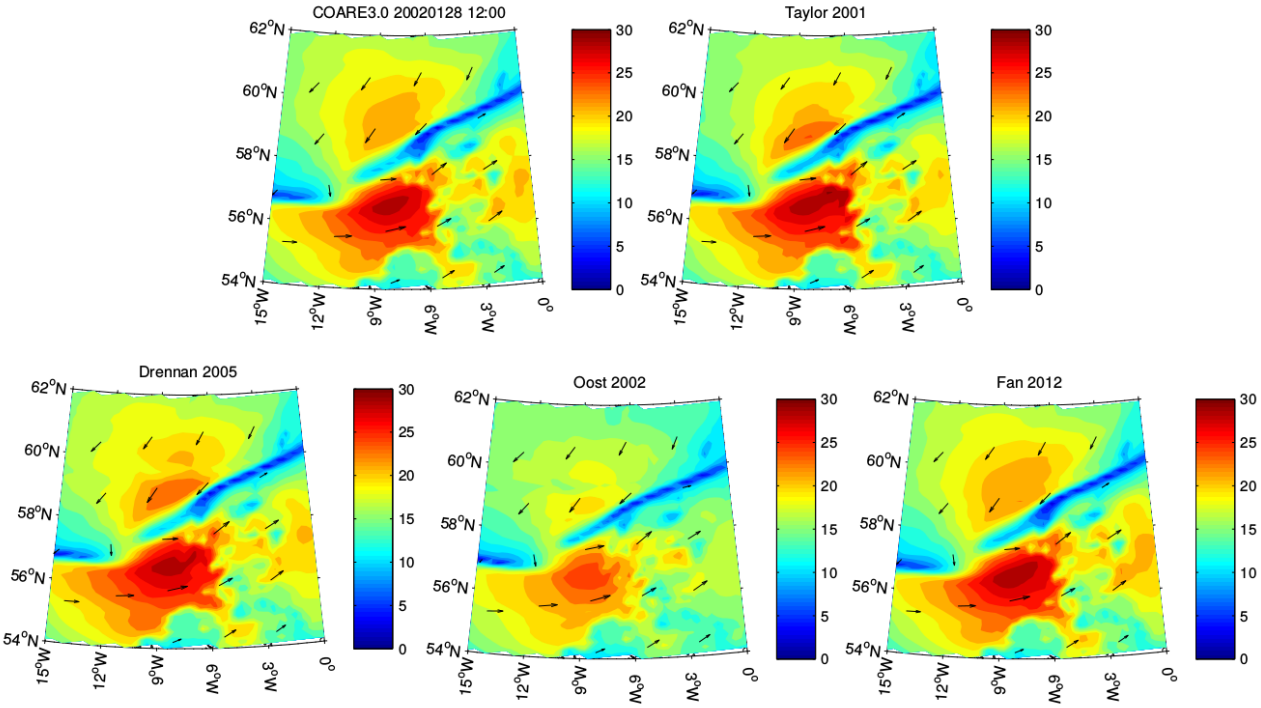

Figure 1B. Snapshot of u_{10} at the storm centre from different coupling approaches.

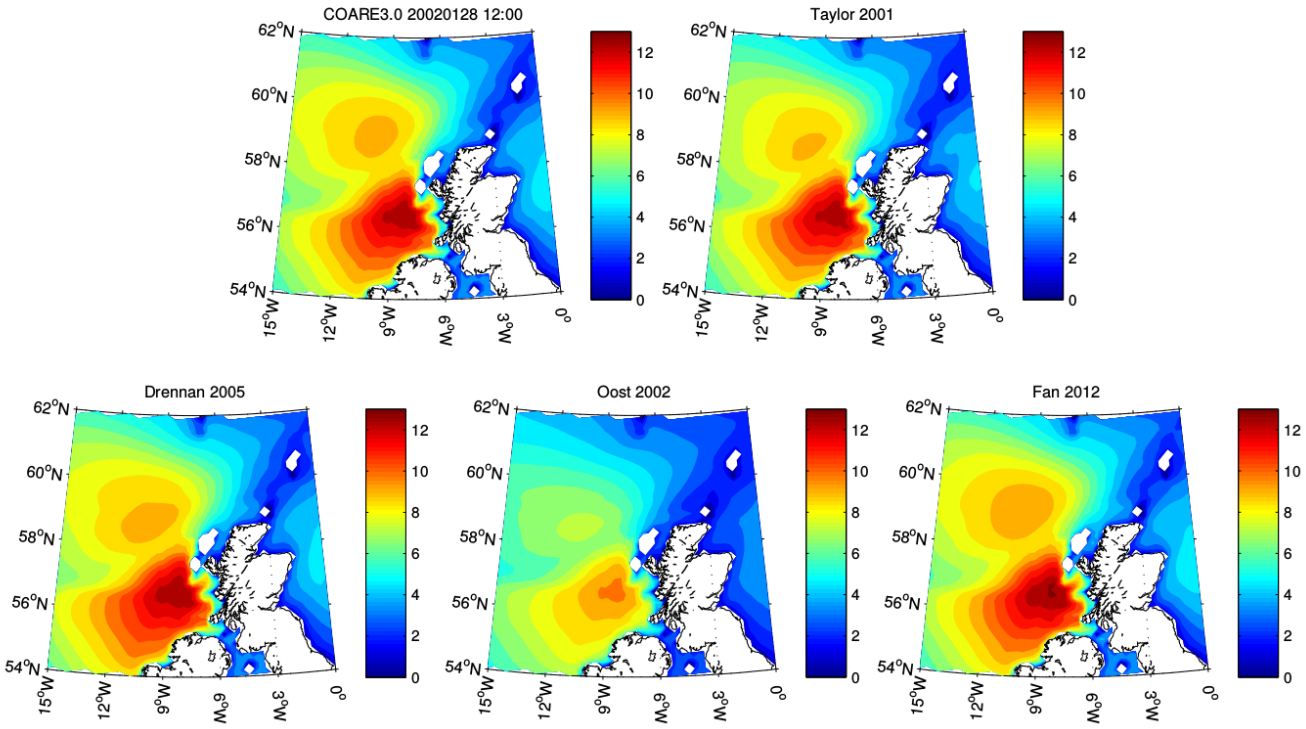

Figure 1C. Same as Figure 1B but shows H_{m0}

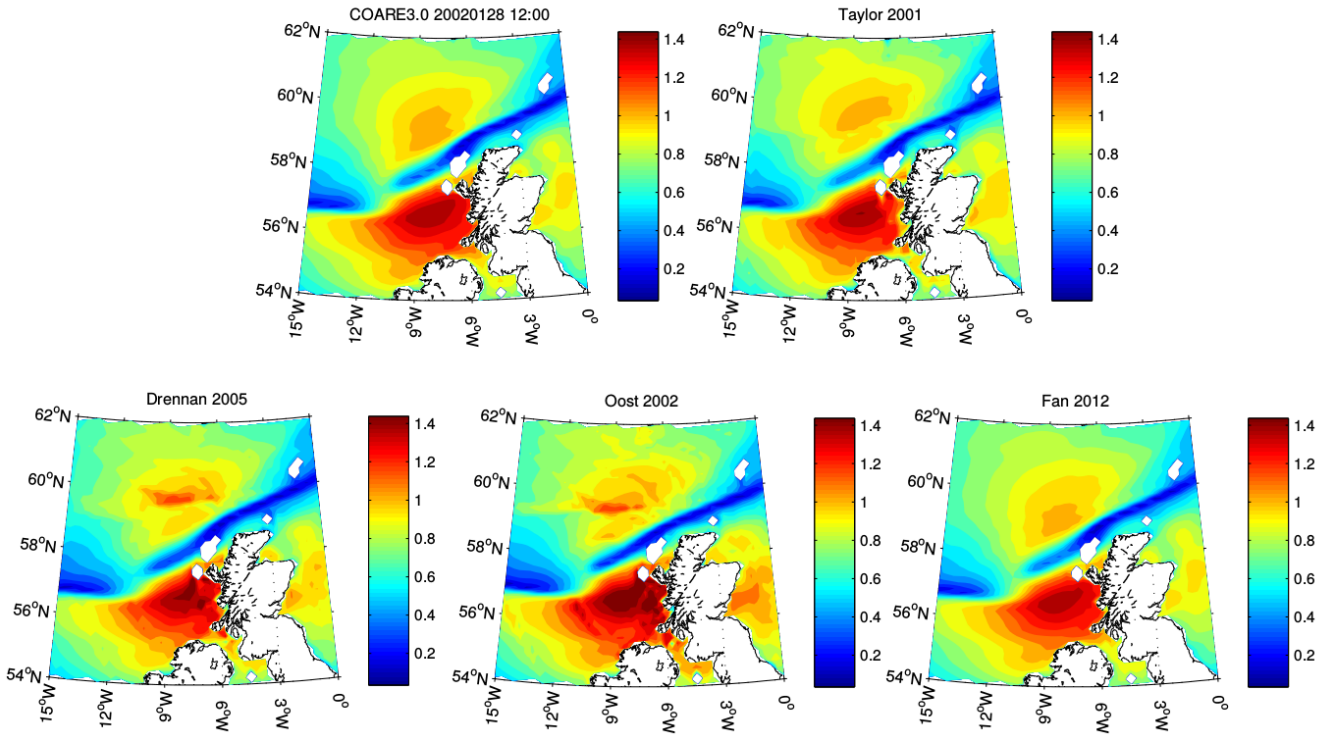

Figure 1D. Same as Figure 1B but shows u_*

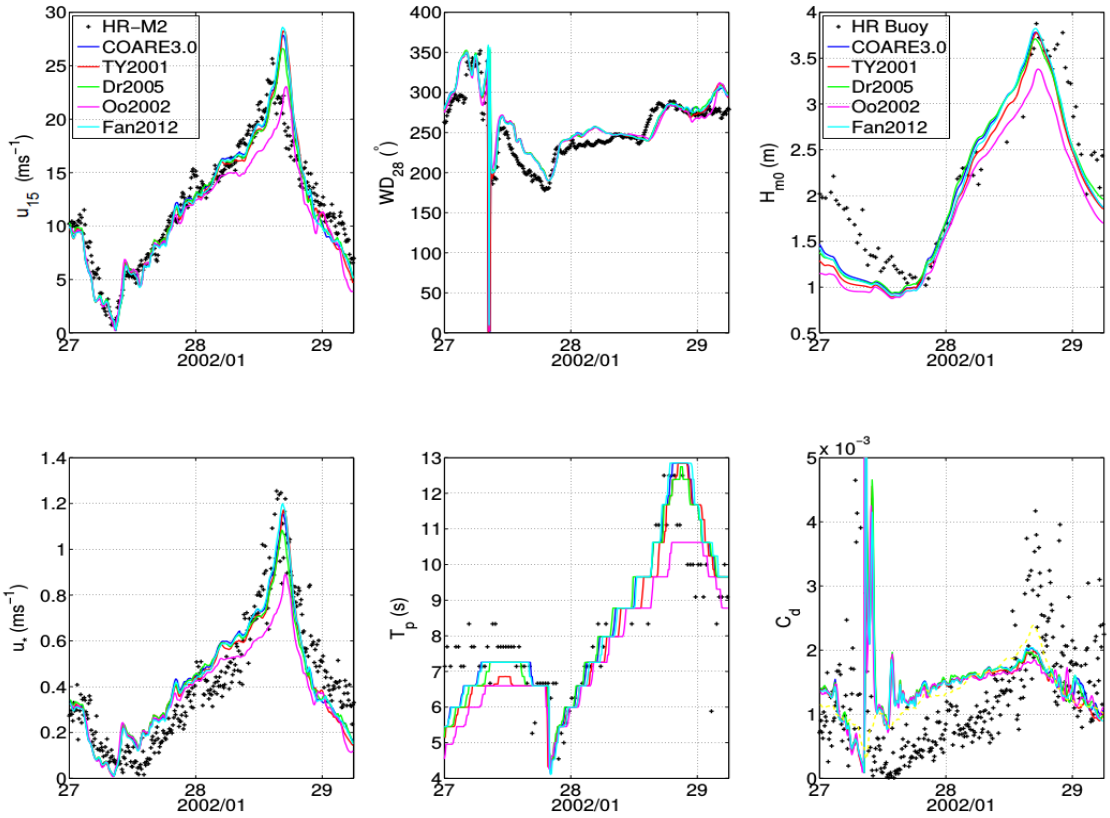

Figure 1E. Time series of wind, wave, and turbulence parameters at Horns Rev during storm Jan 2002

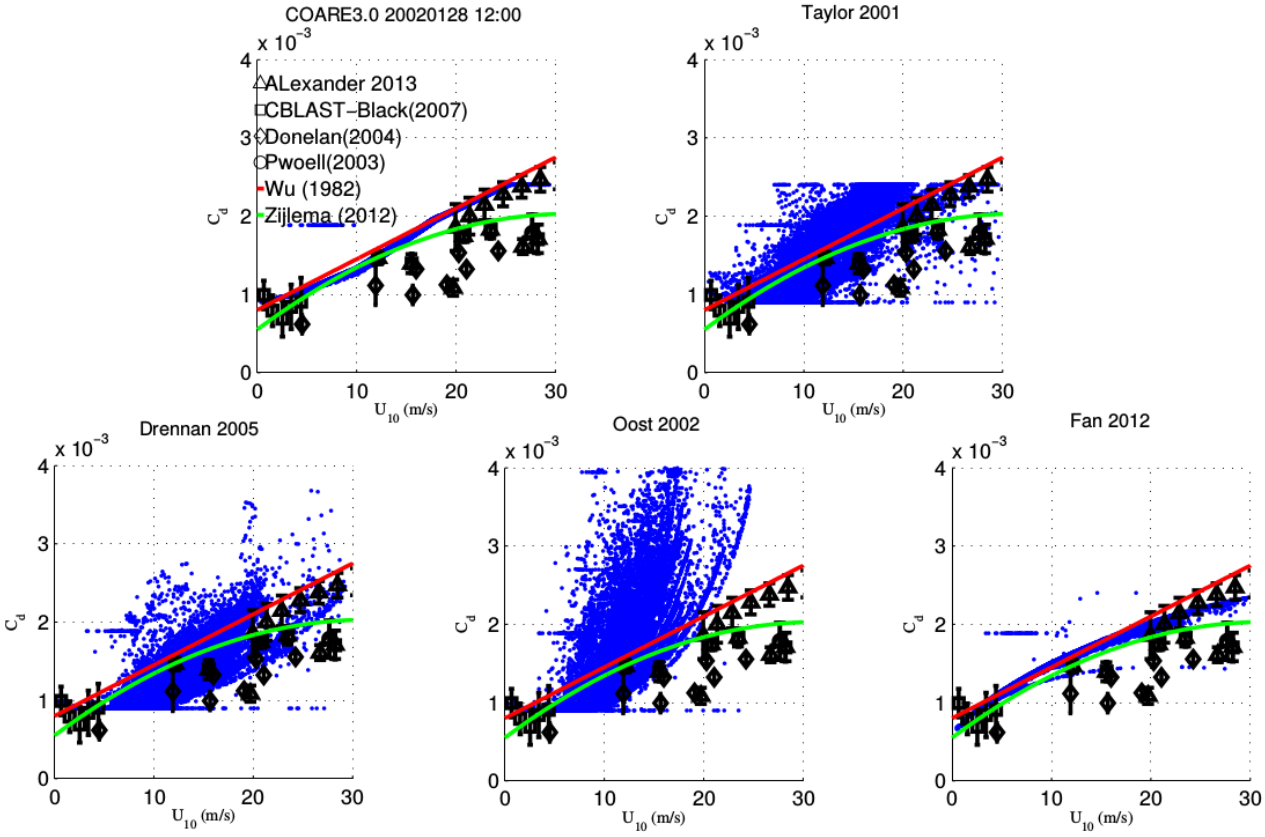

Figure 1F. C_d as a function of u_{10} calculated from different z_0 parameterization approaches.

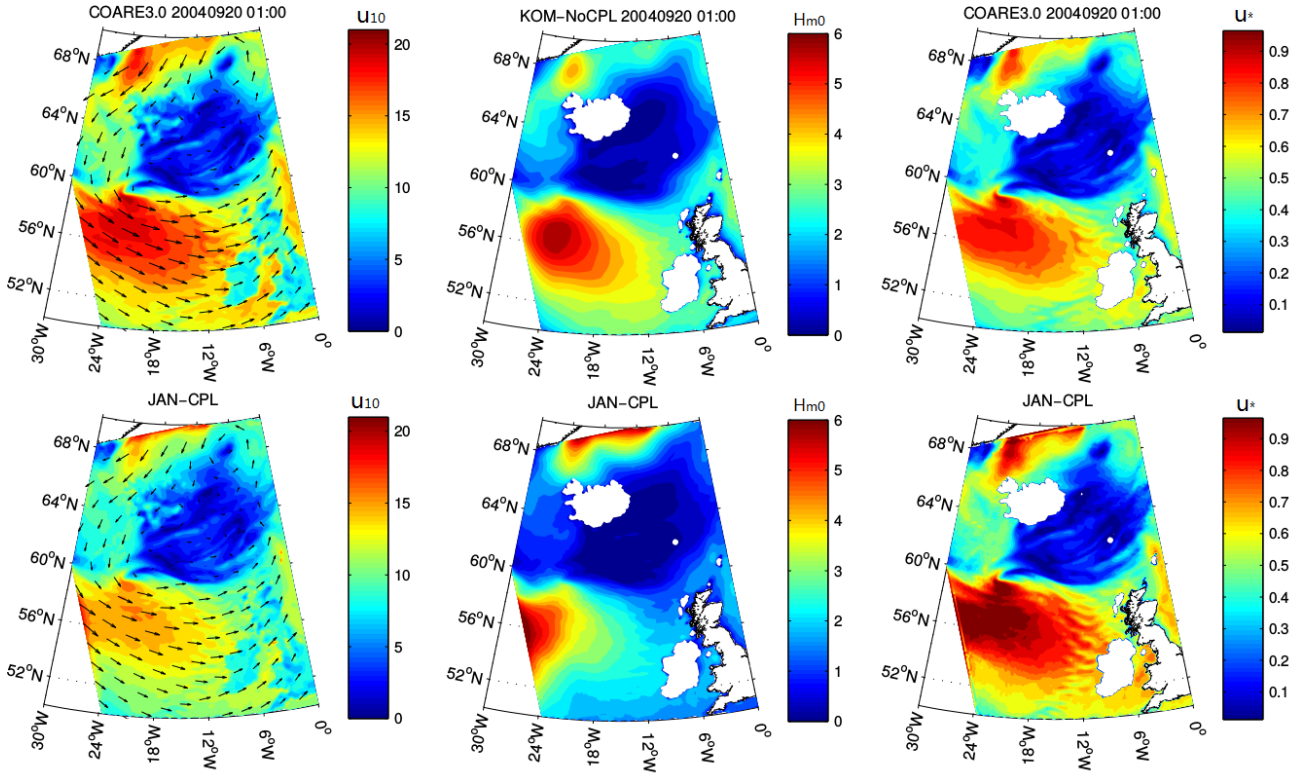

Figure 1G. Spatial distribution of u_{10}, H_{m0}, and u_* from the non-couple simulation and JANS coupled simulation

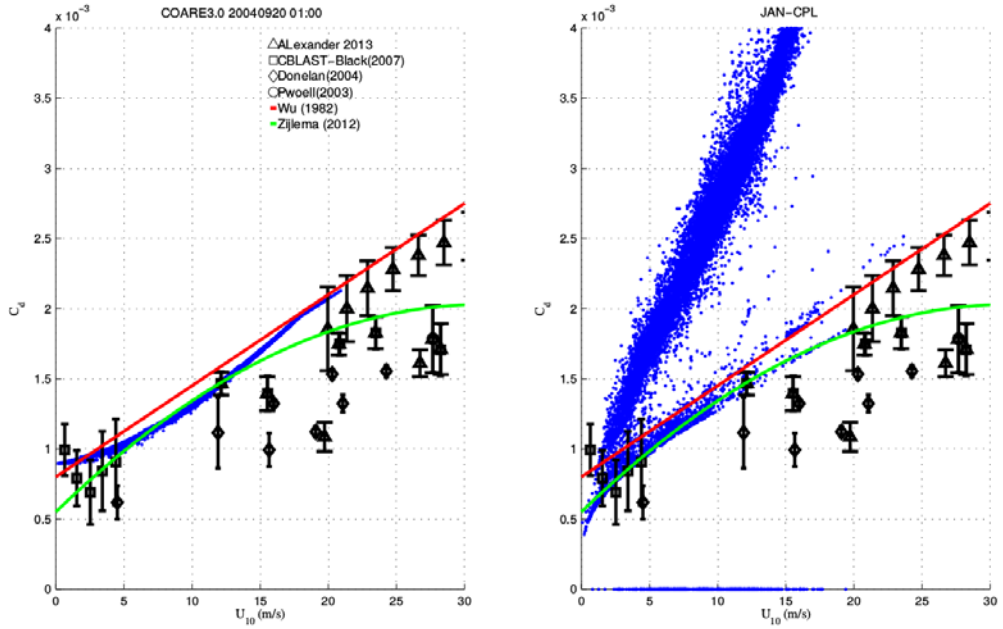

Figure 1H. C_d as a function of u_{10} calculated from the non-coupled (left, COARE3.0) and coupled (right, JANS) simulation.

2. Test of WBLM in idealized fetch-limited study

The Wave Boundary Layer Model (WBLM) as described in report D1.2, is implemented in the 3rd generation ocean wave model SWAN as a new wind-input source function. The WBLM explicitly

estimates the sea surface stress based on the momentum conservation within the air-sea interface, which ensures that the momentum loss from the atmosphere is consistent with the momentum gained by the waves. Meanwhile, the dissipation coefficient is modified to match the new wind-input source function. The following experiments and results have been written as a manuscript of a journal paper: The use of a wave boundary layer model in SWAN, submitted to the Journal of Geophysical Research – Oceans (Du et al. 2016). Here, we briefly overview the main results and conclusions.

The WBLM is first tested in the wave model in the idealized fetch-limited wave evolution study. The general idea of such experiments is to simulate the deep water wave evolution along the fetch under constant offshore wind condition. The simulated significant wave height (H_{m0}) and peak wave frequency (f_p) are evaluated by field measurements according to Kahma and Calkoen (1992, hereafter KC92) and Young (1999, hereafter Y99). The wave spectrum, and 10 meter drag coefficient is also evaluated according to Donelan (1985) and Soloviev (2014), respectively.

The one-dimensional SWAN model is used for the fetch-limited study. The spatial distribution (Δx) is set as follows. For fetch between 0 and 20 km, Δx = 100 m; between 20 km and 100 km, Δx = 400 m; between 100 km and 300 km, Δx = 1 km; between 300 km and 1000 km, Δx = 4 km; between 1000 km and 3000 km, Δx = 10 km. The frequency dimension of the wave spectrum ranges from 0.01 Hz to 10.5 Hz with geometric progression, f(n+1) / f(n) = 1.1. Wind speed at 10m ranges from 5m/s to 60m/s are tested. Four different pairs of wind-input and dissipation source function are tested, including KOM (Kommen, 1984), JANS (Janssen, 1991), WES (var der Westhuysen, 2007), and WBLM. The first three (KOM, JANS, and WES) approaches are originally embedded in SWAN while WBLM is the new one implemented here.

Figure 2A shows H_{m0} as a function of fetch in kilometre. The reference growth curves of KC92 and Y99 are presented in black solid and dashed lines, respectively. Results of KOM, JANS, and WES are presented in blue, red, and orange lines, respectively. Results of WBLM are presented in green lines. It is quite clear that WBLM closely follow the reference growth curves in all fetches and wind speeds, while the three original approaches in SWAN cannot always reproduce the reference growth curves under different fetch and wind speed conditions. Similar conclusions also found in the f_p curves as shown in Figure 1B. WBLM outperforms KOM, JANS, and WES in the idealized fetch-limited studies, both for H_{m0} and f_p with KC92 and Y99 as references.

Figure 2C shows the one dimensional wave spectrum calculated from SWAN in short (5 km) and long (5 km) fetches with 10 m/s wind. The black solid lines are calculated from Donelan et al. (1985) with f_p estimated from KC92. The blue, red, and orange marks are calculated from the three original approaches in SWAN. The green circles are calculated from WBLM. It is clear that WBLM reproduces Donelan et al. (1985) wave spectrum and maintains an f^{-4} high frequency tail.

Figure 2D presents the drag coefficient as a function of wind speed. In the two panels, the black marks with error bars are from field measurements compiled by Soloviev et al. (2014). The blues lines with squares are calculated from Zijlema (2012) which is used by KOM and WES. The orange dashed lines represent the COARE 3.0 algorithm which is used by WRF MYNN surface layer scheme. The red lines with marks in the left panel (panel a) are calculated from JANS. The bars indicate the upper and lower bounds of C_d during the simulation. The green lines with marks in the right panel (panel b) are calculated from WBLM with the same plot configuration as JANS. Roughly speaking, COARE 3.0 algorithm follows the upper bound of the measured data for wind speed less than 30 m/s and extends linearly to higher wind speeds; Zijlema (2012) follows the trend of the measured data but cannot explain the variance of C_d at each wind speed; JANS explains the variance of C_d at each wind speed by accounting the wind-wave interaction, but obviously it overestimates C_d significantly. The WBLM not only follows the trend of the measured data for wind speed less than 40m/s but also covers a certain range of its variance. For wind speed greater than 40m/s, C_d from WBLM does not drop with u_{10} as the

measurement does. We attributed this to different processes such as sea spray (e.g. Chen and Yu, 2016), which needs further investigations.

Based on the above results, we conclude that the new WBLM wind-input and dissipation source functions can be used in the 3rd generation ocean wave model for idealized fetch-limited wind wave simulations. It not only improves the wave simulation but also have the potential of improving wind-wave coupling systems by providing reliable wind stress estimation at the air-sea interface.

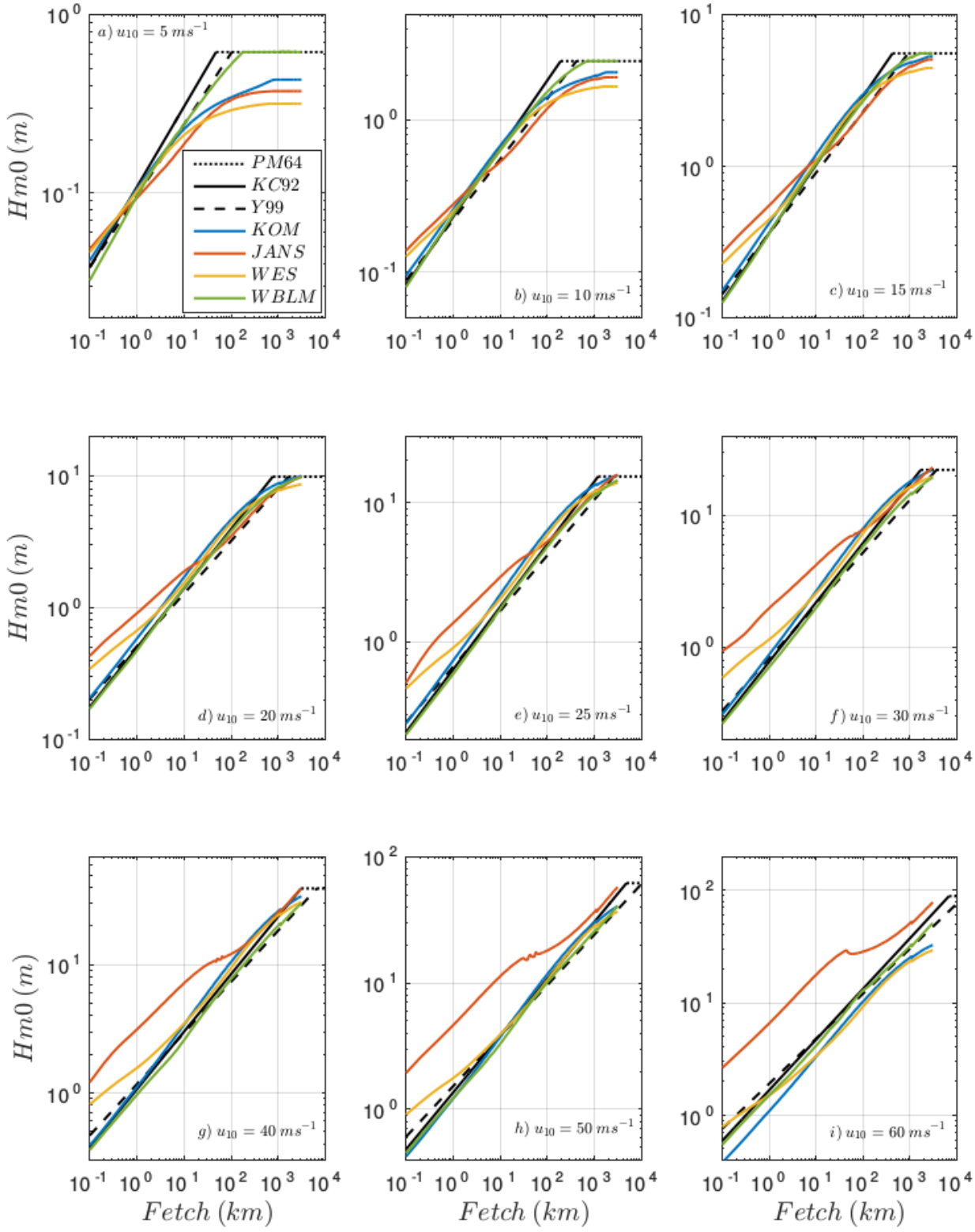

Figure 2A. Significant wave height (H_{m0}) as a function of fetch in kilometre.

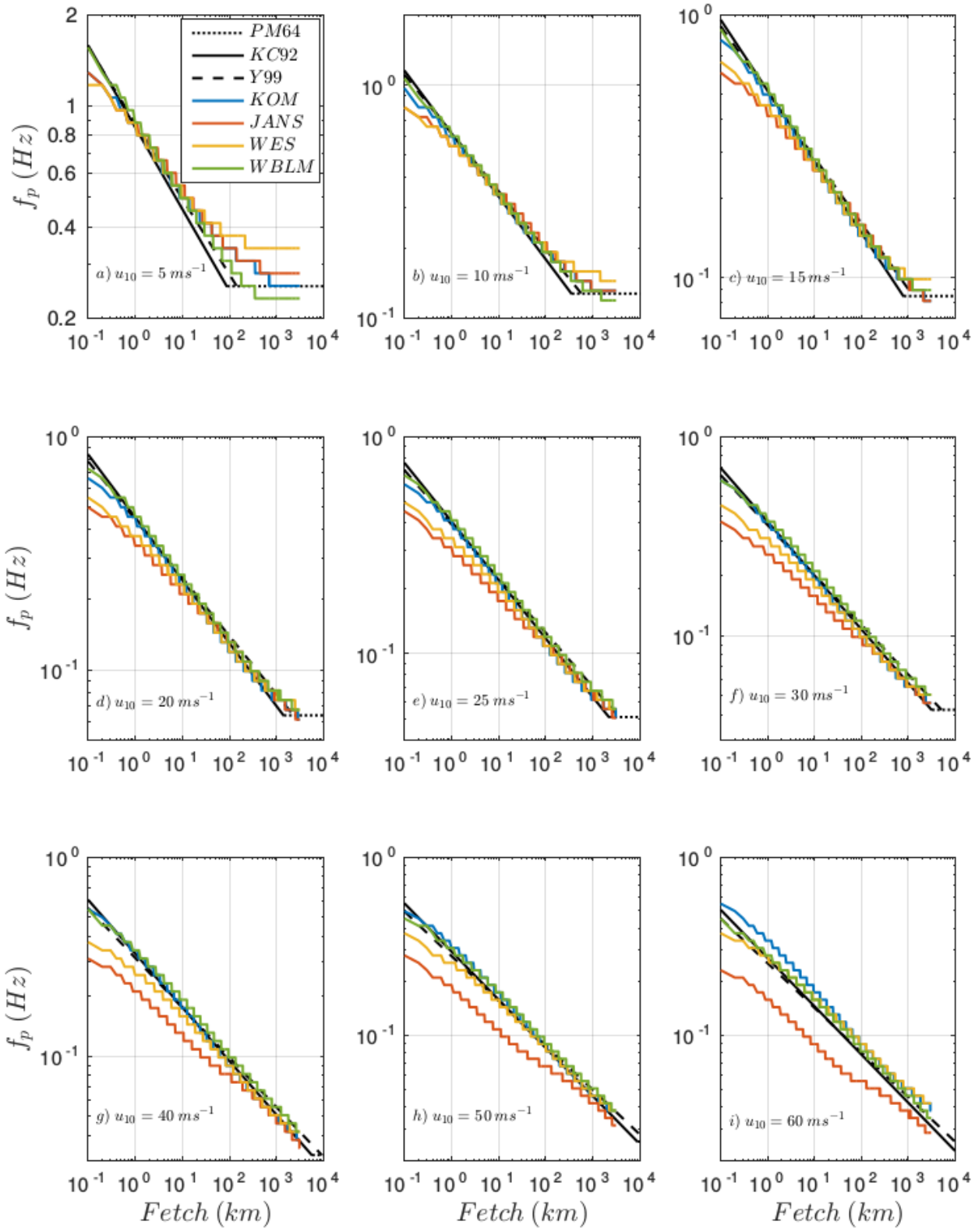

Figure 2B. Peak wave frequency (f_p) as a function of fetch in kilometre.

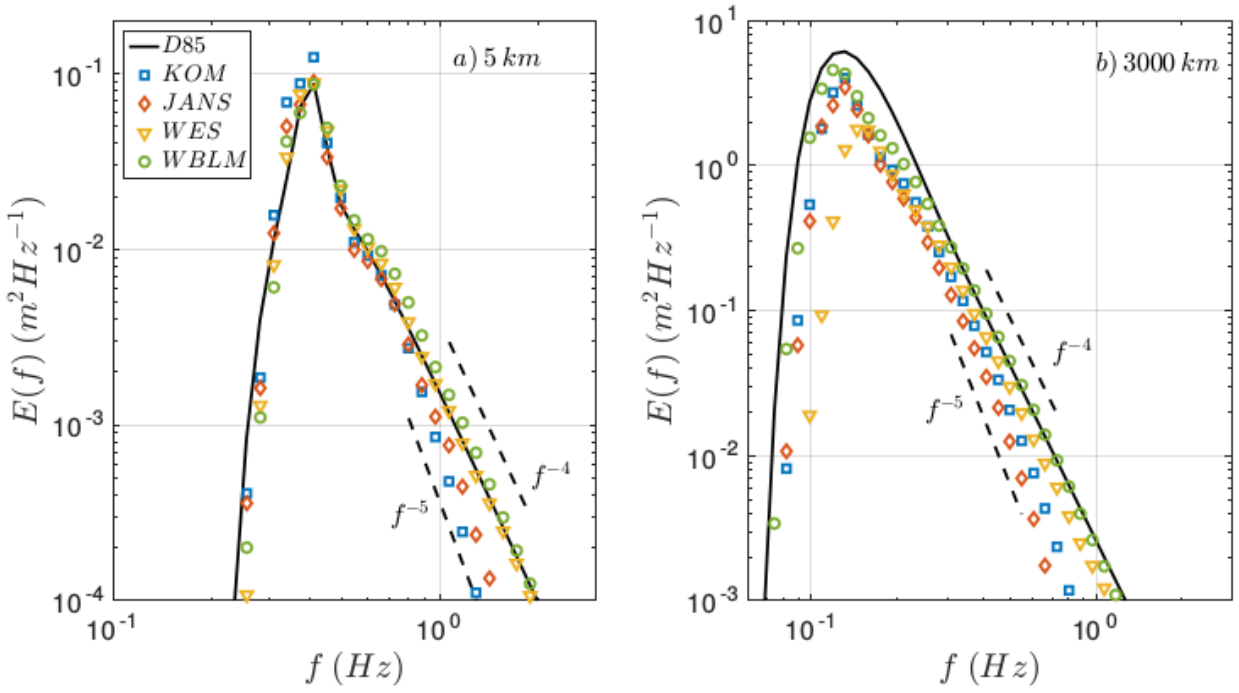

Figure 2C. One-dimensional wave spectrum at short fetch (5 km) and long fetch (3000 km). Both with wind speed of 10 m/s after 72 hours simulation.

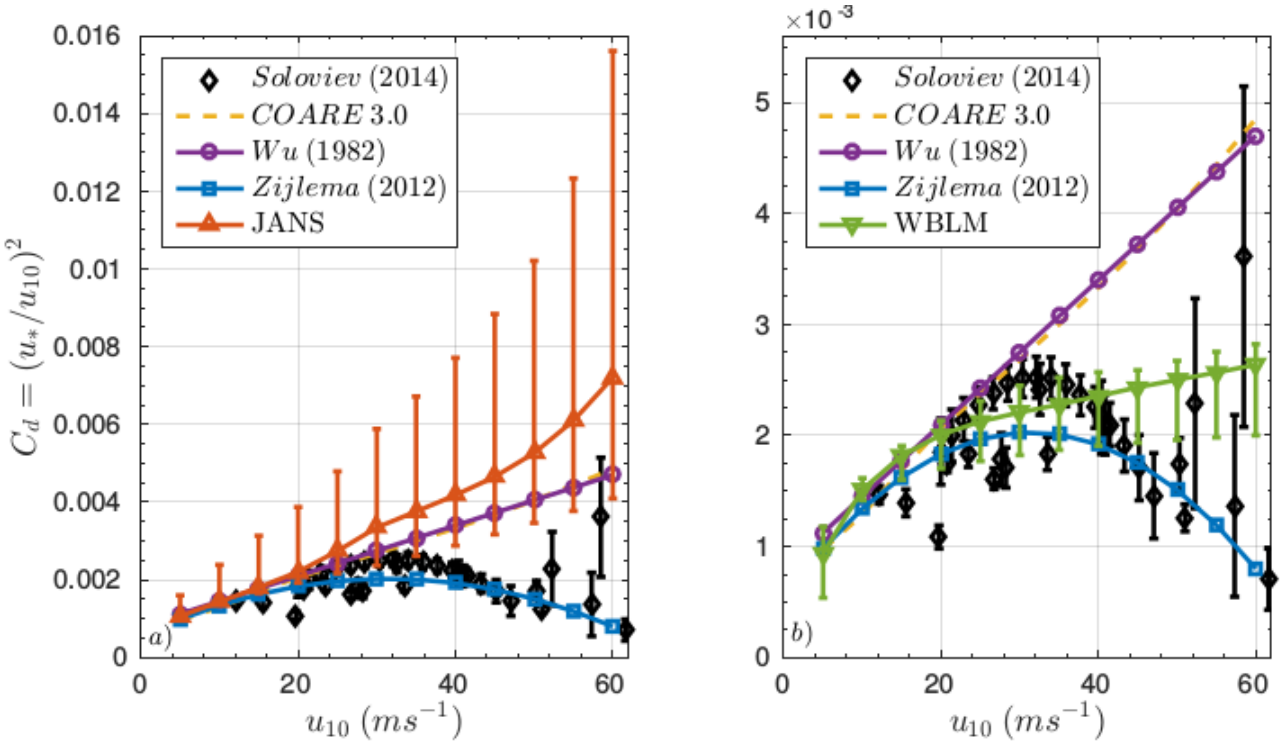

Figure 2D. Drag coefficient (C_d) as a function of wind speed.

3. Test of WBLM in fetch-limited condition using measured wind

The WBLM introduced in section 2 is further tested in a simple, fetch-limited wave simulations of real conditions. The objective of this experiment is to test the numerical stability of WBLM, and to investigate its behaviors in the real storm simulations.

The experiments are designed as follows. A small model domain around Horns Rev as shown in Figure 3A is set up. The reason that we focus on Horns Rev is that we have combined wind, wave, and especially turbulent measurements for several years. Horns Rev is located to west coast of Denmark, so that if the wind blows from the east, the impact of open boundaries in the wave modelling in the north, west, and south to the waves at Horns Rev can be neglected. Since the area is relatively small (about 10 km × 10 km around Horns Rev), the spatial variation of 10 m wind is ignored. Thus the wave model can be forced by the wind speed measured at Horns Rev M2 extending to the whole model domain. It should be noted that there are still some uncertainties in this experiment design. First, Horns Rev is a shallow water site (about 10 m deep). The wave dissipation due to bottom friction cannot be neglected. Here we choose the widely used JONSWAP (Hasselmann et al. 1973) bottom friction dissipation source function for all the experiments. Second, although the effective area is relatively small, the spatial variation of wind speed cannot be completely neglected. The wind speed gradient caused by the sheltering of the coast line may still cause some uncertainties.

Four storm events with winds at M2 from the east are selected based on the following four conditions:

a. The east wind (direction between 80 and 150 deg.) lasts for at least 2 days.

b. Measurements of wind, wave, and turbulent measurements are all available at Horns Rev M2.

c. Neutral condition.

d. The 10 m wind speed at Horns Rev during the storm peak is larger than 10 m/s.

In SWAN ,we use a spatial resolution of 600 m, 1 min time step, 36 directions, and frequency ranges from 0.03 to 10 Hz. For each storm, KOM, JANS, and WBLM source terms are tested.

Figure 3B to 3E show the time series of wind speed, wind direction, significant wave height (H_{m0}) and friction velocity (u_*) at Horns Rev M2, measured and modelled during four storms, see the *x*-axes for the time of the storms. In each of the four figures, the top two panels show the wind speed and direction measured at Horns Rev wind mast 2. Wind speed is measured at 15 m above the water level. It is converted into 10 m wind speed using a logarithm law and interpolated to every 10 min per record in order to be used by SWAN. Wind direction is measured at 28 m height. As we can see, during those storms, the wind direction changes slowly between 80 and 150 degree, which means that the winds are almost always from the east.

In the bottom two panels, the black dots show the significant wave height measured by the buoy located in the south of Horns Rev 1 wind farm and the friction velocity measured by sonic anemometer at 50 m of Horns Rev wind mast 2, respectively. Accordingly, modelled H_{m0} and u_* using KOM, JANS, and WBLM approaches are plotted on top of the measurement data, and presented with blue, red, and green lines, respectively.

Over all, it is clearly seen that JANS tends to overestimate H_{m0} and u_*, especially during the storm peak, which is consistent with the conclusion of idealized fetch-limited study in section 2.

The use of the KOM approach gives rather reasonable u_* which is also consistent with the idealized fetch-limited study. C_d calculated from Zijlema (2012) follows the trend of the measurement data (Figure 2D). Although the Zijlema (2012) relation of C_d and wind speed does not contain a wave dependence, considering that the wind speed during the four storms are less than 20 m/s, the variation of C_d at each wind speed are relatively small, so the wave impact to the value of u_* at one single point is not significant. The KOM approach also gives rather good estimation of H_{m0} when the wind speed is lower than 12 m/s. However, at the storm peak, when the wind speed is higher than 12 m/s, KOM approach overestimates H_{m0}, even though u_* is consistent with the measurements. The phenomenon that KOM approach overestimates H_{m0} using a reasonable u_* is because it does not take account of the momentum conservation. If the momentum conserves, an overestimation of the wave growth should be result in an overestimation of the u_*.

The green lines show the H_{m0} and u_* calculated with WBLM approach. Generally, the simulated H_{m0} and u_* follow the measurements quite well during the four storms, which indicate that the WBLM can improve both the wave simulation and stress estimation at the same time. However, it is also seen that the time series of H_{m0} are too smooth that it misses the small variations on the time scale of several hours. This is attributed to the method that we used in determining the dissipation coefficient. The dissipation coefficient is currently proportional to the wind-input source function. It shows excellent fetch-limited growth curves in the idealized study with constant wind speed. However, when the wind speed varies with time, the wave growth/decay rate will be reduced because higher wind-input results in higher dissipation, lower wind-input results in lower dissipation. Thus, the dissipation coefficient still needs further investigation.

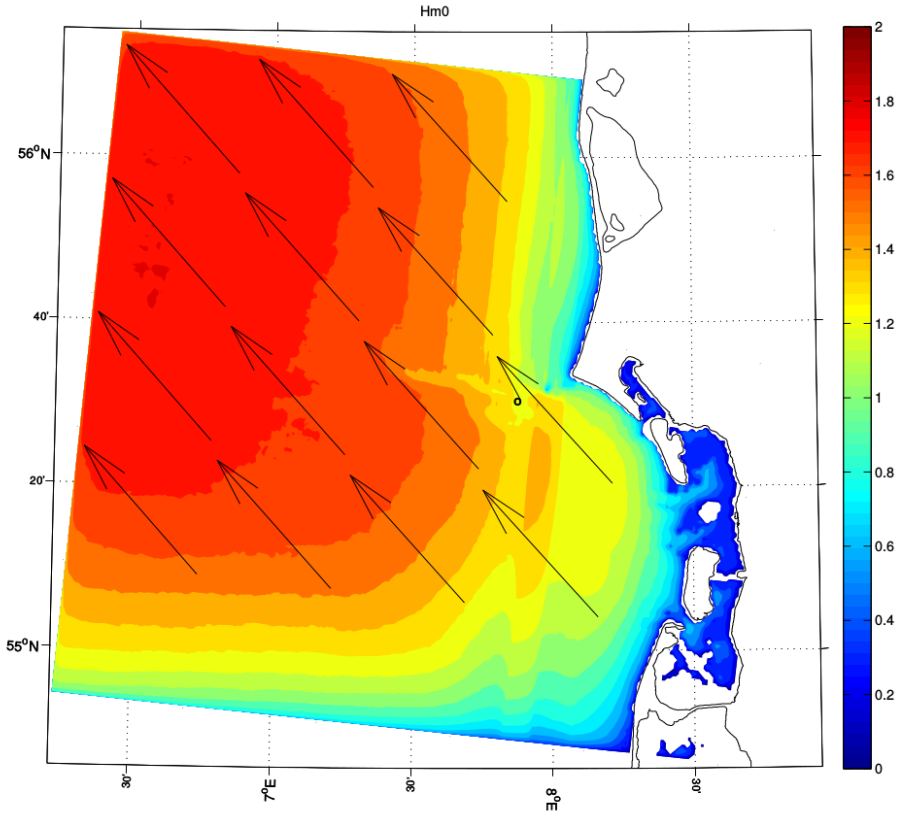

Figure 3A. Example of wind (arrows) and wave field (colours) around Horns Rev. The black circle indicates the location of Horns Rev wind mast 2.

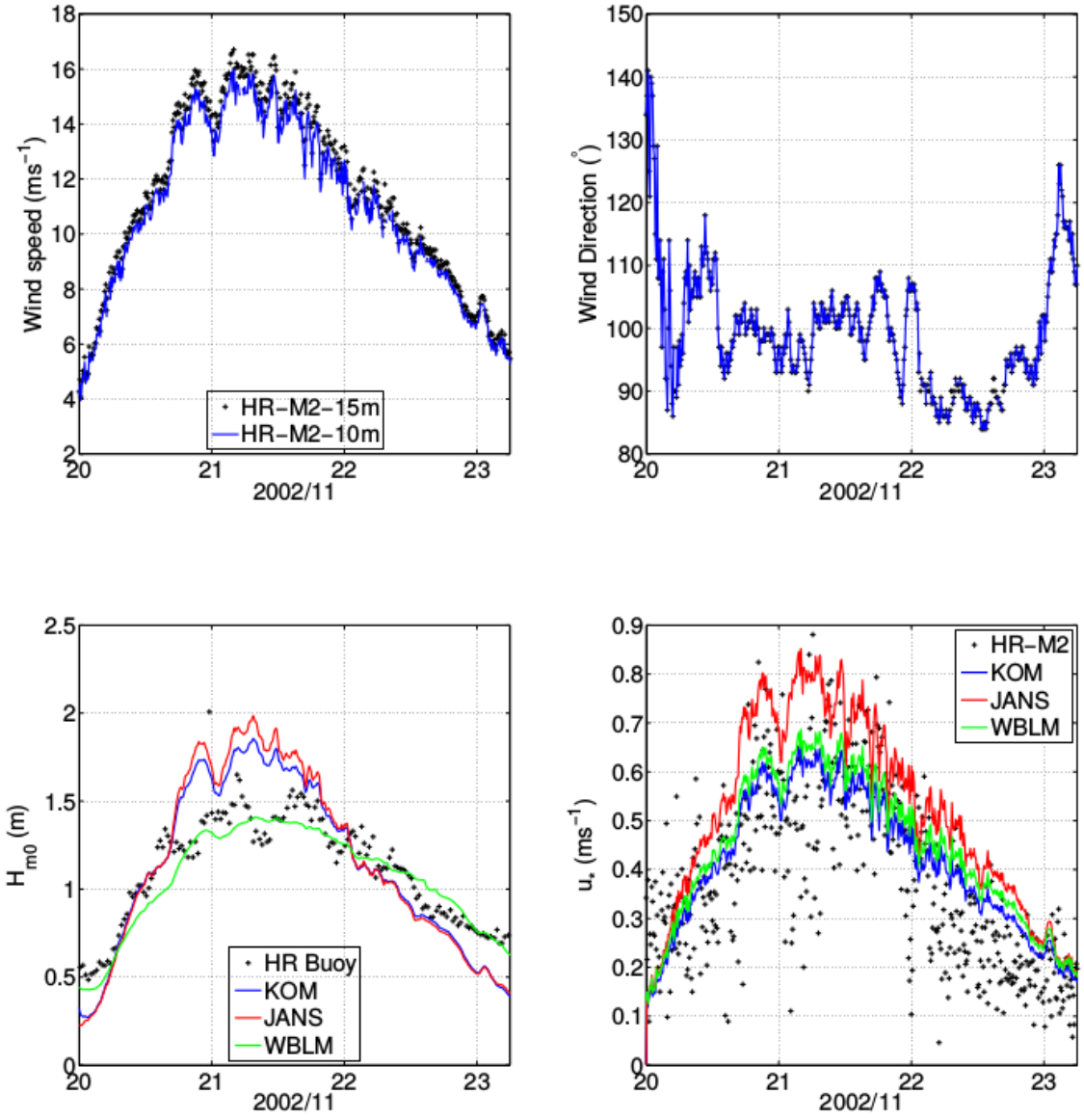

Figure 3B. Time series of wind speed, wind direction, significant wave height, and friction velocity during 2002/11/20 – 2002/11/23.

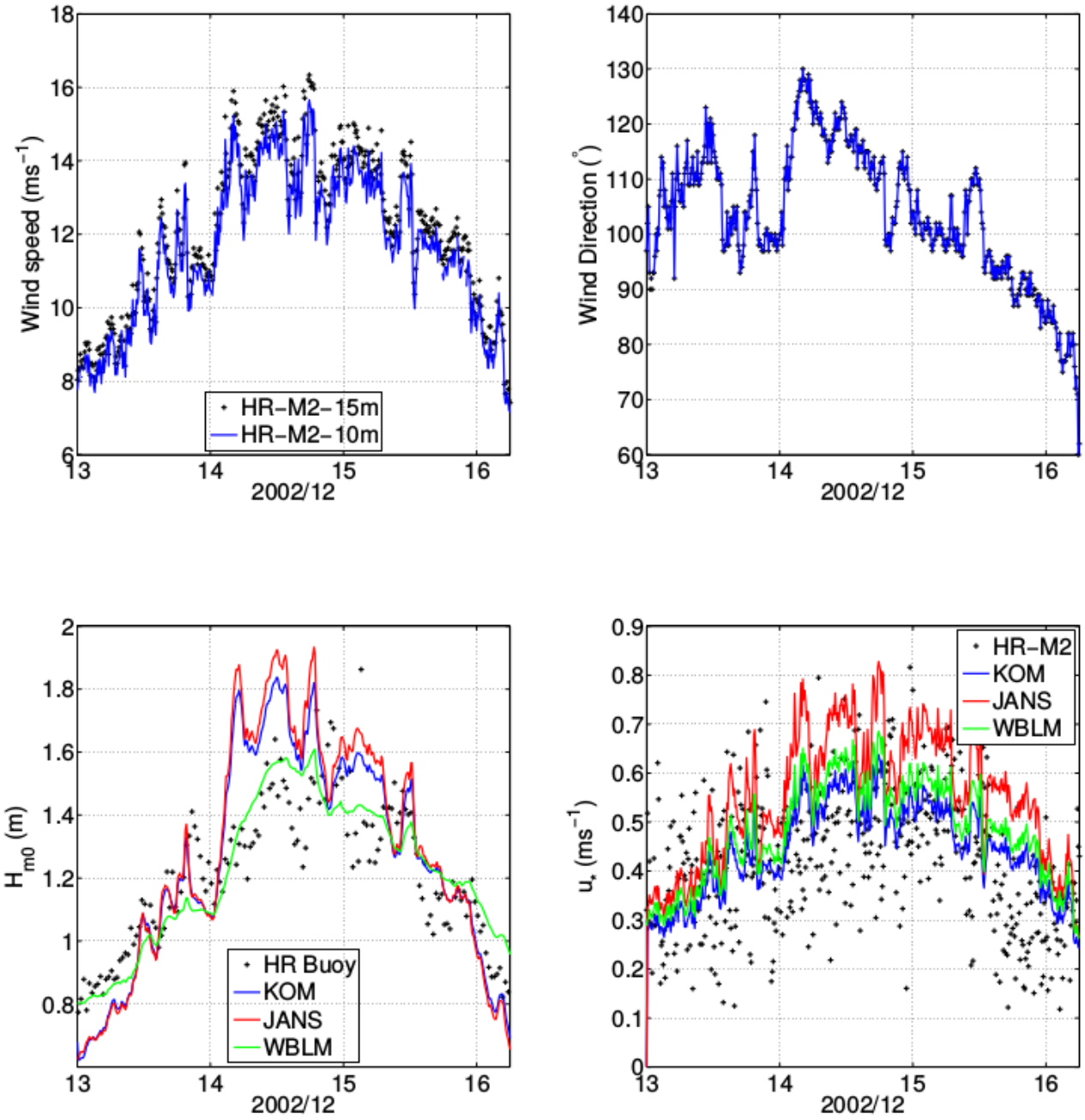

Figure 3C. Time series of wind speed, wind direction, significant wave height, and friction velocity during 2002/12/13 – 2002/12/15.

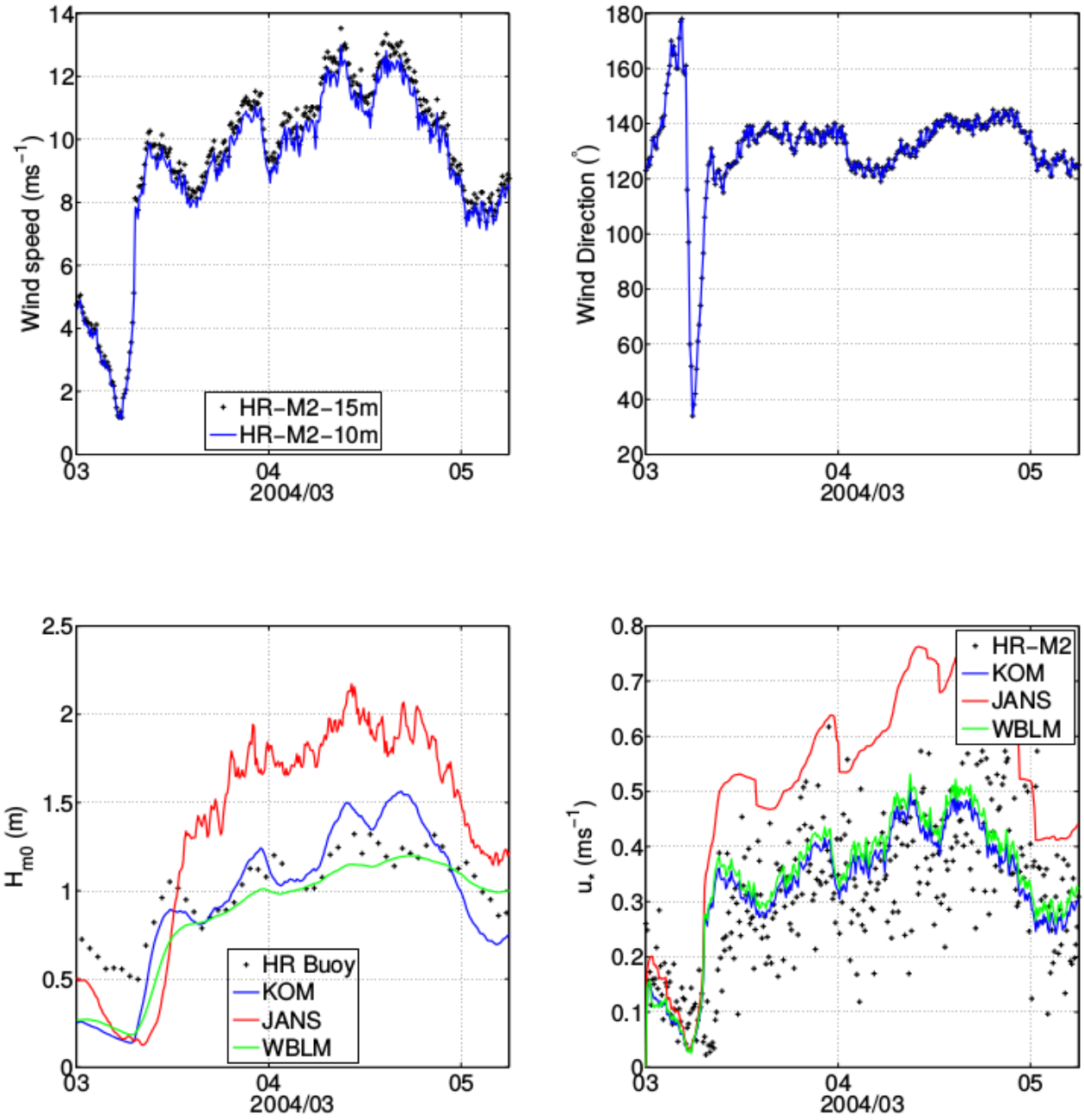

Figure 3D. Time series of wind speed, wind direction, significant wave height, and friction velocity during 2004/03/03 – 2004/03/06.

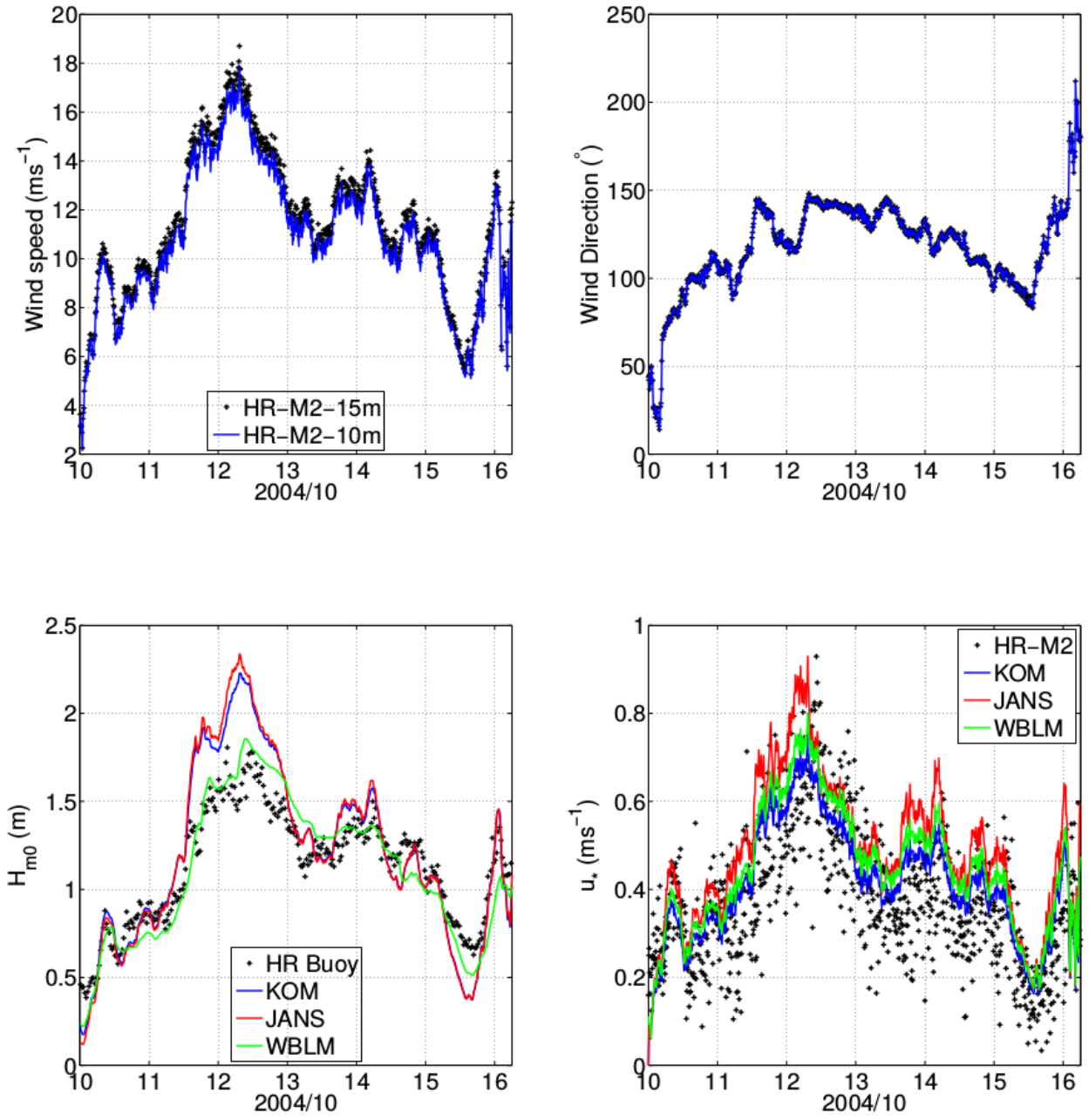

Figure 3E. Time series of wind speed, wind direction, significant wave height, and friction velocity during 2004/10/10 – 2004/10/16.

4. Sensitivity test of stress-coupling approach during storms

The WBLM is implemented in the online coupling system. Considering the conditions of wind direction, atmospheric stability, and measurements availability, 9 North Sea storms were chosen for the sensitivity test for the new stress-coupling approach. These storms are listed in Table 4A. The model domains are shown in Figure 4A and the model setups for WRF and SWAN are listed in Table 4B.

Figure 4B shows a snapshot of u_{10} during an offshore storm non-coupled simulation at 06:00 12nd Oct. 2004. The interested areas are the storm centre, which is located southwest of iceland and the Danish coastal zones. Figure 4C and Figure 4D show a snapshot of u_{10} and u_* around the storm centre, respectively. It is clearly seen that the u_{10} difference caused by stress-coupling is quite significant. With

maximum u_{10} of 22 m/s, the coupling brings about ±3 m/s u_{10} difference. The maximum difference is found in both highest and lowest wind speed areas. It should be noted that the high wind speed area over Island shows no difference between coupled and non-coupled simulations. This indicates that the difference of u_{10} in the ocean surface is caused directly by the air-sea interaction instead of phase shift. Figure 4F and Figure 4G show a snapshot of u_{10} and u_* at the west coast of Denmark, respectively. Even though the wind speed in the Danish west coastal zones is relatively low, the coupling still causes a maximum 10% difference. From the spatial distribution of u_*, it is also seen that in the nearshore zones, the coupled simulation has higher u_* than the not coupled simulation, which is consistent with the concept that young waves are rougher than old waves. Figure 4I shows C_d as a function of u_{10} at 06:00 12nd Oct. 2004. It is clear that C_d estimated from WBLM in the coupling experiments better overlap with the measurements, compared with KOM and JANS. Compared with Figure 2D in section 2, we can see that in real cases, as the wind and wave field becomes more complex, C_d estimated from WBLM explains better the wider distribution of the measurement data.

Figure 4J to Figure 4Q show a snapshot at 18:00 20th Sep. 2004 during an onshore storm. In the storm centre, the wind-wave coupling shows similar sensitivity test results as for the offshore storm. However, in the Danish west coastal zones, the coupling causes more changes for the onshore storm than for the offshore storm. The maximum difference in u_{10} reaches about 30% of the maximum wind speed. The largest difference is found in the cellular structure areas. The coupling impact on u_{10} also propagates to the land surface. Different from the offshore case, there is no significant increase of u_* in the nearshore zones in the coupling experiment, because the waves propagate from the west and they are not young waves. From Figure 4Q, it is also seen that C_d is very well predicted by WBLM.

In this section, H_{m0} is not presented. The reason is that the dissipation coefficient is still under calibration for real storm simulation so that the waves tend to be underestimated by the WBLM. Despite that, it is found that the stress-coupling method can improve the wind field significantly by providing reliable wind stress.

Table 4A. Selected North Sea storms for the sensitivity test of stress-coupling

Storm	**WD at H.R.**	**Stability**	**Measurements**
From 2002/01/27 To 2002/01/30	West	Unstable	WS, WD, U*, Hm0, Tp
From 2002/11/20 To 2002/11/23	East	Neutral	WS, WD, U*, Hm0, Tp
From 2002/12/13 To 2002/12/16	East	Neutral	WS, WD, U*, Hm0, Tp
From 2002/03/03 To 2002/03/06	East	Neutral	WS, WD, U*, Hm0, Tp
From 2004/10/10 To 2004/10/16	East	Neutral	WS, WD, U*, Hm0, Tp
From 2004/02/22 To 2004/02/24	North West	Neutral	WS, WD, U*, Hm0, Tp
From 2004/09/19 To 2004/09/25	North West	Neutral	WS, WD, U*, Hm0, Tp
From 2015/11/28 To 2015/12/02	West		Wave spectrum RUNE
From 2015/12/03 To 2015/12/08	South West		Wave spectrum RUNE

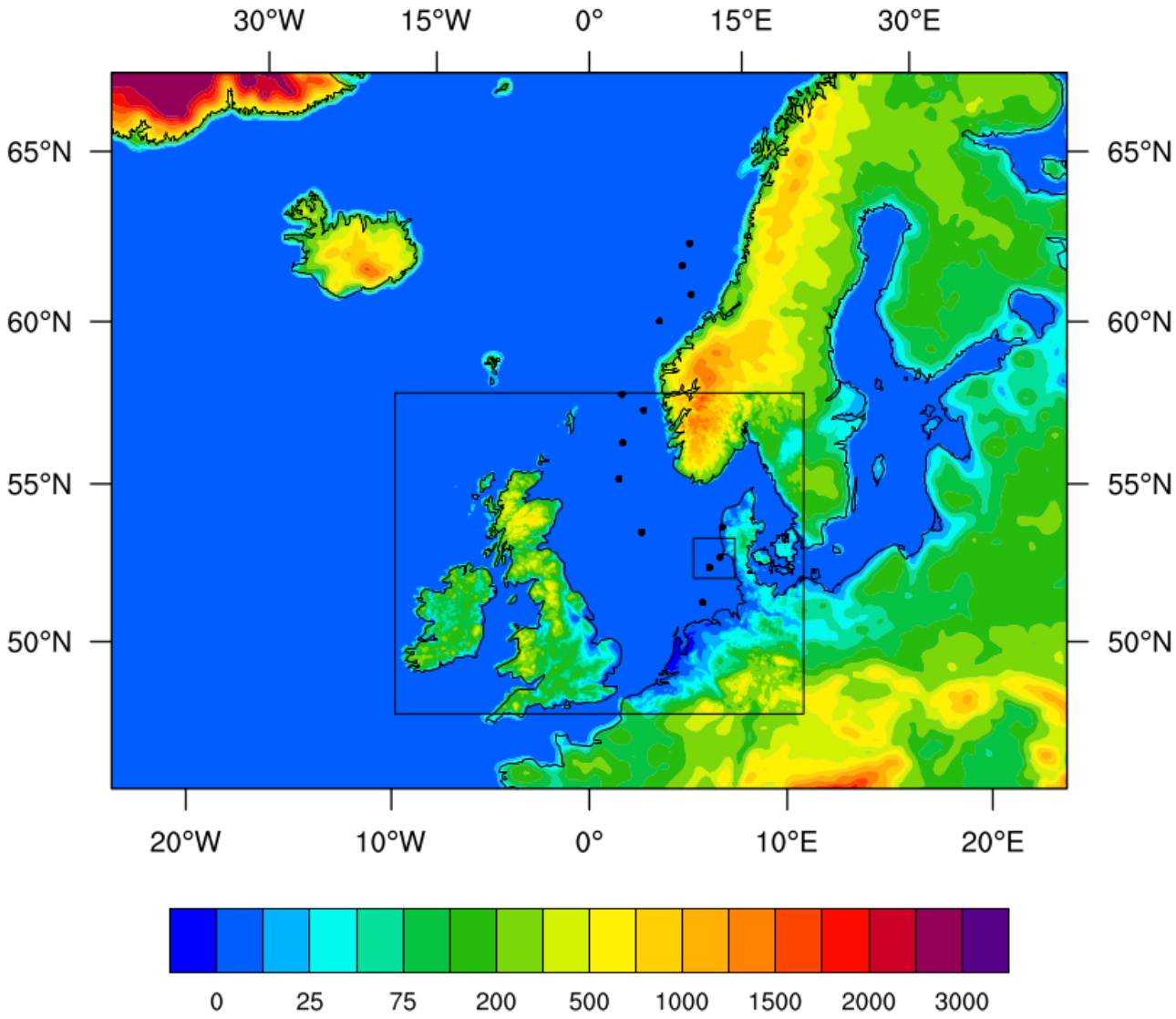

Figure 4A. Model domains

Table 4B. Model setups

Model	**Initial**	**Boundary**	**Spatial resolution (km)**	**Time step (Seconds)**	**PLB /Sin**	**Send**	**Receive**
WRF	CFSR	CFSR	15, 3, 0.6	60, 12, 2.4	MYNN 3.0	u_{10}, v_{10}	H_{m0}, T_p, L_p, z_0
SWAN	JONSWAP spectrum	Fully absorb	15, 3, 0.6	60, 60, 60	KOM, WBLM	H_{m0}, T_p, L_p, z_0	u_{10}, v_{10}

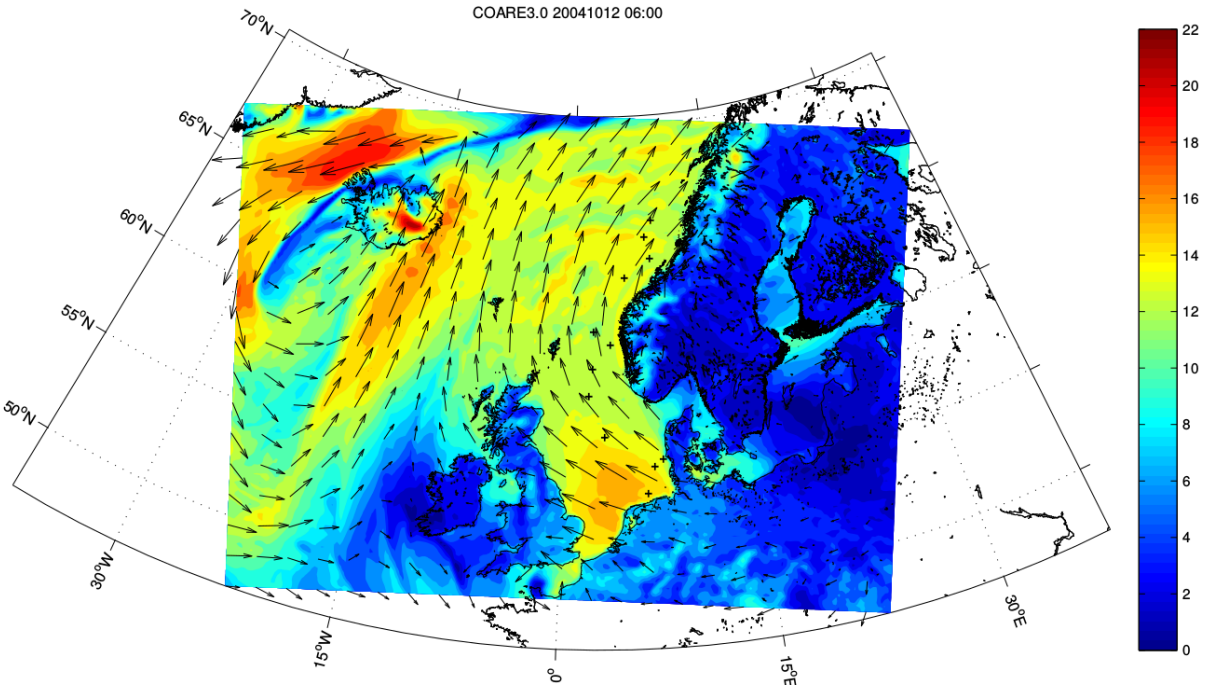

Figure 4B. Snapshot of u_{10} at 06:00 12nd Oct. 2004 from not coupled WRF simulation.

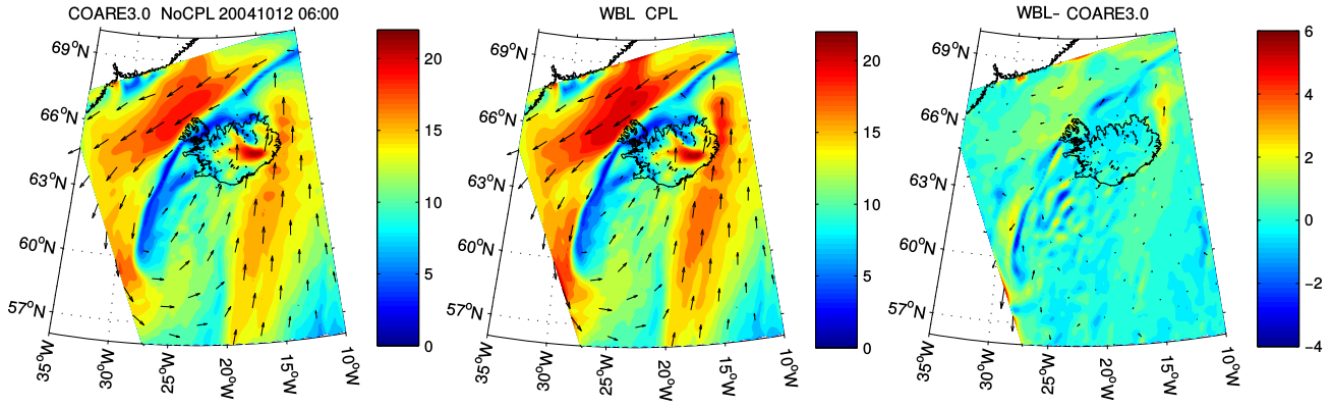

Figure 4C. Snapshot of u_{10} at the storm centre including not coupled (left), WBLM coupled (middle), and the difference between them (right).

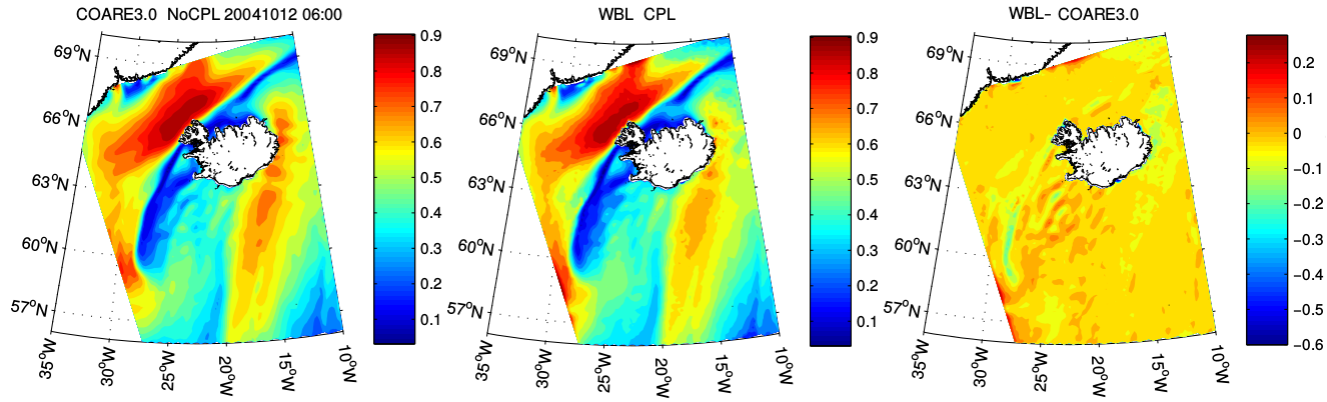

Figure 4D. The same plot as Figure 4C but plots u_*.

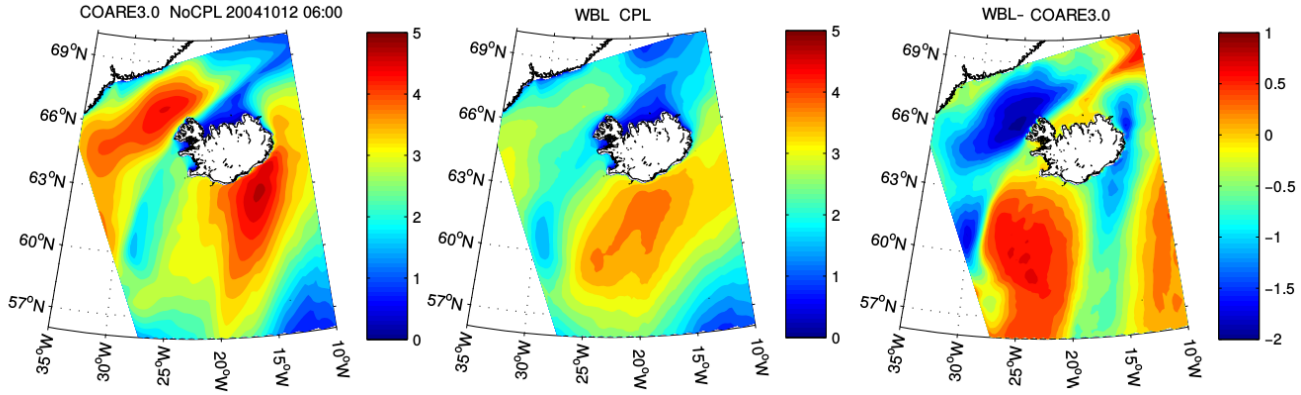

Figure 4E. The same plot as Figure 4C but plots H_{m0}.

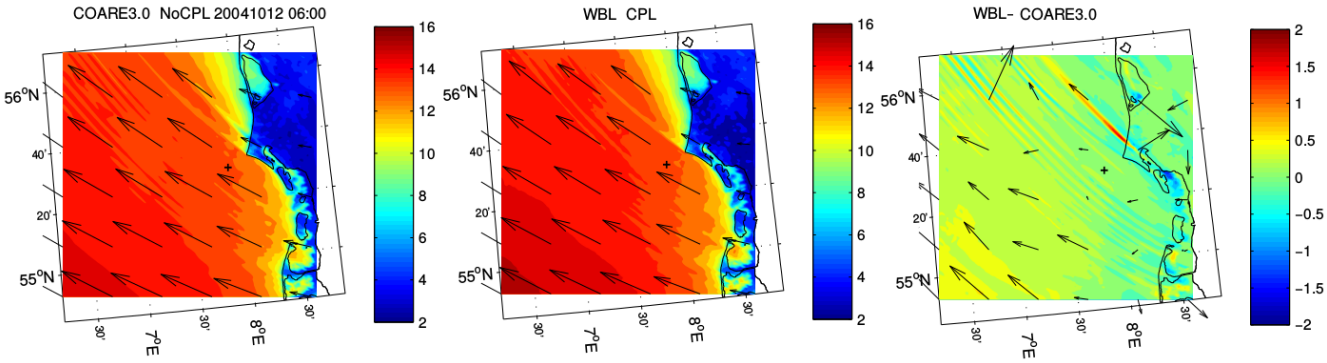

Figure 4F. Snapshot of u_{10} at the Danish west coastal zones including not coupled (left), WBLM coupled (middle), and the difference between them (right).

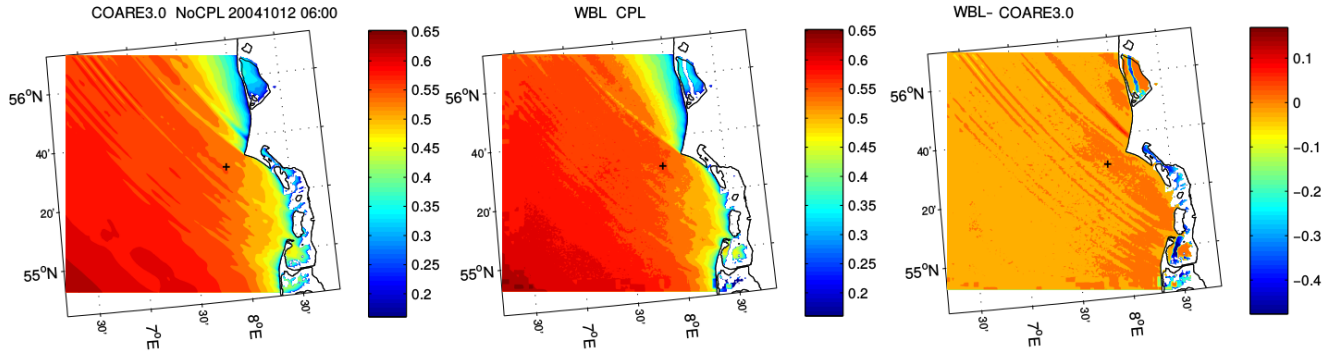

Figure 4G. The same plot as Figure 4F but plots u_*.

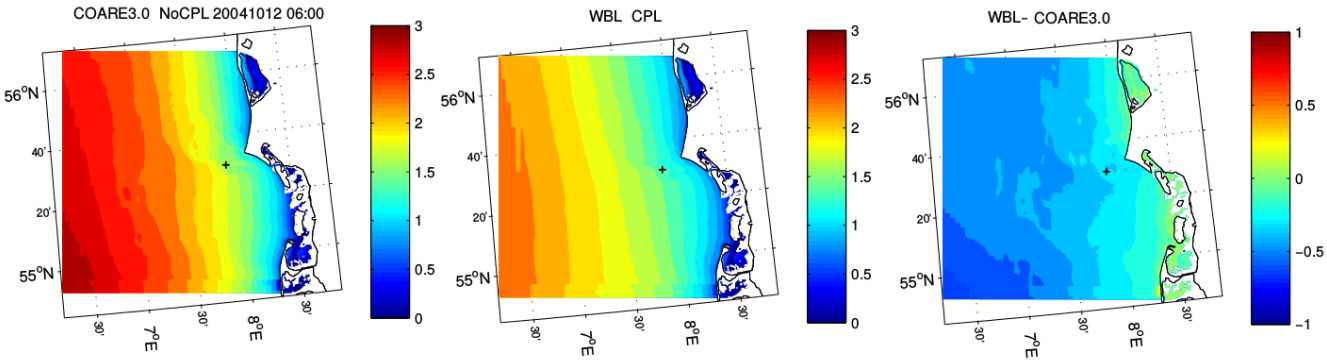

Figure 4H. The same plot as Figure 4F but plots H_{m0}.

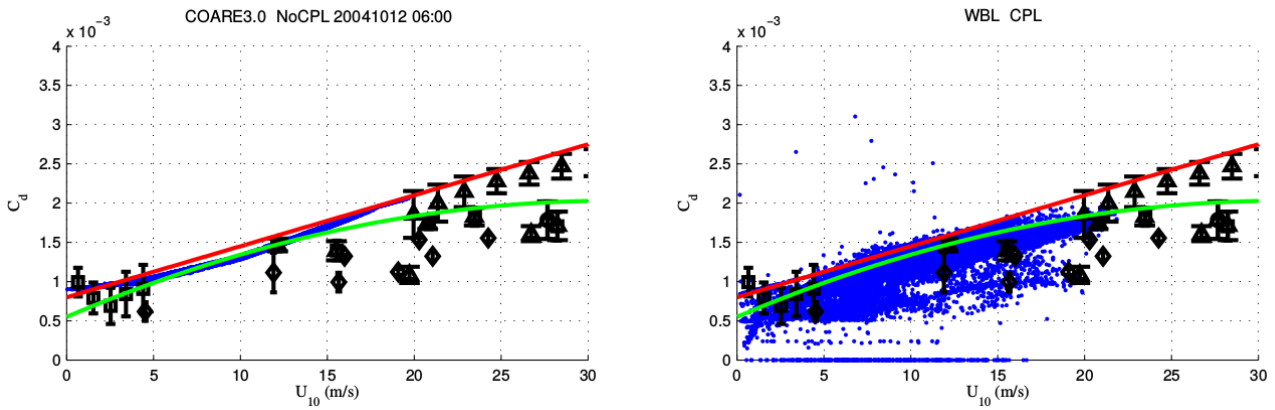

Figure 4I. C_d as a function of u_{10} at 06:00 12nd Oct. 2004. The red is from JANS, the blue is from KOM and the green is from WBLM.

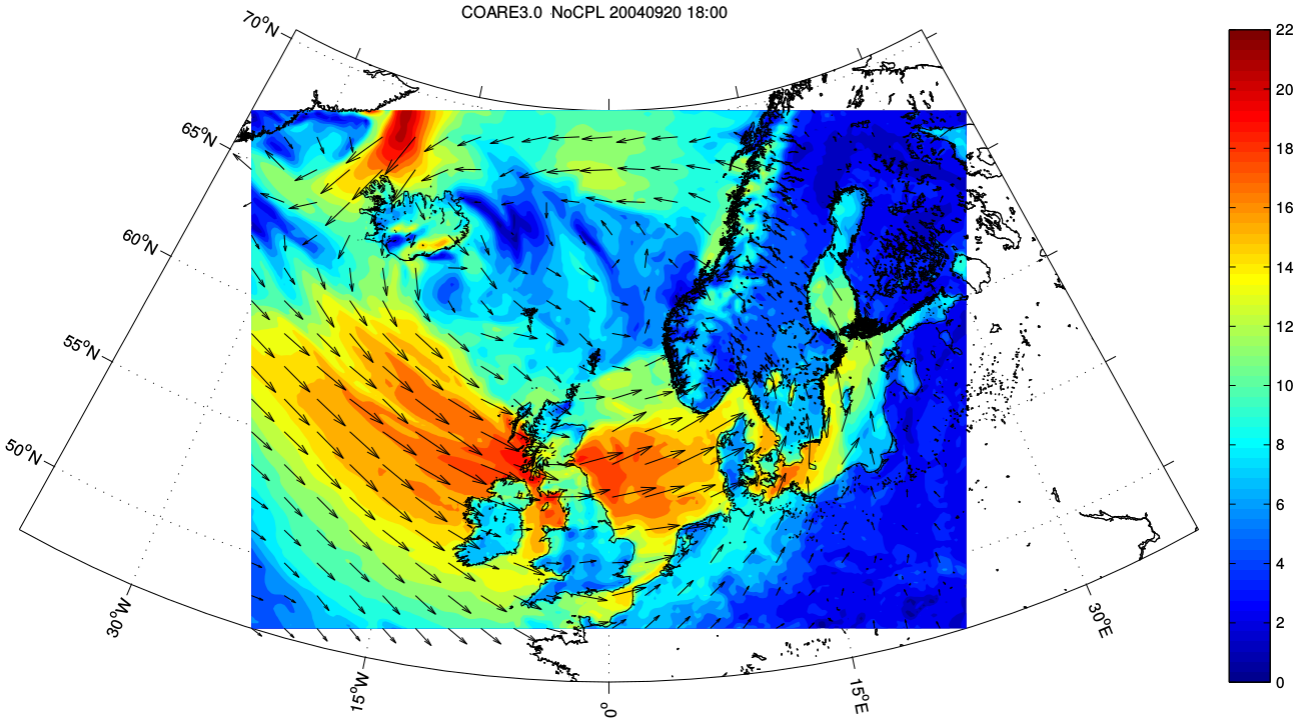

Figure 4J. Snapshot of u_{10} at 18:00 20th Sep. 2004 from not coupled WRF simulation.

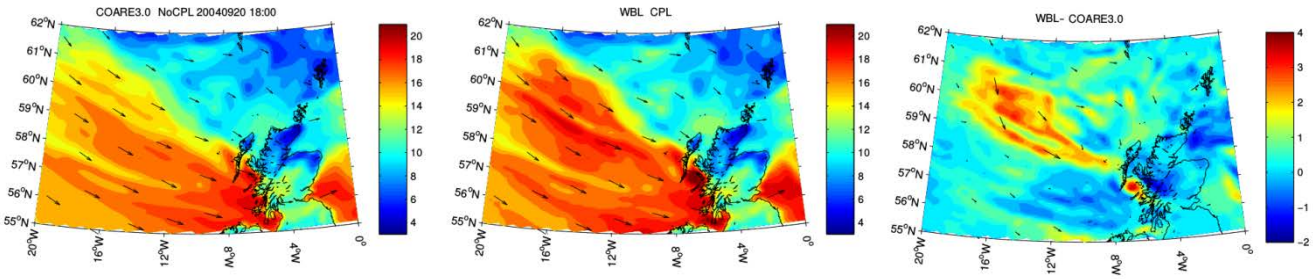

Figure 4K. Snapshot of u_{10} at the storm centre including not coupled (left), WBLM coupled (middle), and the difference between them (right).

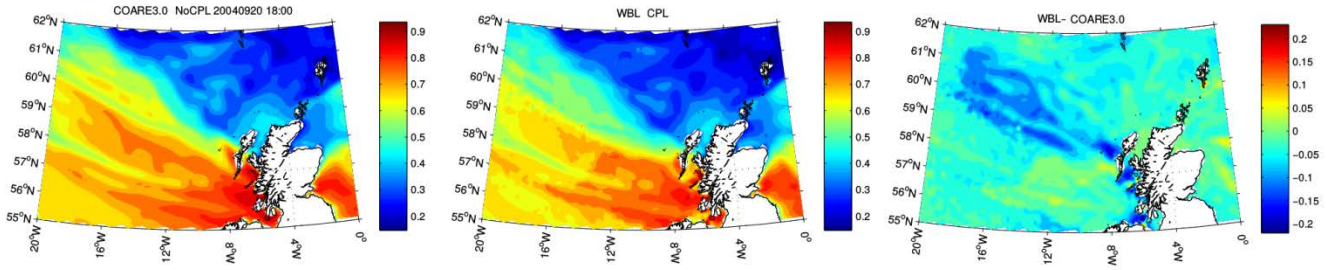

Figure 4L. The same plot as Figure 4K but plots u_*.

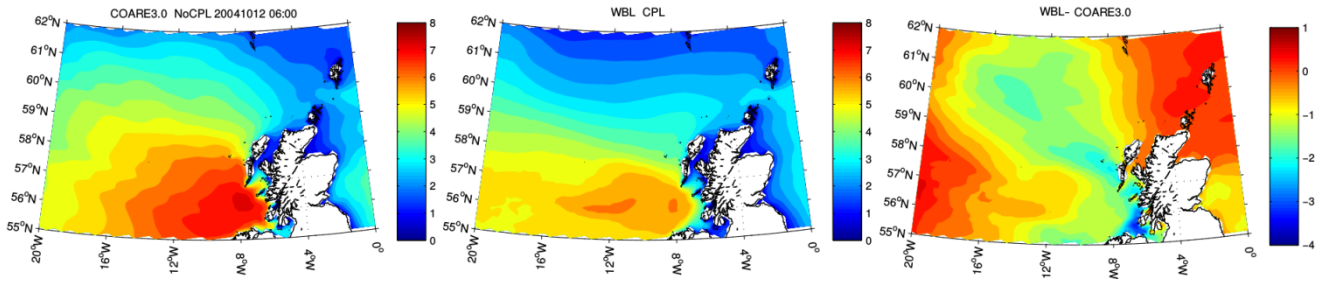

Figure 4M. The same plot as Figure 4K but plots H_{m0}.

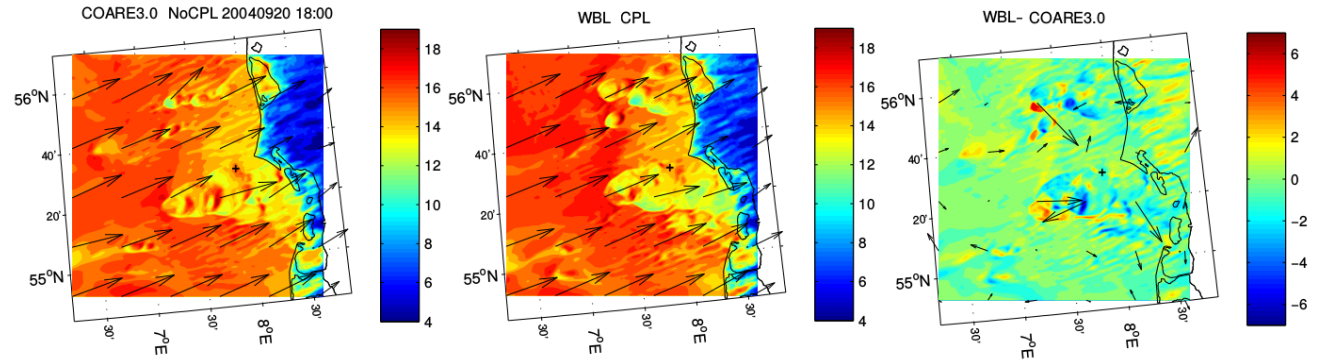

Figure 4N. Snapshot of u_{10} at the Danish west coastal zones including not coupled (left), WBLM coupled (middle), and the difference between them (right).

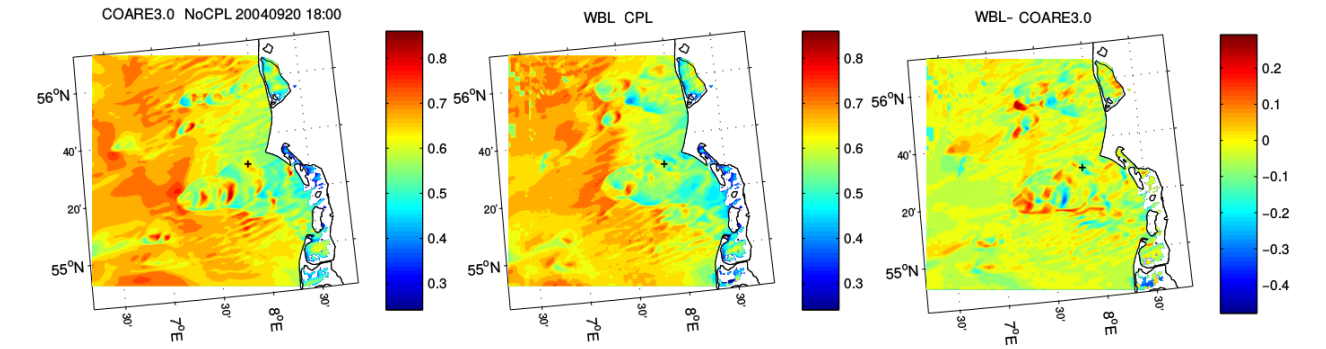

Figure 4O. The same plot as Figure 4N but plots u_*.

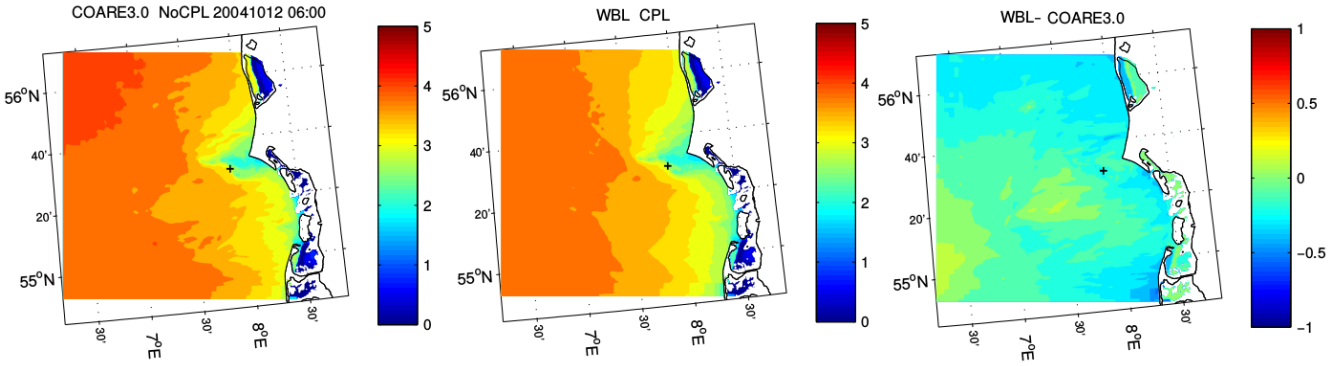

Figure 4P. The same plot as Figure 4N but plots H_{m0}.

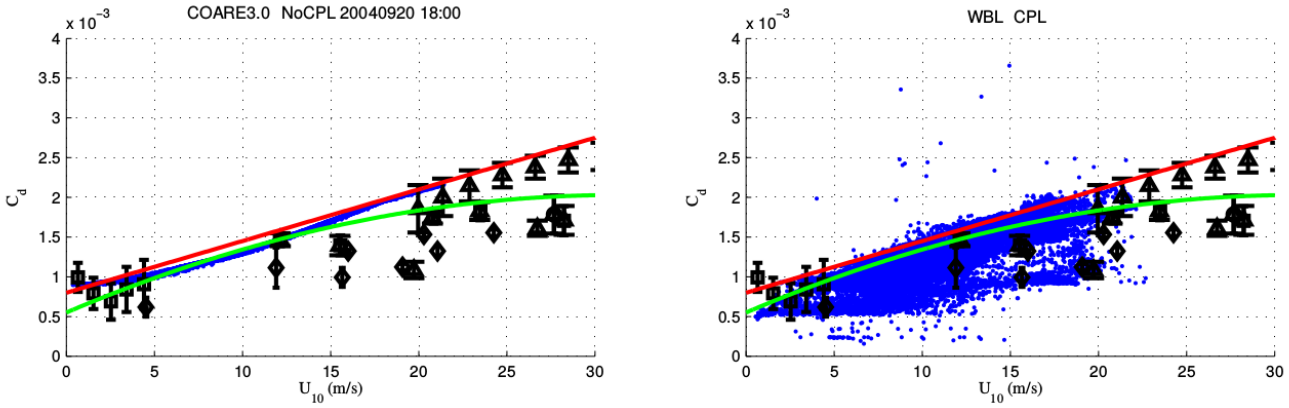

Figure 4Q. C_d as a function of u10 at 18:00 20th Sep. 2004

5. Efficiency and improvements of the coupling system

Several improvements have been done to the coupling system to increase the model efficiency and numerical stability. In COAWST, the parallel algorithm of SWAN distributes computation nodes equally in space (Figure 5A, left panel). This approach has two defects. One is that if we use many nodes in the computation, some of the nodes may only have land point. This may cause errors when the model allocating arrays in these empty nodes. The other is that SWAN only calculates water points, if the nodes equally distributes in space, the loads of the nodes are not balanced. A proper way is to distribute the nodes based on the water points. As shown in Figure 5A (right panel), the nodes are not equally distributed in space, but they are equally distributed in water points. Thus it not only balanced the load of the nodes, but also do not have empty node problems. There are also some other small changes in the use of MCT functions, remapping approaches, and time controls to make the model more stable.

One big issue is the efficiency of the WBLM. The WBLM has to find the solutions of many equations in the four dimensional space (x, y, σ, θ) in every time step. So it is quite time consuming. At the beginning, it takes 3-4 times of the other approaches in SWAN such as KOM, JANS, etc. Several steps were done to improve its efficiency. First, the calculation of WBLM in σ space is reduced to the range in which the wind input is positive. This reduces the computation time of WBLM from 3-4 times of KOM to 2 times of KOM. Second, the calculation of source functions was divided into 4 quadrants in SWAN. So the WBLM was calculated 4 times in each time step. Since the WBLM has to integrate over all the directions, it only needs to calculate 1 time and save the value for next 3 sweeps. This reduces the time from 2 times of KOM to 1.5 times of KOM. Finally, when SWAN is parallel, the boundaries in each node are overlapped. So more nodes, more overlaps, and more duplicated computation. Now,

each node sends its data to a common array in the first sweep, and grabs data from the common array in the following 3 sweeps. This reduces the time from 1.5 times of KOM to 1.1 times of KOM. With these optimizations, now the WBLM is almost as efficient as the other wind input source functions.

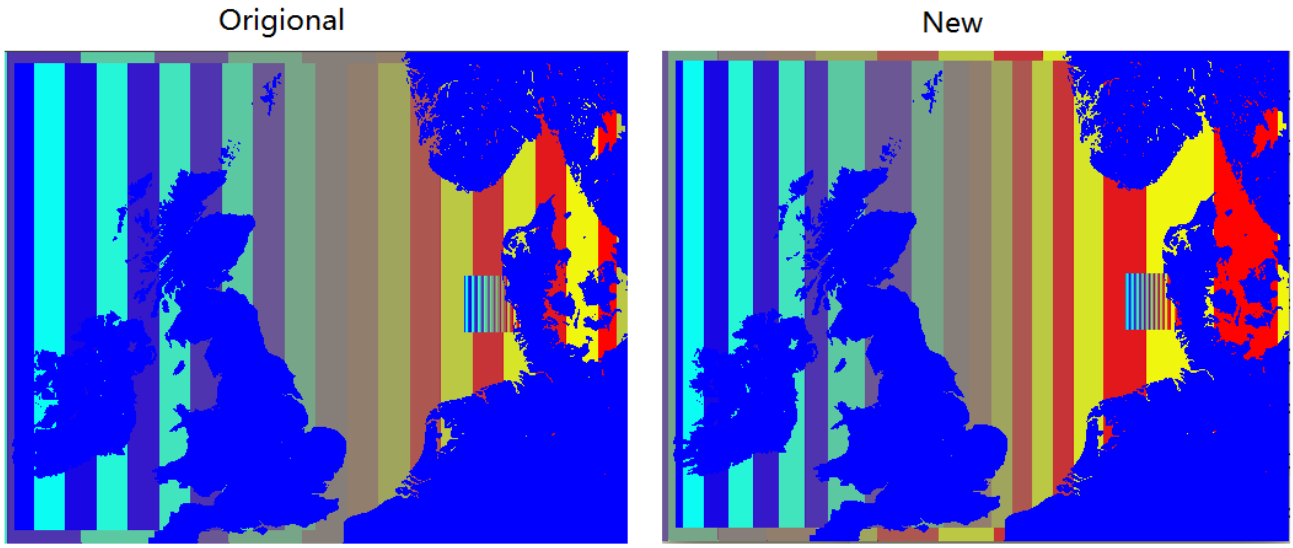

Figure 5A. SWAN parallel approaches in COAWST

Reference

Chen, S. S., Zhao, W., Donelan, M. a., & Tolman, H. L. (2013). Directional Wind–Wave Coupling in Fully Coupled Atmosphere–Wave–Ocean Models: Results from CBLAST-Hurricane. *Journal of the Atmospheric Sciences*, *70*(10), 3198–3215. http://doi.org/10.1175/JAS-D-12-0157.1

Davis, C., Wang, W., Chen, S. S., Chen, Y., Corbosiero, K., DeMaria, M., … Xiao, Q. (2008). Prediction of Landfalling Hurricanes with the Advanced Hurricane WRF Model. *Monthly Weather Review*, *136*(6), 1990–2005. http://doi.org/10.1175/2007MWR2085.1

Drennan, W. M., Taylor, P. K., & Yelland, M. J. (2005). Parameterizing the Sea Surface Roughness. *Journal of Physical Oceanography*, *35*(5), 835–848. http://doi.org/10.1175/JPO2704.1

Du J., Bolaños R. and Larsén X.: The use of a wave boundary layer model in SWAN, submitted to *Journal of Geophysical Research – Ocean*, 2016

Fan, Y., Lin, S.-J., Held, I. M., Yu, Z., & Tolman, H. L. (2012). Global Ocean Surface Wave Simulation Using a Coupled Atmosphere–Wave Model. *Journal of Climate*, *25*(18), 6233–6252. http://doi.org/10.1175/JCLI-D-11-00621.1

Fairall, C. W., Bradley, E. F., Hare, J. E., Grachev, A. A., & Edson, J. B. (2003). Bulk parameterization of air-sea fluxes: Updates and verification for the COARE algorithm. *Journal of Climate*, *16*(4), 571–591. http://doi.org/10.1175/1520-0442(2003)016<0571:BPOASF>2.0.CO;2

Hasselmann, K., Barnett, T. P., Bouws, E., Carlson, H., Cartwright, D. E., Enke, K., … Walden, H. (1973). Measurements of Wind-Wave Growth and Swell Decay during the Joint North Sea Wave

Project (JONSWAP). *Ergnzungsheft Zur Deutschen Hydrographischen Zeitschrift Reihe*, *A(8)*(12), p.95. http://doi.org/citeulike-article-id:2710264

Janssen, P. a. E. M. (1991). Quasi-linear Theory of Wind-Wave Generation Applied to Wave Forecasting. *Journal of Physical Oceanography*, *21*(11), 1631–1642. http://doi.org/10.1175/1520-0485(1991)021<1631:QLTOWW>2.0.CO;2

Kahma, K. K., & Calkoen, C. J. (1992). Reconciling Discrepancies in the Observed Growth of Wind-generated Waves. *Journal of Physical Oceanography*. http://doi.org/10.1175/1520-0485(1992)022<1389:RDITOG>2.0.CO;2

Komen, G. J., Hasselmann, K., & Hasselmann, K. (1984). On the Existence of a Fully Developed Wind-Sea Spectrum. *Journal of Physical Oceanography*, *14*(8), 1271–1285. http://doi.org/10.1175/1520-0485(1984)014<1271:OTEOAF>2.0.CO;2

Oost, W. A., Komen, G. J., Jacobs, C. M. J., & Van Oort, C. (2002). New evidence for a relation between wind stress and wave age from measurements during ASGAMAGE. *Boundary-Layer Meteorology*, *103*(3), 409–438. http://doi.org/10.1023/A:1014913624535

Soloviev, A. V, Lukas, R., Donelan, M. a, Haus, B. K., & Ginis, I. (2014). The air-sea interface and surface stress under tropical cyclones. *Scientific Reports*, *4*, 5306. http://doi.org/10.1038/srep05306

Taylor, P. K., & Yelland, M. J. (2001). The Dependence of Sea Surface Roughness on the Height and Steepness of the Waves. *Journal of Physical Oceanography*, *31*(1996), 572–590. http://doi.org/10.1175/1520-0485(2001)031<0572:TDOSSR>2.0.CO;2

van der Westhuysen, A. J., Zijlema, M., & Battjes, J. A. (2007). Nonlinear saturation-based whitecapping dissipation in SWAN for deep and shallow water. *Coastal Engineering*, *54*(2), 151–170. http://doi.org/10.1016/j.coastaleng.2006.08.006

Young, I. R. (1999). Wind Generated Ocean Waves Chapter 5 Fetch and duration limited growth. In *Elsevier Science* (pp. 83–131). http://doi.org/10.1016/S1571-9952(99)80007-5

Zijlema, M., Van Vledder, G. P., & Holthuijsen, L. H. (2012). Bottom friction and wind drag for wave models. *Coastal Engineering*, *65*, 19–26. http://doi.org/10.1016/j.coastaleng.2012.03.002

WIND ENERGY
Wind Energ. 2016; **00**:1–9
DOI: 10.1002/we

RESEARCH ARTICLE

Impact of Sea Surface Roughness Parametrization on North Sea Storm Simulation

Imberger, Marc and Du, Jianting ‡

‡ DTU Wind - Department of Wind Energy, Technical University of Denmark, Denmark.

ABSTRACT

A two-domain nested wind-wave coupling system based on the ocean-atmosphere-wave-sediment transport model (COAWST, [29]), containing the mesoscale atmospheric Weather Research and Forecast (WRF, [25]) model and the spectral ocean wave model Simulating Waves Nearshore (SWAN, [3]) is used to investigate the influence of different state-of-the-art parametrizations for the sea surface roughness z_0 on North Sea storm simulations. Five parametrizations proposed by Fairall et al. [12], Taylor and Yelland [27], Drennan et al. [6], Oost et al. [24] and Fan et al. [13] are applied in two North Sea storm simulations covering 0000 UTC 27 Jan 2002 to 1200 UTC 29 Jan 2002 and 1200 UTC 21 Nov 2002 and 1800 UTC 23 Nov 2002. It is shown, that the parametrization proposed by Oost et al. [24] yield to the highest sea surface roughness while Fairall et al. [12] and Fan et al. [13] yield to lower roughness lengths. The comparison of simulated values (wind speed at 10m height, wave height and peak time period) and provided measurements at three measuring sites showed that the sea surface parametrization of Oost et al. [24] is too high to be representative for the North Sea region, because it underestimates the wind speed and wave height strongly. Furthermore is detected that the estimations of the individual sea surface roughness parameterizations differ more, when the wind and wave conditions are more extreme (high wind speeds and high waves). The bad estimation of the wind speed and the wave height at measuring site 'Troll-A' points out, that the selected resolution need to be increased to eliminate the error due to interpolation between widely distributed grid points.

KEYWORDS

wind-wave coupling, sea surface roughness, COAWST, SWAN, WRF, North Sea, storm simulation

Correspondence

Imberger, Marc, DTU Wind Energy, Risø Campus, Frederiksborgvej 399, 4000 Roskilde, Denmark. Email: s151241@student.dtu.dk

Received . . .

1. INTRODUCTION

This paper deals with the impact of sea surface roughness parameterizations on storm simulations with focus on their applicability for the North Sea region, because a suitable estimation of the sea surface roughness is necessary to describe the interaction between the sea surface and the atmosphere sufficiently and therefore provide good estimations of the wind and wave conditions in the focus area. The obtained knowledge about wind and wave conditions, especially under extreme conditions, can be used to optimize operational processes or the design of floating turbines or regular wind turbines at offshore and coastal sides. Since the wind and wave conditions cannot be determined separately due to moment transformation between atmosphere and ocean [16], a two-way wind-wave coupling system is used. The coupling system used in this paper is based on the ocean-atmosphere-wave-sediment transport model (COAWST, [29]), which contains the mesoscale atmospheric Weather Research and Forecast (WRF, [25]) model and the spectral ocean wave model Simulating Waves Nearshore (SWAN, [3]).

Different approaches to parameterize the sea surface roughness z_0 were proposed in the past, based on the earliest parametrization of Charnock [4]. Janssen [15] propose an approach where the sea surface roughness depends on wave-induced stress and the wind speed at 10m height. Johnson et al. [17] introduce a wave age based formulation which is determined from a least square fit of different datasets from different sites. Taylor and Yelland [27] follow a different

Prepared using weauth.cls [Version: 2010/06/17 v1.00]

approach which is based on the wave steepness and which was determined by three datasets. Oost et al. [24] consider not only the wave-age but also the wave steepness and their formulation bases on the 1996 ASGAMAGE experiment. A wave independent approach, where the Charnock parameter only depends on the wind speed in 10m height, is proposed by Fairall et al. [12]. Drennan et al. [6] come up with a wave age dependent formulation determined by a data fit considering five field campaigns with a wide range of wave ages. Fan et al. [13] develop a formulation depending on wind speed and wave age. It is based on the output of a 29 year free-running simulation using an atmosphere-wave coupled model.

Some of the mentioned approaches are already analyzed with regard to their applicability. Olabarrieta et al. [23] investigate the interaction between atmosphere ocean and waves during Hurricane Ida and Nor'Ida (North Atlantic) using COAWST and compare the three roughness expressions proposed by Taylor and Yelland [27], Oost et al. [24] and Drennan et al. [6]. The authors show that the parametrization proposed by Oost et al. [24] yield to the best results with regard to the prediction of wind and wave growth while the approaches developed by Taylor and Yelland [27] and Drennan et al. [6] yield better results with regard to surface currents and storm surge. Bolaños et al. [2] investigate the reaction of an atmosphere model on the sea surface roughness parametrization for a coastal location in west Denmark. The authors use WRF and the spectral wave model MIKE 21 SW, developed by DHI. The model is realized in an offline (uncoupled) mode. They show that Taylor and Yelland [27] overestimates significant wave heights and time periods for Horns Rev 1 and that the higher values for the sea surface roughness determined by the approach of Janssen [15] are significant for coastal water. Du et al. [7] point out, that the expression of z_0 is especially influencing open ocean sites and that Janssen [15] yield to better results for the significant wave hight for the analyzed QuickSCAT data set.

Section 2 of this paper is dedicated to the coupling procedure, the used model domains and used computational grids and to the configuration of WRF and SWAN. Additionally, a description of the measurement data, which are used for validation, is given. The results are presented in Section 3 and discussed in Section 4.

2. METHODS

This section describes the used methods and configurations. Section 2.1 presents the coupling procedure and the communication between WRF and SWAN. The chosen model domains and computational grids for WRF and SWAN are described in Section 2.2. The configuration of WFR and SWAN is explained in Section 2.3 respectively 2.4 and the investigated sea surface roughness approaches are clarified in Section 2.5. Section 2.6 describes the simulated time period and the measurement data.

2.1. Coupling Procedure and Communication between WRF and SWAN

The Weather Research and Forecast (WRF) is used as mesoscale atmospheric module within the scope of this investigation. Within the COAWST model system, WRF determines wind speeds at 10m above the sea surface and passes the values to SWAN. The third-generation wave model SWAN passes then wave parameters (significant wave height, wave period and wave length) back to WRF. The sea surface roughness calculation is part of WRF. The communication between WRF and SWAN is managed by the Model Coupling Toolkit (MCT, [20]).

2.2. Model Domains and Computational Grid

WRF and SWAN are configured two-domain nested. The geographic location of the domains is shown in Figure 2.2.

Within this domains, WRF and SWAN are using both a curvilinear computational grid with the same resolution and the same number of grid points. The grid details are summarized in Table I.

Additionally, WRF uses 46 vertical eta-levels in both domains.

2.3. Weather Research and Forecast Settings

The enhanced bulk scheme based on Thompson et al. [28] is used to parameterize precipitation and the Rapid Radiative Transfer Model (RRTM) physics scheme based on Mlawer et al. [21] is applied to describe long wave radiation. Dudhia shortwave scheme [8] is used for shortwave radiation. The Noah Land-surface model [9] with four soil layers and without

	Domain I	Domain II
grid points in horizontal direction [.]	200	351
grid points in vertical direction [.]	150	243
spatial resolution [km]	18	6

Table I. Details of the curvilinear computational grid used by WRF and SWAN.

Wind Energ. 2016; **00**:1–9 © 2016 John Wiley & Sons, Ltd.
DOI: 10.1002/we
Prepared using weauth.cls

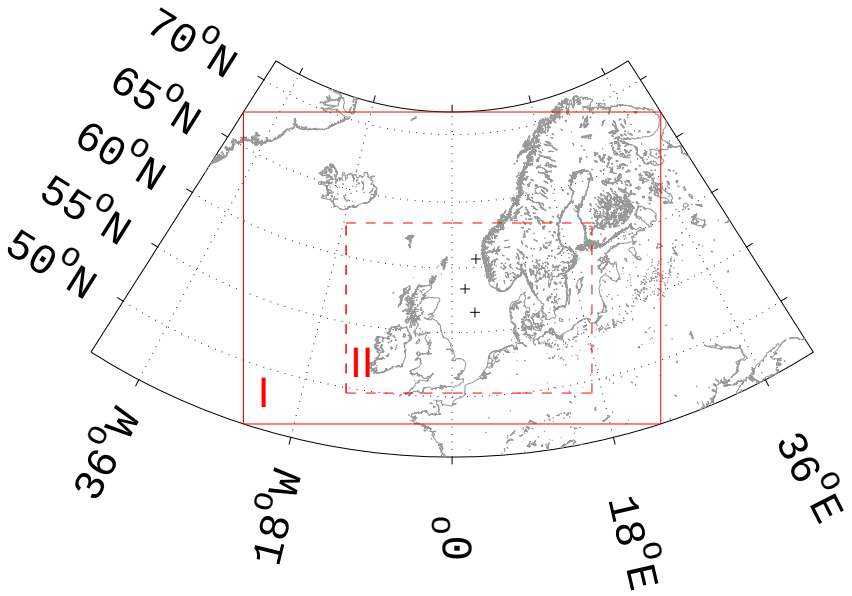

Figure 1. Geographic location of the model domains. The plus signs indicate the position of the measuring sites 'Troll-A','Sleipner-A' and 'Ekofisk' (from north to south).

urban canopy model is applied and the planetary boundary layers are modeled using the Mellor-Yamada Nakanishi Niino (MYNN) scheme according to Nakanishi and Niino [22]. Modified Kain-Fritsch scheme [18] is used in both domains to parameterize cumulus. Boundary-layer physics and cumulus physics are called every time step, while the radiation physics are called every two minutes. Vertical-Velocity damping with a damping coefficient of $\gamma_w = 0.05\,\mathrm{ms}^{-2}$ is activated and the damping depth is set to $z_{damp} = 5\,\mathrm{km}$. The NCEP Climate Forecast System Reanalysis (CFSR) dataset [10] with a grid resolution of 38 km is used to provide necessary initial and boundary conditions for WRF.

2.4. Simulating Waves Nearshore Settings

The spectral wave model SWAN is operating in an non-stationary two dimensional mode. The spectral directional resolution $\Delta\theta$ is set to $\Delta\theta = 10\,^\circ$ covering the full circle. The resolution in frequency space Δf depends on the frequency itself due to logarithmic distribution of the frequency bins and is set to $\Delta f = 0.1f$. The lowest frequency bin f_{min} is selected to $f_{min} = 0.03\,\mathrm{Hz}$. A JONSWAP spectrum with a peak enhancement parameter of $\gamma_f = 3.3$ is used as initial wave spectrum. For the source and sink term of the underlying governing equations (cf. [1]), the following parameters are set:

- Wave growth due to wind is assumed to be exponential using the expression presented in Komen et al. [19] including the drag coefficient parametrization proposed by Zijlema et al. [30],
- white-capping is considered in the same way as stated in Komen et al. [19] with a white-capping dissipation rate of $C_{ds} = 2.36 \cdot 10^{-5}$,
- quadruplet wave interactions are considered using the explicit Discrete Interaction Approximation formulated by Hasselmann and Hasselmann [14],
- depth-induced wave breaking is considered by using constant breaker index of $\gamma = 0.8$ and
- bottom friction is considered by using JONSWAP with constant friction coefficient of $C_b = 0.038\,\mathrm{m}^2\mathrm{s}^{-3}$.

The bathymetry data for SWAN is retrieved from the EMODnet Digital Terrain Model (DTM) [11], which has a spatial resolution of 0.125 arc minutes.

2.5. Investigated Sea Surface Roughness Expressions

Generally, the sea surface roughness is calculated as stated in Equation (1), whereby $\hat{z}_0$ depends on the underlying approach to estimate the sea surface roughness.

$$z_0 = \hat{z}_0 + \frac{0.11\nu}{u_*} \tag{1}$$

Independently from the selected approach, a smooth flow limit following Smith [26] is added to $\hat{z}_0$ to consider the roughness length for a smooth ocean surface. ν is the kinematic viscosity and u_* is the friction velocity. The following approaches to estimate $\hat{z}_0$ are analyzed in this paper:

Approach 1: Fairall et al. (2003)

The approach from Fairall et al. is the method in WRF when the MYNN surface layer scheme is used . It is independent from the coupling procedure, since it is only based on the friction velocity u_* and the gravity g. It is also based on the formulation by Charnock [4], except that the Charnock parameter α is not constant but depends on the wind speed at 10m height U_{10} (cf. Equation (2)).

$$\begin{aligned} \hat{z}_0 &= \frac{\alpha\left(U_{10}\right) u_*^2}{g} \\ \alpha\left(U_{10}\right) &= \begin{cases} 0.011 & \text{for} \quad U_{10} \leq 10\,\mathrm{ms}^{-1} \\ 8.75 \cdot 10^{-4} U_{10} + 2.25 \cdot 10^{-3} & \text{for} \quad 10\,\mathrm{ms}^{-1} < U_{10} < 18\,\mathrm{ms}^{-1} \\ 0.018 & \text{for} \quad U_{10} \geq 18\,\mathrm{ms}^{-1} \end{cases} \end{aligned} \tag{2}$$

Approach 2: Taylor & Yelland (2001)

Taylor & Yelland introduce an approach to estimate the roughness based on the wave steepness, which is defined as the ratio between the significant wave height H_{m0} and the wave length L_p (at the peak of the frequency spectrum). Its mathematical formulation is given in Equation (3).

$$\hat{z}_0 = 1200 H_{m0} \left(\frac{H_{m0}}{L_p}\right)^{4.5} \tag{3}$$

An upper and lower limit for the sea surface roughness according to Davis et al. [5] has to be applied for stability reasons.

Approach 3: Drennan et al. (2002)

Drennan et al. propose a roughness length formulation which takes the significant wave height H_{m0} and the wave age into account. The wave age is defined as the ratio between the wave phase speed at peak frequency c_p and the friction velocity u_*. The roughness length $\hat{z}_0$ is then calculated according to Equation (4).

$$\hat{z}_0 = 3.35 H_{m0} \left(\frac{u_*}{c_p}\right)^{3.5} \tag{4}$$

Approach 4: Oost et al. (2002)

The approach of Oost et al. considers not only wave age but also the wave steepness due to the consideration of L_p. The roughness length is calculated as stated in Equation (5).

$$\hat{z}_0 = \frac{25}{\pi} L_p \left(\frac{u_*}{c_p}\right)^{4.5} \tag{5}$$

Approach 5: Fan et al. (2012)

Fan et al. proposed a formulation which is also based on Charnock [4]. The Charnock parameter α is considered as wind speed dependent (given at 10m height), which is similar to Fairall et al. [12]. However, the relation is proposed differently (cf. Equation (6)).

$$\begin{aligned} \hat{z}_0 &= \frac{\alpha\left(U_{10}\right) u_*^2}{g} \\ \alpha\left(U_{10}\right) &= \frac{0.023}{1.0568^{U_{10}}} \left(\frac{c_p}{u_*}\right)^{0.012 U_{10}} \end{aligned} \tag{6}$$

Wind Energ. 2016; **00**:1–9 © 2016 John Wiley & Sons, Ltd.
DOI: 10.1002/we
Prepared using weauth.cls

2.6. Analyzed Storm Events and Measurements

Each of the approaches presented in Section 2.5 is analyzed with respect to two different storm events, which took place during January (simulation case 'JAN02') and November (simulation case 'NOV02') in 2002 in the North Sea. JAN02 covers the time range between 0000 UTC 27 Jan 2002 and 1200 UTC 29 Jan 2002, which is dominated by wind coming from west. NOV02, covers 1200 UTC 21 Nov 2002 and 1800 UTC 23 Nov 2002. This storm is dominated by wind coming from east and south-east. To validate the results, measurement data from three measuring sites ('Ekofisk', 'Sleipner-A' and 'Troll-A') is used. Their positions within the model domain can be seen in Figure 1. The wind speed at 10m height U_{10}, the significant wave height H_{m0} and the peak wave period T_p are chosen as relevant parameters.

3. RESULTS

Figure 2 depicts the sea surface roughness exemplarily for 1800 UTC 21 Nov 2002 (part of the NOV02 simulation) depending on the used approach. The red marks indicate the measuring sites. It can be seen, that the parametrization proposed by Oost et al. [24] calculates high roughness values compared to the other approaches. Fairall et al. [12] or Fan et al. [13] estimate the roughness length lower, followed by Drennan et al. [6] and Taylor and Yelland [27].

To validate the simulation, relevant values at the position at the measuring sites are extracted. Figure 3 shows the time series of U_{10}, H_{m0} and T_p for the NOV02 simulation (right column) and the JAN02 simulation (left column) at the 'Ekofisk' measuring site. The time series at 'Sleipner-A' and 'Troll-A' are depicted in Figure 4 respectively Figure 5.

Figure 3 shows that the estimated wind speed is slightly overestimated and relatively independent from the used sea surface roughness formulation. One exception from that is the approach proposed by Oost et al. [24], which estimates the wind speed lower than the other approaches. This effect becomes more visible when the wind speeds are high (cf. hour 44 in the JAN02 simulation). The same effect can be detected in the estimation of the significant wave height. Generally, the wave height is underestimated by all approaches. The peak wave period is estimated well, whereby the approach proposed by Oost et al. [24] yield to the lowest wave period.

The comparison of the simulated and measured data at measuring site 'Sleipner-A' (cf. Figure 4) reveals a more accurate estimation in the wind speed while the wave heights are generally underestimated. The difference between the different sea surface roughness expressions is small. Also in this case, Oost et al. [24] estimates the lowest wind speed. The peak wave period is reproduced quite accurate by all approaches.

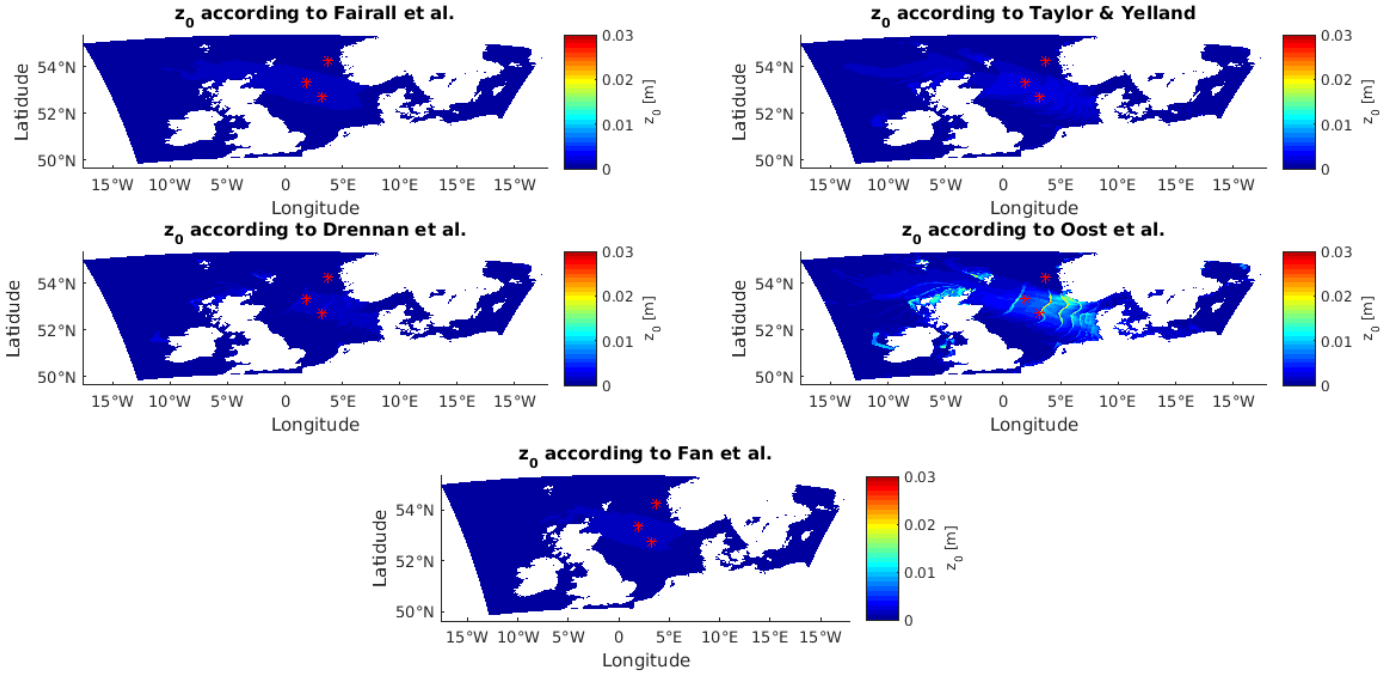

Figure 2. Sea surface roughness for 1800 UTC 21 Nov 2002 using different approaches. Oost et al. [24] yield to the highest values for the roughness, while the approaches proposed by Fairall et al. [12] and Fan et al. [13] yield to the lowest. The red marks indicate the position of the measuring sites. A land mask is used to focus only on the sea surface roughness.

The evaluation of the simulations at 'Troll-A' (see Figure 5) disagree with previous observations from 'Ekofisk' and 'Sleipner-A'. The wind speed is estimated badly and the fluctuations in the estimated values is high although the measurements vary not that much. This phenomenon is independent from the selected sea surface roughness approach. The wave height is underestimated in the JAN02 simulation, but relatively good estimated in the NOV02 simulation, although faster changes in the wave height are not covered (cf. hour 40 or hour 55 in the NOV02 simulation). The peak wave period is quite good estimated in the NOV02 simulation.

4. DISCUSSION

From the results presented in Section 3 can be concluded that the selected sea surface roughness approach has an impact on the estimation of wind speed and wave height, whereby its impact depends on the sea state and the wind speed: The heavier the wind and wave conditions are (high waves and high wind speeds), the bigger is the influence of the used parametrization for the roughness length. The comparison with the measuring sites 'Ekofisk' and 'Sleipner-A' point out that Oost et al. [24] is not suitable to describe storm conditions in the investigated domains, because the approach estimates the roughness length too high which causes a low value for the estimated wind speed and wave height. Differences between the other sea surface roughness approaches under normal conditions are visible but not strong. In order to explain the general underestimation of the wave height at 'Sleipner-A', further knowledge about the wind and wave directions and the water depth is needed. Looking at the results obtained by the JAN02 simulation, the underestimation might be caused by

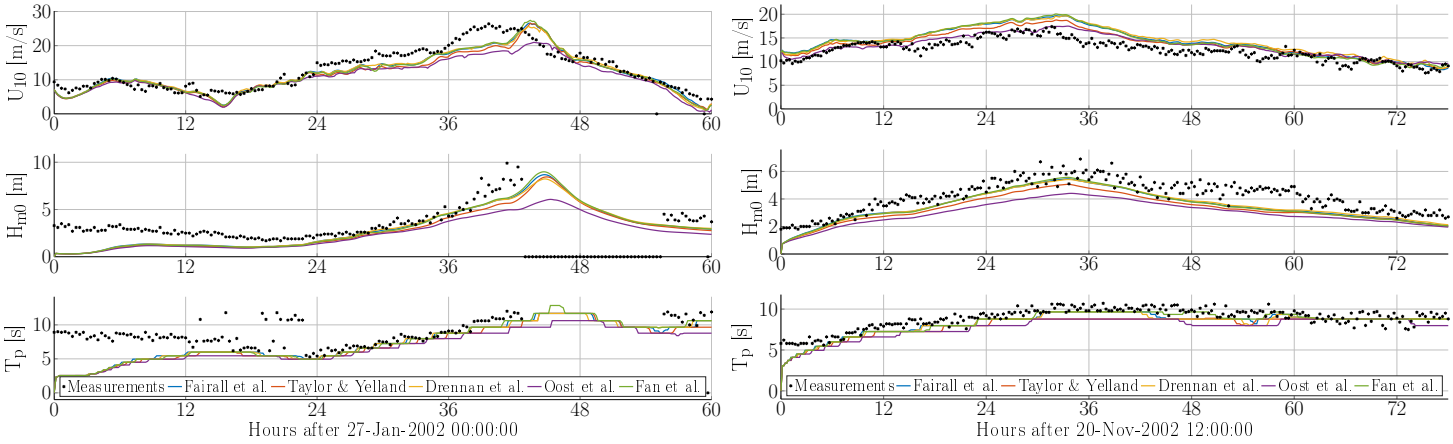

Figure 3. Simulated and measured wind speed at 10m height U_{10} (top), significant wave height H_{m0} (middle) and peak wave period T_p (bottom) for NOV02 (right column) and JAN02 (left column) simulation at measuring site 'Ekofisk'.

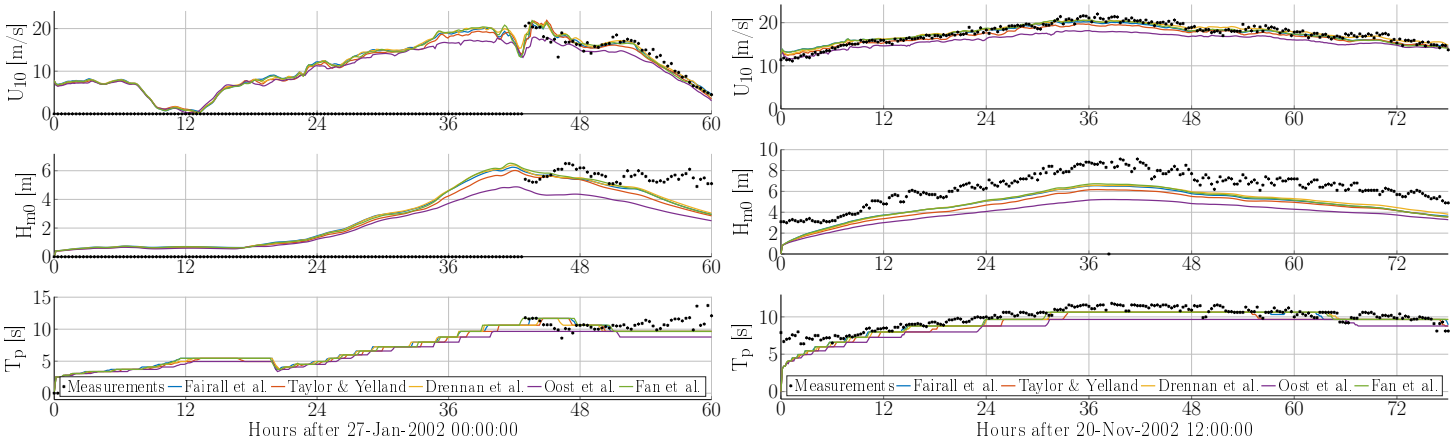

Figure 4. Simulated and measured wind speed at 10m height U_{10} (top), significant wave height H_{m0} (middle) and peak wave period T_p (bottom) for NOV02 (right column) and JAN02 (left column) simulation at measuring site 'Sleipner-A'.

Wind Energ. 2016; **00**:1–9 © 2016 John Wiley & Sons, Ltd.
DOI: 10.1002/we
Prepared using weauth.cls

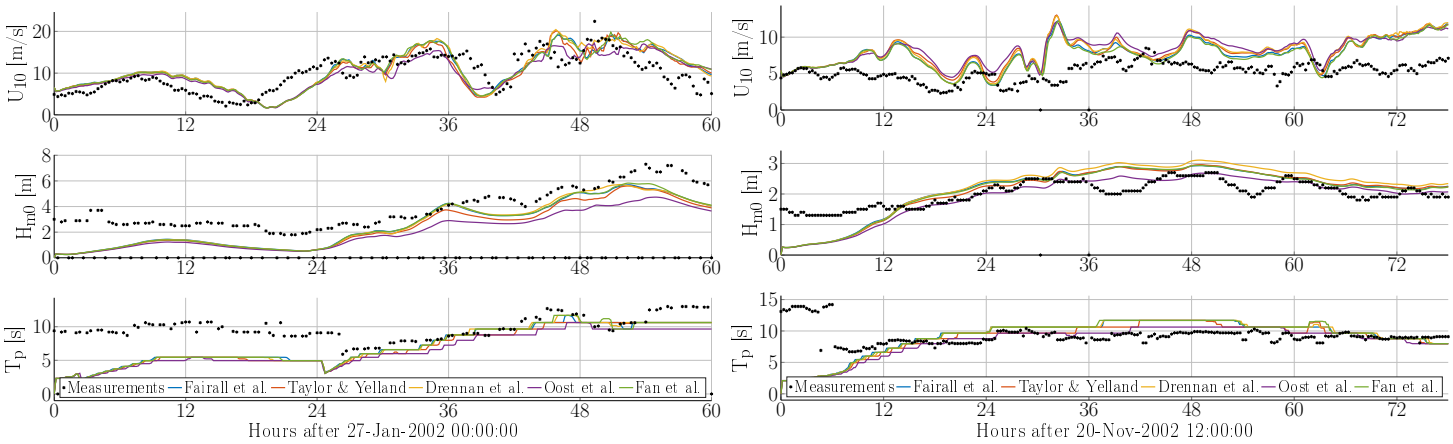

Figure 5. Simulated and measured wind speed at 10m height U_{10} (top), significant wave height H_{m0} (middle) and peak wave period T_p (bottom) for NOV02 (right column) and JAN02 (left column) simulation at measuring site 'Troll-A'.

some specific atmospheric conditions during November, because such a high underestimation of the wave height is not detected in this simulation. However, the low amount of measurements at 'Sleipner-A' during January makes it difficult to use the data for analysis purposes. Because the general underestimation is not that obvious at the measuring site 'Ekofisk', which is relatively close to 'Sleipner-A', there might be some local changes in the conditions. This can be only detected by a simulation with a higher resolution. Furthermore, the comparison with measuring site 'Troll-A' showed that the used computational grid is too rough. The coupling configuration is not able to estimate the wind conditions for this measuring site and all estimations independently from the used sea surface roughness approach are equally bad. This could be due to the close position of the measuring site to the Norwegian coast, where the wind conditions change faster due to the complex topography. Since coastal zones require a higher spatial resolution (cf. [7]), a investigation with higher resolution of the second domain or a third domain is necessary to determine the causes. The results obtained within the first hours of the simulation can be only considered with caution, because impact of the initial conditions cannot be excluded and might sill influencing the results.

[Still to do: comparison with other papers]

ACKNOWLEDGMENT

The authors acknowledge the EMODnet Bathymetry portal, which provide the the bathymetry data as well as the research group of the NCEP Climate Forecast System Reanalysis project which provide initial and boundary conditions for WRF. The authors acknowledge also the Danish Forskel project X-WiWa (PSO-12020).

REFERENCES

[1] SWAN Scientific and Technical documentation, 2016. URL `http://www.swan.tudelft.nl`.

[2] Rodolfo Bolaños, Xiaoli Guo Larsén, O.S. Petersen, J.R. Nielsen, M. Kelly, H. Kofoed-Hansen, Jianting Du, O.R. Sørensen, S.E. Larsen, A.N. Hahmann, and M. Badger. Coupling atmospherere and waves for coastal wind turbine design. *Proceedings of the Coastal Engineering Conference*, 34:1–11, 2014. ISSN 01613782.

[3] N. Booij, R. C. Ris, and Leo H. Holthuijsen. A third-generation wave model for coastal regions: 1. Model description and validation. *Journal of Geophysical Research*, 104(C4):7649–7666, 1999. ISSN 0148-0227.

[4] H Charnock. Wind stress on a water surface. *Quart. J. Roy. Meteor. Soc.*, 81:639–640, 1955.

[5] Christopher Davis, Wei Wang, Shuyi S. Chen, Yongsheng Chen, Kristen Corbosiero, Mark DeMaria, Jimy Dudhia, Greg Holland, Joe Klemp, John Michalakes, Heather Reeves, Richard Rotunno, Chris Snyder, and Qingnong Xiao. Prediction of Landfalling Hurricanes with the Advanced Hurricane WRF Model. *Monthly Weather Review*, 136 (2008):1990–2005, 2008. ISSN 0027-0644.

[6] William M. Drennan, Hans C. Graber, Daniele Hauser, and Celine Quentin. On the wave age dependence of wind stress over pure wind seas. *Journal of Geophysical Research*, 108(C3):1–13, 2003. ISSN 0148-0227.

[7] Jianting Du, Xiaoli Guo Larsén, and Rodolfo Bolaños. A Coupled Atmospheric and Wave Modeling System for Storm Simulations. In *EWEA Offshore 2015 Conference*, Ballerup, 2015.

[8] Jimy Dudhia. Numerical Study of Convection Observed during the Winter Monsoon Experiment Using a Mesoscale Two-Dimensional Model, 1989. ISSN 0022-4928.

[9] M B Ek, K E Mitchell, Y Lin, E Rogers, P Grunmann, V Koren, G Gayno, and J D Tarpley. Implementation of Noah land surface model advances in the National Centers for Environmental Prediction operational mesoscale Eta model. *Journal of Geophysical Research: Atmospheres*, 108(D22):n/a–n/a, 2003. ISSN 2156-2202.

[10] Saha et al. The NCEP climate forecast system reanalysis. *Bulletin of the American Meteorological Society*, 91(8): 1015–1057, 2010. ISSN 00030007.

[11] European Marine Observation and Data Network (EMODnet). bathymetric metadata and digital terrain model, 2016. URL `http://portal.emodnet-bathymetry.eu/`.

[12] C. W. Fairall, E. F. Bradley, J. E. Hare, A. A. Grachev, and J. B. Edson. Bulk parameterization of air-sea fluxes: Updates and verification for the COARE algorithm. *Journal of Climate*, 16(4):571–591, 2003. ISSN 08948755.

[13] Yalin Fan, Shian-Jiann Lin, Isaac M. Held, Zhitao Yu, and Hendrik L. Tolman. Global Ocean Surface Wave Simulation Using a Coupled AtmosphereWave Model. *Journal of Climate*, 25(18):6233–6252, 2012. ISSN 0894-8755.

[14] S. Hasselmann and K. Hasselmann. Computations and Parameterizations of the Nonlinear Energy Transfer in a Gravity-Wave Spectrum. Part I: A New Method for Efficient Computations of the Exact Nonlinear Transfer Integral, 1985. ISSN 0022-3670.

[15] Peter A. E. M. Janssen. Quasi-linear Theory of Wind-Wave Generation Applied to Wave Forecasting, 1991. ISSN 0022-3670.

[16] Peter A. E. M. Janssen and Pedro Viterbo. Ocean Waves and the Atmospheric Climate, 1996. ISSN 08948755.

[17] H. K. Johnson, J. Højstrup, H. J. Vested, and S.E. Larsen. On the Dependence of Sea Surface Roughness on Wind Waves. *Journal of Physical Oceanography*, 28(9):1702–1716, 1998. ISSN 0022-3670.

[18] John S. Kain. The KainFritsch Convective Parameterization: An Update. *Journal of Applied Meteorology*, 43(1): 170–181, 2004. ISSN 0894-8763.

[19] G. J. Komen, K. Hasselmann, and K. Hasselmann. On the Existence of a Fully Developed Wind-Sea Spectrum, 1984. ISSN 0022-3670.

[20] J. Larson, Robert Jacob, and Everest Ong. The Model Coupling Toolkit: A New Fortran90 Toolkit for Building Multiphysics Parallel Coupled Models. *International Journal of High Performance Computing Applications*, 19(3): 277–292, 2005. ISSN 1094-3420.

[21] Eli J. Mlawer, Steven J. Taubman, Patrick D. Brown, Michael J. Iacono, and Shepard A. Clough. Radiative transfer for inhomogeneous atmospheres: RRTM, a validated correlated-k model for the longwave. *Journal of Geophysical Research*, 102(D14):16663, 1997. ISSN 0148-0227.

[22] Mikio Nakanishi and Hiroshi Niino. Development of an Improved Turbulence Closure Model for the Atmospheric Boundary Layer. *Journal of the Meteorological Society of Japan*, 87(5):895–912, 2009. ISSN 0026-1165.

[23] Maitane Olabarrieta, John C. Warner, Brandy Armstrong, Joseph B. Zambon, and Ruoying He. Ocean-atmosphere dynamics during Hurricane Ida and Nor'Ida: An application of the coupled ocean-atmosphere-wave-sediment transport (COAWST) modeling system. *Ocean Modelling*, 43-44:112–137, 2012. ISSN 14635003.

[24] W. A. Oost, G. J. Komen, C. M J Jacobs, and C. Van Oort. New evidence for a relation between wind stress and wave age from measurements during ASGAMAGE. *Boundary-Layer Meteorology*, 103(3):409–438, 2002. ISSN 00068314.

[25] W.C. Skamarock, J.B. Klemp, J. Dudhi, D.O. Gill, D.M. Barker, M.G. Duda, X.-Y. Huang, Wei Wang, and J.G. Powers. A Description of the Advanced Research WRF Version 3. *Technical Report*, (June):113, 2008. ISSN 1477870X.

[26] Stuart D. Smith. Coefficients for sea surface wind stress, heat flux, and wind profiles as a function of wind speed and temperature. *Journal of Geophysical Research: Oceans*, 93(C12):15467–15472, 1988. ISSN 21699291.

[27] Peter K. Taylor and Margaret J. Yelland. The Dependence of Sea Surface Roughness on the Height and Steepness of the Waves. *Journal of Physical Oceanography*, 31:572–590, 2000.

[28] Gregory Thompson, Roy M. Rasmussen, and Kevin Manning. Explicit Forecasts of Winter Precipitation Using an Improved Bulk Microphysics Scheme. Part I: Description and Sensitivity Analysis. *Monthly Weather Review*, 132 (2):519–542, 2004. ISSN 0027-0644.

[29] John C. Warner, Brandy Armstrong, Ruoying He, and Joseph B. Zambon. Development of a Coupled Ocean-Atmosphere-Wave-Sediment Transport (COAWST) Modeling System. *Ocean Modelling*, 35(3):230–244, 2010. ISSN 14635003.

[30] M. Zijlema, G. Ph Van Vledder, and L. H. Holthuijsen. Bottom friction and wind drag for wave models. *Coastal Engineering*, 65:19–26, 2012. ISSN 03783839.

Appendix E: M1.7 updated

M1.7 Subroutines for the estimation of the sea spray heat fluxes and 2D fields of sea spray heat fluxes effect on the roughness

Xiaoli G. Larsén, Nikhil Garg, Jianting Du, Rodolfo Bolaños, Mark Kelly

This is an updated version of the report with the same title, attached in Interim Report IV.

Deliverable 1.16 documents the experiments and the results from these experiments related to sea surface temperature and sensible heat fluxes.

The subroutine was written by Garg N. (Garg 2015) within the cooperation between X-WiWa and DHI's program at School of Mechanical and Aerospace Engineering, Nanyang Technological University.

This subroutine implements the spray model developed by Andreas E. for tropical cyclones in a series of his and his colleagues' articles (Andreas E. 1989, 1990, 1992, 1995, 1996, 2005; Andreas et al. 1999, 2011, 2012). The intention here is to find out if this spray scheme brings as much impact in the storm characteristics in the mid-latitude storms as in the tropical cyclones.

The impact of implementing the spray model is that the drag coefficient increases with wind speed up to about 40 m/s and starts to decreases with it at stronger winds, see Figure 1.

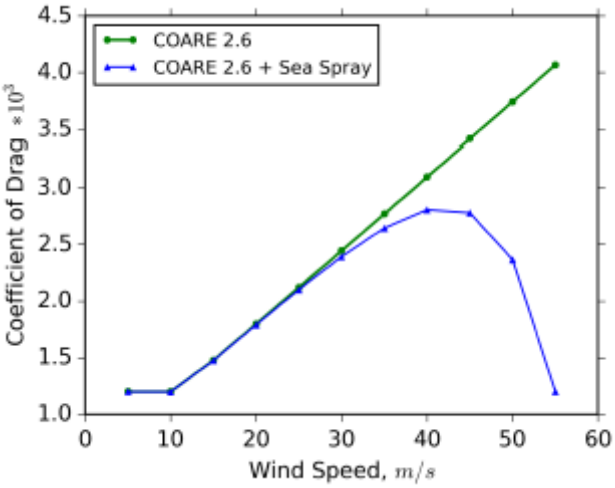

Figure 1. Drag coefficient as a function of wind speed at 10 m, with and without the sea spray model. (Garg 2015)

In Wu et al. (2015), the sea spray generation function (SSGF) from Kudryavsev (2006) was used. Additionally, SSGF was introduced as a function of wave age through the Charnock coefficient α based on the study of Carlsson et al. (2009), where $\alpha=0.05(c_p/u_*)^{-0.4}$. Effectively, this results in similar dependence of the drag coefficient on the wind speed as Figure 1. The study of Wu et al. (2015) suggests that, considering sea spray impact on wind stress (and not on heat fluxes) will intensify the storms (in terms of minimum sea level pressure and maximum wind speed) but has little effect on the storm tracks. Considering the impact of sea spray on heat fluxes only (and not on stress) can improve the model performance regarding air temperature, but it has little effect on the storm intensity and storm track performance. The model performs best if the spray effects on both the stress and heat are considered. However, the improvement is rather marginal, in comparison with measurements (see Figures 2, 3 and 4).

Based on these findings from Garg (2015) and Wu et al. (2015), it is decided that we do not continue the implementation of the subroutine for sea spray effect in the modeling system, since the effort is big, cost is considerable and the effect is not convincing.

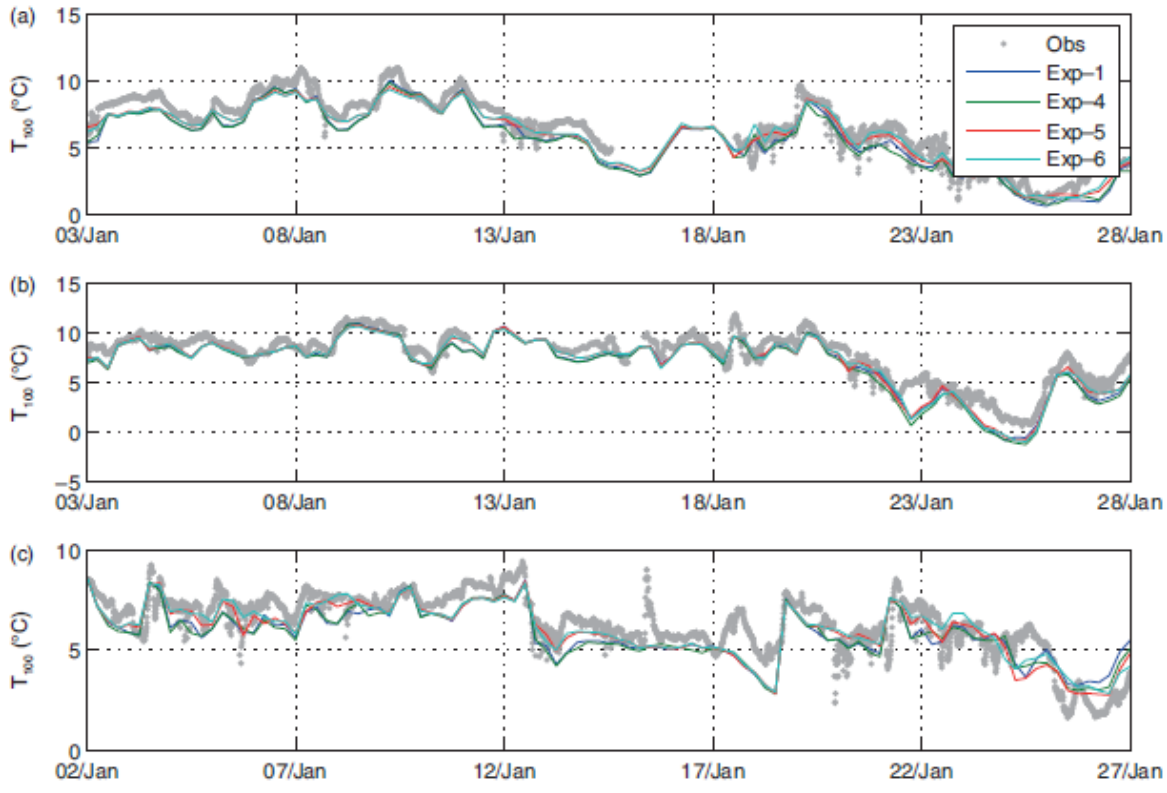

Fig. 6. Same as in Fig. 4, but for temperature measured at a height of 100 m compared with the second model layer (about 100 m).

Figure 2. Comparison of modeled and measured temperatures at 100 m at FINO 1. Exp 6 is where SSGF is used both to the stress and heat and it outperforms the other experiments, but only marginally. (from Wu et al. 2015)

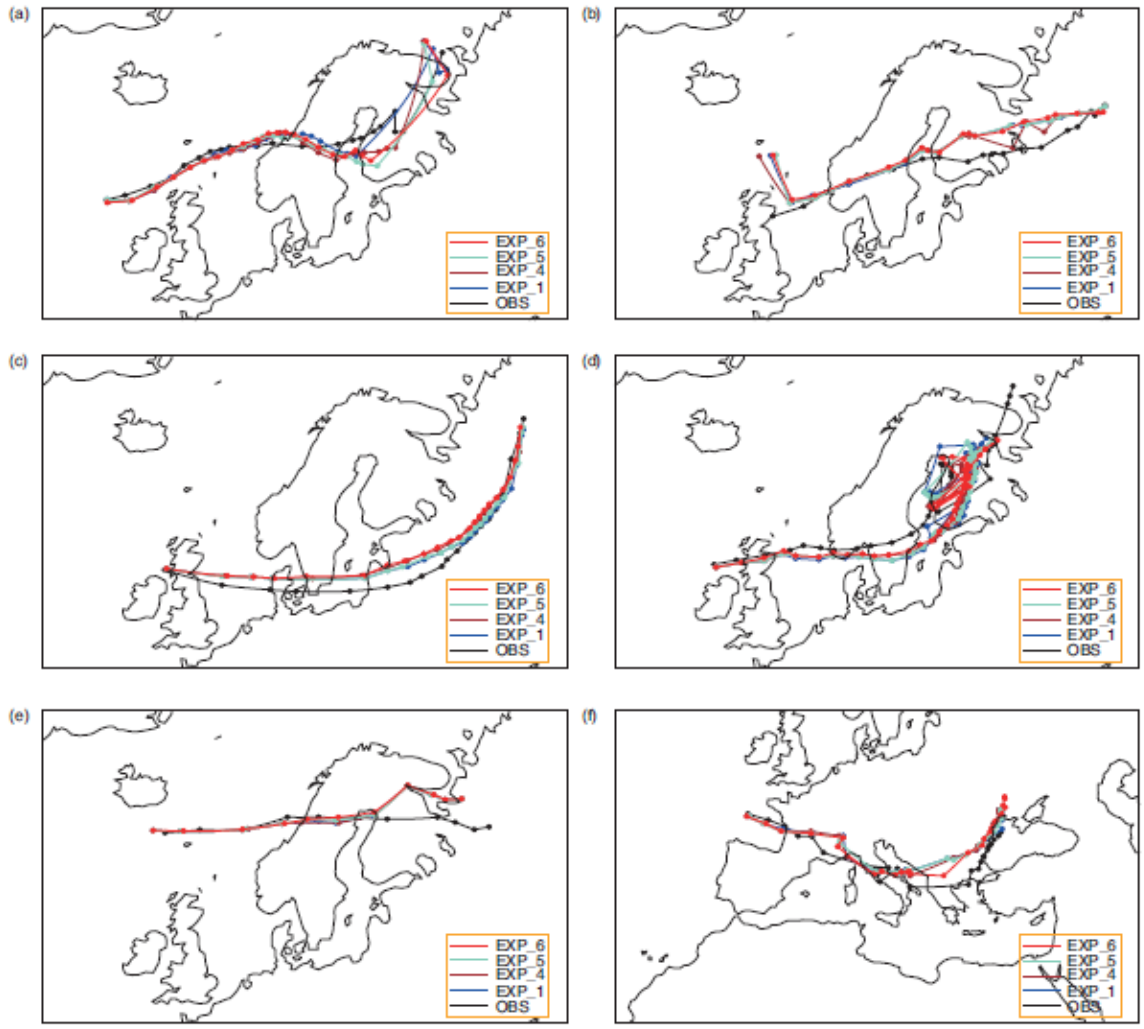

Fig. 8. The storm tracks represented by the minimum sea level pressure every three hours: (a) Gero, (b) Erwin/Gudrun, (c) Kyrill, (d) Ulli, (e) Patrick and (f) Klaus.

Figure 3. Comparison of modeled and measured storm tracks for 6 storms. Exp 6 is where SSGF is used both to the stress and heat and it outperforms the other experiments, but only marginally. (from Wu et al. 2015)

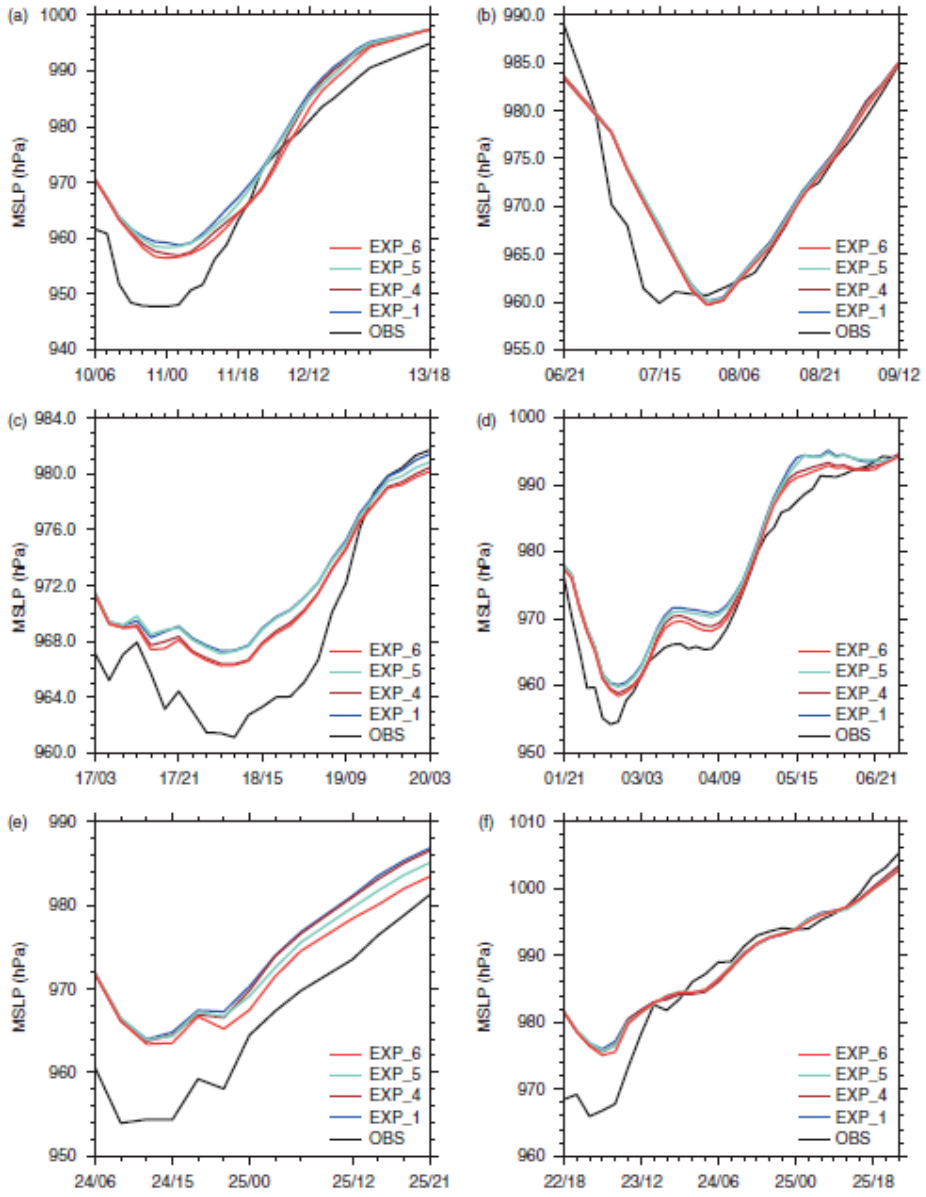

Fig. 9. The minimum sea level pressure of different storms over time: (a) Gero, (b) Erwin/Gudrun, (c) Kyrill, (d) Ulli, (e) Patrick and (f) Klaus.

Figure 4. Comparison of modeled and measured storm center pressure for 6 storms. Exp 6 is where SSGF is used both to the stress and heat and it outperforms the other experiments, but only marginally. (from Wu et al. 2015)

References: (Members in X-WiWa are underlined)

E.L. Andreas. Thermal and size evolution of sea spray droplets. Technical Report 89-11, U.S. Army Cold Regions Research and Engineering Laboratory, June 1989.

E.L. Andreas. Time constants for the evolution of sea spray droplets. *Tellus B*, 42(5), November 1990. ISSN 1600-0889, 0280-6509. doi:10.3402/tellusb.v42i5.15241.

E.L. Andreas. Sea spray and the turbulent air-sea heat fluxes. *Journal of Geophysical Research: Oceans (1978-2012)*, 97(C7): 11429–11441, 1992.

E.L. Andreas. The Temperature of Evaporating Sea Spray Droplets. *Journal of the Atmospheric Sciences*, 52(7):852–862, April 1995.ISSN 0022-4928, 1520-0469. doi: 10.1175/1520-0469(1995) 052<0852:TTOESS>2.0. CO;2.

E.L. Andreas. Reply. *Journal of the Atmospheric Sciences*, 53(11):1642–1645, June 1996. ISSN 0022-4928, 1520-0469. doi:10.1175/1520-0469(1996)053<1642:R>2.0.CO;2.

E.L. Andreas. A New Sea Spray Generation Function for Wind Speeds up to 32 m s -1. *Journal of Physical Oceanography*, 28(11): 2175–2184, November 1998. ISSN 0022-3670, 1520-0485. doi:10.1175/1520-0485(1998)028<2175:ANSSGF>2.0.CO;2.

E.L. Andreas. Approximation formulas for the microphysical properties of saline droplets. *Atmospheric Research*, 75(4):323–345, June 2005. ISSN 01698095. doi: 10.1016/j.atmosres.2005.02.001.

E.L. Andreas. Spray-Mediated Enthalpy Flux to the Atmosphere and Salt Flux to the Ocean in High Winds. *Journal of Atmospheric Sciences*, 40(3):608–619, 2010.

E.L. Andreas. Fallacies of the Enthalpy Transfer Coefficient over the Ocean in High Winds. *Journal of Atmospheric Sciences*, 68(7): 1435–1445, 2011.

E.L. Andreas and J. DeCosmo. Sea spray production and influence on air-sea heat and moisture fluxes over the open ocean. In *Air-Sea Exchange: Physics, Chemistry and Dynamics*, pages 327–362. Springer, 1999.

Garg Nikhil (2015): On the effects of sea spray in coupled atmosphere-ocean-wave modeling – Revisiting models and field data. Power Point Presentation, Wind Energy Seminar at DTU, December 2015.

Kudryavtsev V. (2006): On the effect of sea drops on the atmospheric boundary layer. J. Geophys. Res. Oceans (1978 - 2012), 111 (C7), C07020.

L. Bianco, J.W. Bao, C.W. Fairall, and S.A. Michelson. Impact of sea-spray on the atmospheric surface layer. *Boundary-layer meteorology*, 140(3):361–381, 2011.

S.S. Chen, M.A. Donelan, M. Curcic, C. Lee, S. Chen, J. Doyle, S. Gabersek, S. Wang, R. Allard, T. Campbell, T. Smith, J. Michalakes, and R. Foster. A Unified Air-Sea Interface for Fully Coupled Atmosphere-Wave-Ocean Models for Improving Intensity Prediction of Tropical Cyclones. (Accessed on September 15, 2013), 2012. URL http://www.nopp.org/wp-content/uploads/2012/06/2012Miami_NOPP_TC_Chen_etal.pptx.

Wu L., Rutgersson A., Sahlée E. and Larsén X. (2015): The impact of waves and sea spray on modeling storm track and development. Tellus A 2015, 67, 27967.